Supporting Information

Synthesis and Stereochemistry of Chiral Aza-boraspirobifluorenes with Tetrahedral Boron stereogenic Centers

Yusuke Yoshigoe[1*], Keiichiro Hashizume[1], Shinichi Saito[1*]

[†]*Department of Chemistry, Faculty of Science, Tokyo University of Science, Shinjuku, Tokyo 162-8601, Japan*

Table of Contents

1. General

All reactions were carried out under an argon atmosphere unless otherwise noted. All reagents were purchased from commercial sources (TCI, Wako, and Aldrich) and used without further purification unless otherwise noted. Unless otherwise noted, flame-dried flasks or flame-dried Schlenk tubes were used for the reactions. NMR spectra were recorded on JEOL ECZ 400S, and Bruker-Biospin AVANCE NEO 400 (400 MHz for ^{1}H NMR, 100 MHz for ^{13}C NMR, 368 MHz for ^{19}F NMR, and 128 MHz for ^{11}B NMR) spectrometers. Proton and carbon chemical shifts are reported relative to the residual solvent ($CHCl_3$ (δ 7.24 for ^{1}H NMR, and δ 77.16 for ^{13}C NMR)) used as an internal reference. Fluorine chemical shifts are reported relative to hexafluorobenzene (δ -164.9) as an external reference. Borane chemical shifts are reported relative to the trifluoroborane diethyl ether complex (δ 0.0) as an external reference. Multiplicity is indicated by s (singlet), d (doublet), t (triplet), q (quartet), quint (quintet), or m (multiplet). Coupling constants, *J*, are reported in Hz. IR spectra were recorded on a JASCO FT/IR-4600 spectrometer equipped with a diamond ATR module. GPC separation was performed on JAI NEXT equipped with a YMC-GPC T-30000 (21.2 mm ID × 600 mm L) column using $CHCl_3$ as the eluent. Thin layer chromatography (TLC) was performed on Merck silica gel 60F-254 plates. Column chromatography was performed using Kanto Chemical silica gel 60N (spherical, neutral 50–60 μm). High-resolution mass spectra (HR-MS) were obtained by using Sciex ESI-MS X500R (for ESI-MS) with a quadrupole time-of-flight (QTOF) mass analyzer, or JEOL JMS-700 (for EI-MS).

2. Detailed Procedure of Synthesis

Synthesis of pyridine-borane complex (2)[1]

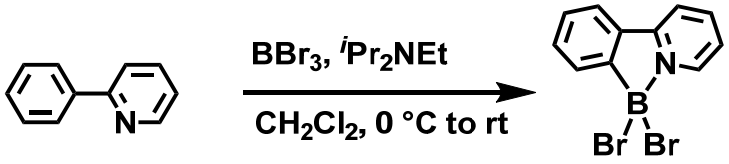

2

To a solution of 2-phenylpyridine (310 mg, 2.00 mmol, 1.00 equiv) and $^{i}Pr_2NEt$ (259 mg, 2.00 mmol, 2.00 equiv) in CH_2Cl_2 (2.0 mL), BBr_3 (1.0 M in CH_2Cl_2, 6.0 mL, 6.0 mmol, 3.0 equiv) was added at 0 °C. After being stirred at room temperature for 24 h, a saturated K_2CO_3 aqueous solution was added to the reaction mixture. The organic layer was separated and the aqueous layer was extracted with CH_2Cl_2. The combined organic layer was washed with water and brine and dried over $MgSO_4$. After removal of the solvent, the resulting solid was washed with hexane to give **2** as a white solid (462 mg, 1.42 mmol, 71% yield).

^{1}H NMR (400 MHz, $CDCl_3$): δ 8.94 (d, *J* = 5.5 Hz, 1H), 8.15 (t, *J* = 7.8 Hz, 1H), 7.91 (d, *J* = 8.2 Hz, 1H), 7.86 (d, *J* = 7.3 Hz, 1H), 7.74 (d, *J* = 7.8 Hz, 1H), 7.55 (t, *J* = 7.3 Hz, 2H), 7.40 (t, *J* = 7.5 Hz, 1H). These values are consistent with those reported in the literature. [1]

Synthesis of 2,2-Dibromobiphenyl derivatives

2,2'-Dibromo-5-methyl-1,1'-biphenyl (4)

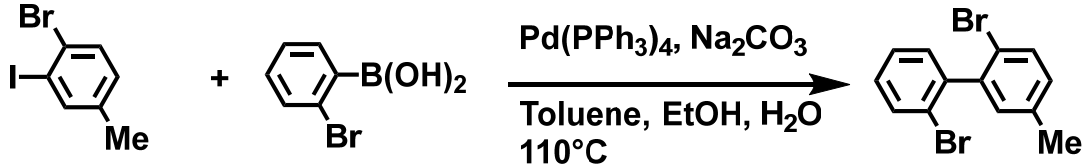

4

To a mixture of 2-bromophenylboronic acid (4.42 g, 22.0 mmol, 1.10 equiv), $Pd(PPh_3)_4$ (1.16 g, 1.00 mmol, 5 mol %) and Na_2CO_3 (4.24 g, 40 mmol, 2 equiv), 1-bromo-1-iodo-5-methylbenzene (5.94 g, 20.0 mmol, 1.00 equiv), toluene (80 mL), ethanol (40 mL) and H_2O (40 mL) were added. After being stirred at 110 °C overnight, the mixture was cooled to room temperature. The organic layer was separated and the aqueous layer was extracted with MTBE. The combined organic layer was washed with brine and dried over Na_2SO_4. After removal of the solvent, the crude reaction mixture was purified by column chromatography (hexane) to give **4** as a white solid (6.00 g, 18.4 mmol, 92% yield). R_f = 0.46 (silica gel, hexane).

^{1}H NMR (400 MHz, $CDCl_3$): δ 7.64 (d, *J* = 7.8 Hz, 1H), 7.52 (d, *J* = 7.8 Hz, 1H), 7.35 (td, *J* = 8.0, 1.4 Hz, 1H), 7.27-7.18 (m, 2H), 7.08-7.00 (m, 2H), 2.33 (s, 3H); **^{13}C NMR (100 MHz, $CDCl_3$)**: δ 142.3, 141.9, 137.2, 132.7, 132.4, 131.7, 131.1, 130.4, 129.4, 127.2, 123.7, 120.2, 21.1; **IR (ATR, ν/cm^{-1})**: 3059, 2930, 2329, 1457, 751; **HRMS (EI)**: calcd. for $C_{13}H_{10}Br_2$, 323.9149; Found, 323.9151.

2-Bromo-3'-methoxybiphenyl (S1)[2]

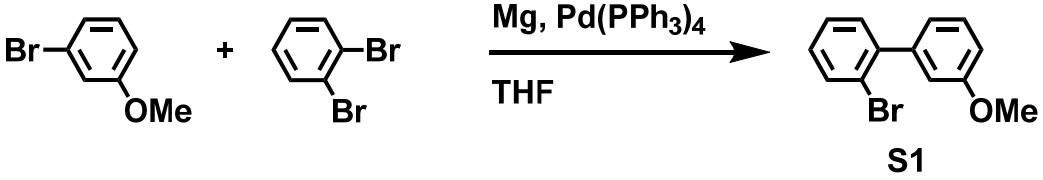

S1

To a suspension of iodine-activated magnesium turnings (240 mg, 10.0 mmol, 1.00 equiv) in anhydrous THF (11 mL), 1-bromo-3-methoxybenzene (1.87 g, 10 mmol, 1.0 equiv) was added at 0 °C. After refluxing for 2 hours, the suspension was added to a suspension of 1,2-dibromobenzene (2.44 g, 10.3 mmol, 1.03 equiv) and $Pd(PPh_3)_4$ (169 mg, 0.146 mmol, 1.5 mol%) in anhydrous THF (11 mL) at 0 °C. After being stirred at 40 °C for 48 hours, a saturated K_2CO_3 aqueous solution was added to the reaction mixture. The organic layer was separated and the aqueous layer was extracted with MTBE. The combined organic layer was washed with brine and dried over $MgSO_4$. After removal of the solvent, the crude reaction mixture was purified by column chromatography (hexane and EtOAc) to give **S1** as a colorless oil (1.12 g, 4.25 mmol, 43% yield). R_f = 0.40 (silica gel, hexane : EtOAc = 30 : 1).

^{1}H NMR (400 MHz, $CDCl_3$): δ 7.69 (dd, *J* = 8.4, 0.8 Hz 1H), 7.39-7.35 (m, 3H), 7.25-7.21 (m, 1H), 7.01 (dt, *J* = 7.5, 1.0 Hz, 1H), 6.98-6.94 (m, 2H), 3.87 (s, 1H). These values are consistent with those reported in the literature. [2]

2,2'-Dibromo-5-methoxy-1,1'-biphenyl (S2)[3]

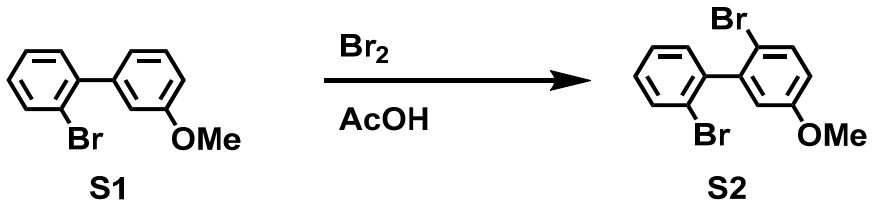

S1 **S2**

To a solution of 2-bromo-3'-methoxybiphenyl (1.10 g, 4.18 mmol, 1.00 equiv) in acetic acid (9.0 mL), bromine (0.26 mL, 5.0 mmol, 1.2 equiv) was added. After being stirred at room temperature overnight, a saturated $Na_2S_2O_3$ aqueous solution was added to the

reaction mixture. The organic layer was separated and the aqueous layer was extracted with CH_2Cl_2. The combined organic layer was washed with brine and dried over $MgSO_4$. After the removal of the solvent, the crude reaction mixture was purified by column chromatography (hexane and EtOAc) to give **S2** as a colorless oil (1.30 g, 4.20 mmol, 89% yield). R_f = 0.38 (silica gel, hexane : EtOAc = 30 : 1).

^{1}H NMR (400 MHz, $CDCl_3$): δ 7.65 (d, *J* = 8.0 Hz, 1H), 7.52 (d, *J* = 8.8 Hz 1H), 7.38-7.33 (m, 1H), 7.28-7.20 (m, 2H), 6.83-6.76 (m, 2H), 3.79 (s, 3H). These values are consistent with those reported in the literature. [3]

2,2'-Dibromo-5-(trifluoromethyl)-1,1'-biphenyl (S3)

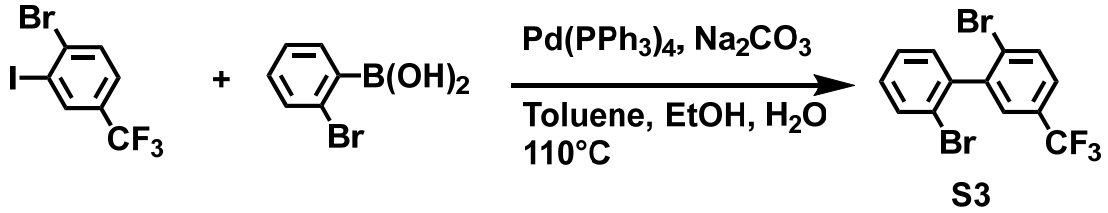

S3

To a mixture of 2-bromophenylboronic acid (843 mg, 4.20 mmol, 1.05 equiv), $Pd(PPh_3)_4$ (324 mg, 0.280 mmol, 7 mol %) and Na_2CO_3 (848 mg, 8.00 mmol, 2.00 equiv), 2-bromo-1-iodo-5-(trifluoromethyl)-benzene (1.40 g, 4.00 mmol, 1.00equiv), toluene (16 mL), ethanol (8 mL) and H_2O (8 mL) were added. After being stirred at 110 °C for 5 h, the mixture was cooled to room temperature. The organic layer was separated and the aqueous layer was extracted with MTBE. The combined organic layer was washed with brine and dried over Na_2SO_4. After the removal of the solvent, the crude reaction mixture was purified by column chromatography (hexane) to give **S3** as a pink solid (1.38 g, 3.62 mmol, 91% yield). R_f = 0.51 (silica gel, hexane).

^{1}H NMR (400 MHz, $CDCl_3$): δ 7.80-7.76 (m, 1H), 7.67 (dd, *J* = 8.0, 1.0 Hz, 1H), 7.51-7.47 (m, 2H), 7.39 (td, *J* = 7.5, 1.3 Hz 1H), 7.28 (td, *J* = 7.5, 1.8 Hz 1H), 7.24-7.21 (m, 1H); **^{13}C NMR (100 MHz, $CDCl_3$)**: δ 142.9, 140.9, 133.4, 132.9, 130.9, 130.1, 129.9 (q, J_F = 32.7 Hz), 128.0 (q, J_F = 3.6 Hz), 127.8, 127.5, 126.2 (q, J_F = 3.6 Hz), 123.9 (q, J_F = 272.5 Hz), 123.4; **^{19}F NMR (375 MHz, $CDCl_3$)**: δ -61.0; **IR (ATR, ν/cm^{-1})**: 3058, 1608, 1562, 1405 1336, 1174, 1139; **HRMS (EI)**: calcd. for $C_{13}H_7Br_2F_3$, 377.8867; Found, 377.8866.

2,2'-Dibromo-4-methyl-1,1'-biphenyl (S4) [4]

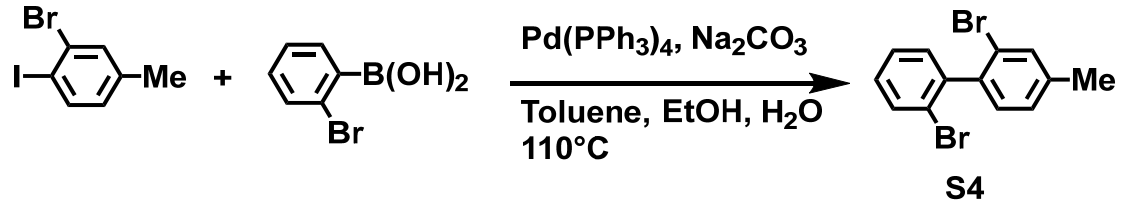

S4

To a mixture of 2-bromophenylboronic acid (2.21 g, 11.0 mmol, 1.10 equiv), $Pd(PPh_3)_4$ (578 mg, 0.500 mmol, 5 mol %) and Na_2CO_3 (2.12 g, 20.0 mmol, 2.00 equiv), 2-bromo-1-iodo-4-methylbenzene (2.97 g, 10.0 mmol, 1.00 equiv), toluene (40 mL), ethanol (20 mL) and H_2O (20 mL) were added. After being stirred at 110 °C overnight, the mixture was cooled to room temperature. The organic layer was separated and the aqueous layer was extracted with MTBE. The combined organic layer was washed with brine, and dried over Na_2SO_4. After removal of the solvent, the crude reaction mixture was purified by column chromatography (hexane) to give **S4** as a colorless oil (2.86 g, 8.78 mmol, 88% yield). R_f = 0.49 (silica gel, hexane).

^{1}H NMR (400 MHz, $CDCl_3$): δ 7.64 (d, *J* = 7.8 Hz, 1H), 7.49 (s, 1H), 7.34 (dt, *J* = 7.1, 1.2 Hz, 1H), 7.25-7.20 (m, 2H), 7.16 (d, *J* = 7.8 Hz, 1H), 7.11 (d, *J* = 7.8 Hz, 1H), 2.38 (s, 1H). These values are consistent with those reported in the literature. [4]

2,2'-Dibromo-4-methoxy-1,1'-biphenyl (S5)[4]

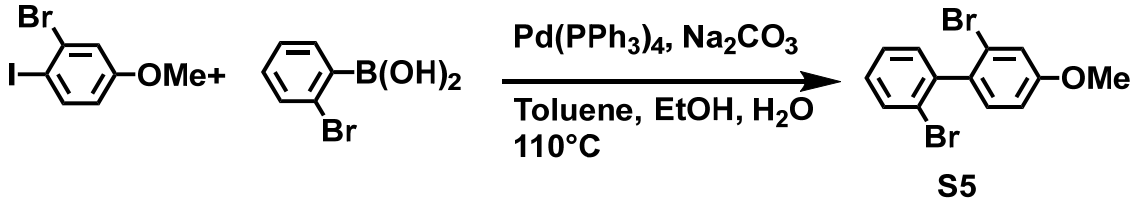

S5

To a mixture of 2-bromophenylboronic acid (884 mg, 4.40 mmol, 1.10 equiv), $Pd(PPh_3)_4$ (324 mg, 0.28 mmol, 7 mol %) and Na_2CO_3 (848 mg, 8.00 mmol, 2.00 equiv), 2-bromo-1-iodo-4-methoxybenzene (1.25 g, 4.00 mmol, 1.00 equiv), toluene (16 mL), ethanol (8 mL) and H_2O (8 mL) were added. After being stirred at 110 °C overnight, the mixture was cooled to room temperature. The organic layer was separated and the aqueous layer was extracted with MTBE. The combined organic layer was washed with brine and dried over Na_2SO_4. After removal of the solvent, the crude reaction mixture was purified by column chromatography (hexane) to give **S5** as a white solid (1.02 g, 3.00 mmol, 75% yield). R_f = 0.44 (silica gel, hexane : CH_2Cl_2 = 10 : 1).

^{1}H NMR (400 MHz, $CDCl_3$): δ 7.66-7.62 (m, 1H), 7.34 (td, 1H, *J* = 7.5, 1.3 Hz), 7.25-

7.19 (m, 3H), 7.13 (d, J = 8.5 Hz, 1H), 6.90 (dd, J = 8.5, 2.5 Hz, 1H), 3.83 (s, 3H). These values are consistent with those reported in the literature. [4]

2,2'-Dibromo-4-(trifluoromethyl)-1,1'-biphenyl (S6)[5]

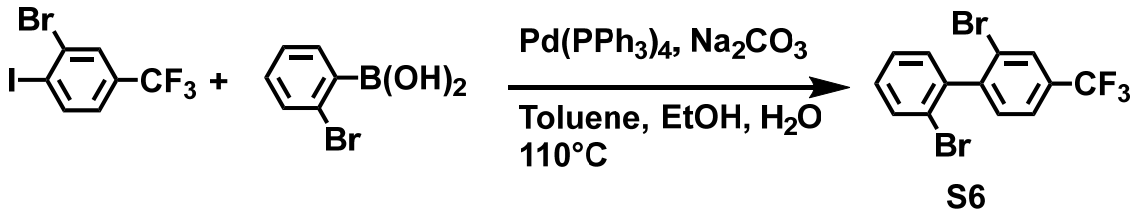

S6

To a mixture of 2-bromophenylboronic acid (843 mg, 4.20 mmol, 1.05 equiv), $Pd(PPh_3)_4$ (324 mg, 0.280 mmol, 7 mol %) and Na_2CO_3 (848 mg, 8.00 mmol, 2.00 equiv), 2-bromo-1-iodo-4-(trifluoromethyl)benzene (1.40 g, 4.00 mmol, 1.00 equiv), toluene (16 mL), ethanol (8 mL) and H_2O (8 mL) were added. After being stirred at 110 °C for 5 h, the mixture was cooled to room temperature. The organic layer was separated and the aqueous layer was extracted with MTBE. The combined organic layer was washed with brine and dried over Na_2SO_4. After the removal of the solvent, the crude reaction mixture was purified by column chromatography (hexane) to give **S6** as a colorless oil (1.10 g, 2.88 mmol, 72% yield). R_f = 0.51 (silica gel, hexane).

^{1}H NMR (400 MHz, $CDCl_3$): δ 7.92 (s, 1H), 7.67 (d, J = 7.8 Hz, 1H), 7.62 (d, J = 7.8 Hz, 1H), 7.41-7.34 (m, 2H), 7.28 (td, J = 7.7, 1.5 Hz, 1H), 7.22 (dd, J = 8.0, 1.4 Hz, 1H). These values are consistent with those reported in the literature. [5]

Synthesis of aza-bora spirobifluorenes

Aza-boraspirobifluorene 1a

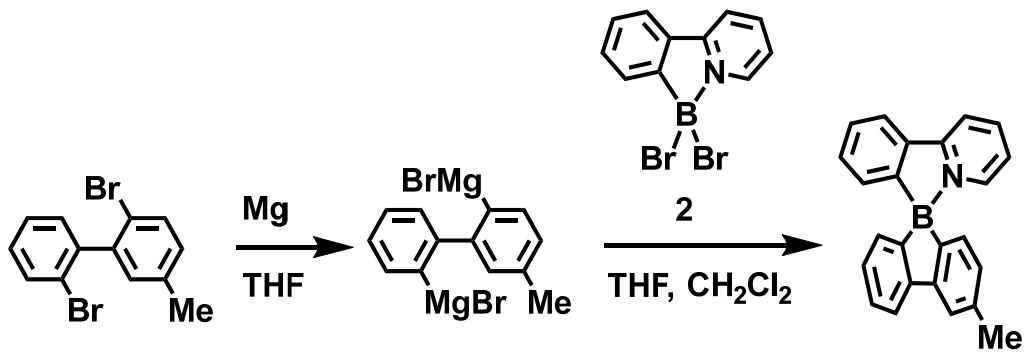

4 3a 1a

To a suspension of iodine-activated magnesium turnings (107 mg, 4.40 mmol, 8.80

equiv), **4** (652 mg, 2.00 mmol, 4.00 equiv) in anhydrous THF (4 mL) was added at 0 °C. The suspension was stirred at room temperature for 10 min. After the supernatant becomes cloudy, Grignard reagent **3a** was prepared by refluxing the mixture for 2 h. A flask was charged with pyridine-borane complex **2** (162 mg, 0.500 mmol, 1.00 equiv) in anhydrous THF (5 mL) and CH_2Cl_2 (5 mL). The THF solution of **3a** was transferred via a cannula at 0 °C. After being stirred at room temperature overnight, saturated NH_4Cl aqueous solution was added to the reaction mixture. The organic layer was separated and the aqueous layer was extracted with $CHCl_3$. The combined organic layer was washed with brine and dried over $MgSO_4$. After removal of the solvent, the crude reaction mixture was purified by column chromatography (hexane and CH_2Cl_2) and GPC to give **1a** as a white solid (56 mg, 0.17 mmol, 34% yield). R_f = 0.48 (silica gel, hexane : CH_2Cl_2 = 3 : 2).

^{1}H NMR (400 MHz, $CDCl_3$): δ 8.03 (dt, *J* = 8.0, 1.0 Hz 1H), 7.98-7.92 (m, 2H), 7.83 (d, *J* = 5.3 Hz, 1H), 7.75 (d, *J* = 7.5 Hz, 1H), 7.61 (s, 1H), 7.40-7.33 (m, 3H), 7.26 (t, *J* = 7.5 Hz, 1H), 7.10 (ddd, *J* = 7.2, 5.8, 1.3 Hz, 1H), 7.00 (tt, *J* = 7.3, 1.0 Hz, 1H), 6.84 (t, *J* = 7.5 Hz, 2H), 6.76 (d, *J* = 7.3 Hz, 1H), 2.41(s, 3H); **^{13}C NMR (100 MHz, $CDCl_3$)**: δ 159.0, 151.4, 151.0, 143.3, 140.5, 137.6, 136.9, 131.1, 130.9, 130.2, 130.1, 127.5, 127.3, 126.5, 126.3, 121.9, 121.5, 120.4, 119.3, 117.9, 21.9 (Note: Three ipso carbons bound to the quadrupolar boron nucleus were not observed.); **^{11}B NMR (128 MHz, $CDCl_3$)**: δ 2.16; **IR (ATR, ν/cm^{-1})**: 3047, 3018, 2982, 2955, 2919, 2858, 1620, 1482; **HRMS (EI)**: calcd. for $C_{24}H_{19}{}^{10}BN$, 345.1798; Found, 345.1801.

Aza-boraspirobifluorene 1b

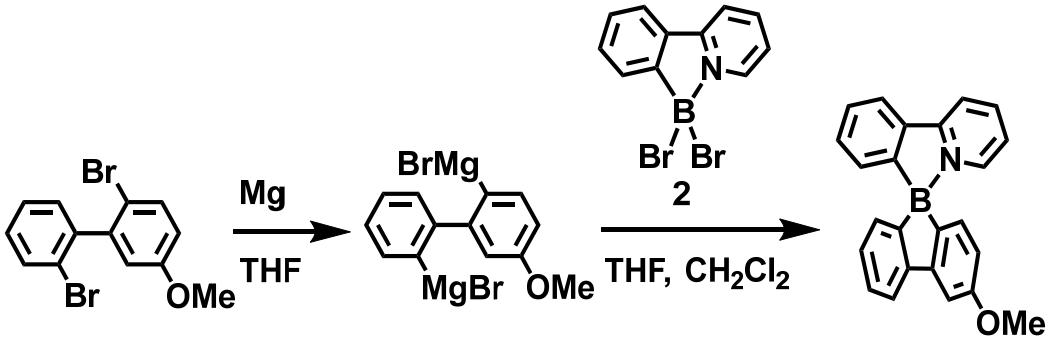

S2 **3b** **1b**

To a suspension of iodine-activated magnesium turnings (107 mg, 4.40 mmol, 8.80 equiv) in anhydrous THF (4 mL), **S2** (684 mg, 2.00 mmol, 4.00 equiv) was added at 0 °C. The suspension was stirred at room temperature for 10 min. After the supernatant

becomes cloudy, refluxing for 2 h, then Grignard reagent **3b** was prepared. A flask was charged with pyridine-borane complex **2** (162 mg, 0.500 mmol, 1.00 equiv) in anhydrous THF (5 mL) and CH_2Cl_2 (5 mL). The THF solution of **3b** was transferred via a cannula at 0 °C. After being stirred at room temperature overnight, saturated NH_4Cl aqueous solution was added to the reaction mixture. The organic layer was separated and the aqueous layer was extracted with $CHCl_3$. The combined organic layer was washed with brine, and dried over $MgSO_4$. After removal of the solvent, the crude reaction mixture was purified by column chromatography (hexane and CH_2Cl_2) and GPC to give **1b** as a white solid (69 mg, 0.20 mmol, 40% yield). R_f = 0.30 (silica gel, hexane : CH_2Cl_2 = 1 : 1).

^{1}H NMR (400 MHz, $CDCl_3$): δ 8.04 (td, *J* = 8.0, 1.0 Hz 1H), 7.98-7.92 (m, 2H), 7.82 (td, *J* = 1.3, 5.8 Hz, 1H), 7.70 (d, *J* = 7.5 Hz, 1H), 7.39-7.30 (m, 4H), 7.26-7.21 (m, 1H), 7.12 (ddd, *J* = 7.2, 6.0, 1.3 Hz, 1H), 6.98 (td, *J* = 6.8, 1.0 Hz, 1H), 6.79 (d, *J* = 7.0 Hz, 1H), 6.75 (d, *J* = 7.8 Hz, 1H), 6.57 (dd, *J* = 7.8, 2.5 Hz, 1H), 3.85 (s, 3H); **^{13}C NMR (100 MHz, $CDCl_3$)**: δ 160.0, 158.9, 152.7, 150.6, 143.2, 140,5 137.6, 131.1, 130.9, 130.8, 130.1, 127.3, 126.8, 126.3, 121.9, 121.5, 119.4, 117.9, 112.1, 105.6, 55.3 (Note: Three ipso carbons bound to the quadrupolar boron nucleus were not observed.); **^{11}B NMR (128 MHz, $CDCl_3$)**: δ 2.18; **IR (ATR, ν/cm^{-1})**: 3048, 2953, 2928, 2830, 1619, 1481; **HRMS (EI)**: calcd. for $C_{24}H_{19}{}^{10}BNO$, 347.1591; Found, 347.1587.

Aza-boraspirobifluorene 1c

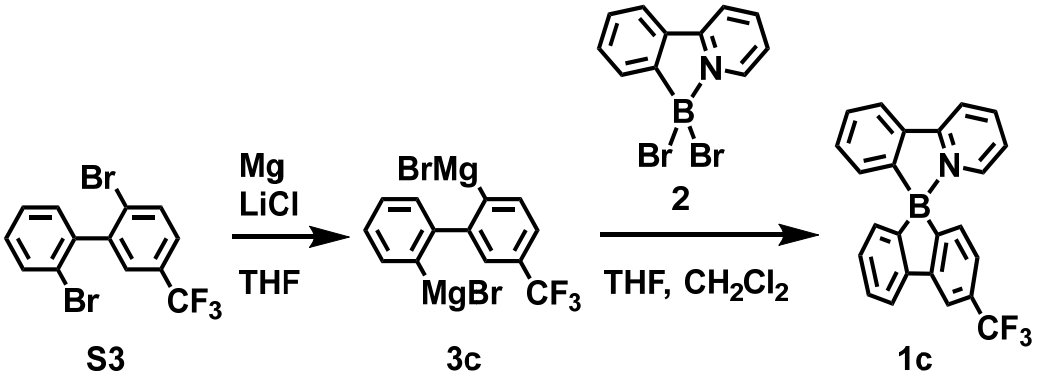

A solution of LiCl in THF was prepared by adding anhydrous THF (10 mL) to LiCl (212 mg, 5.00 mmol, heated to 140 °C under vacuum for 5 h). To a mixture of magnesium turnings (244 mg, 10.0 mmol, 20.0 equiv) and LiCl (10 mL, 0.5 M in THF, 5.00 mmol, 10.0 equiv), DIBAL-H (1 M in THF, 40 μL, 0.04 mmol) was added. After being stirred for 5 min, **S3** (760 mg, 2.00 mmol, 4.00 equiv) was added at 0 °C. After being stirred at

0 °C for 30 min, the Grignard reagent **3c** was prepared. A flask was charged with pyridine-borane complex **2** (162 mg, 0.500 mmol, 1.00 equiv) in anhydrous THF (4 mL), and toluene (1 mL). The THF solution of **3c** was transferred via a cannula at 0 °C. After being stirred at room temperature overnight, saturated NH_4Cl aqueous solution was added to the reaction mixture. The organic layer was separated and the aqueous layer was extracted with $CHCl_3$. The combined organic layer was washed with brine and dried over $MgSO_4$. After removal of the solvent, the crude reaction mixture was purified by column chromatography (hexane and CH_2Cl_2) and GPC to give **1c** as a white solid (39 mg, 0.10 mmol, 20% yield). R_f = 0.49 (silica gel, hexane : CH_2Cl_2 = 3 : 2).

^{1}H NMR (400 MHz, $CDCl_3$): δ 8.08 (dt, *J* = 8.0, 1.3 Hz 1H), 8.02 (td, *J* = 7.2, 1.5 Hz, 1H), 7.98-7.92 (m, 2H), 7.81-7.75 (m, 2H), 7.41-7.26 (m, 4H), 7.22 (d, *J* = 7.3 Hz, 1H), 7.15 (ddd, *J* = 7.3, 5.8, 1.5 Hz, 1H), 7.04 (td, *J* = 7.0, 1.0 Hz, 1H), 6.90 (d, *J* = 7.5 Hz, 1H), 6.86 (d, *J* = 7.0 Hz, 1H); **^{13}C NMR (100 MHz, $CDCl_3$)**: δ 159.2, 151.5, 149.6, 143.2, 141.0, 137.7, 131.4, 130.8, 130.5, 130.2, 129.6 (q, J_F =31.2 Hz), 127.7, 127.5, 126.7, 125.2 (q, J_F = 271.7 Hz), 123.2 (q, J_F = 3.6 Hz), 122.1, 121.7, 119.9, 118.2, 115.8 (q, J_F = 3.6 Hz) (Note: Three ipso carbons bound to the quadrupolar boron nucleus were not observed.); **^{11}B NMR (128 MHz, $CDCl_3$)**: δ 1.80; **^{19}F NMR (375 MHz, $CDCl_3$)**: δ -60.5; **IR (ATR, ν/cm^{-1})**: 3055, 3028, 2957, 2926, 2857, 1621, 1484, 1339; **HRMS (EI)**: calcd. for $C_{24}H_{16}{}^{10}BF_3N$, 385.1359; Found, 385.1364.

Aza-boraspirobifluorene 1d

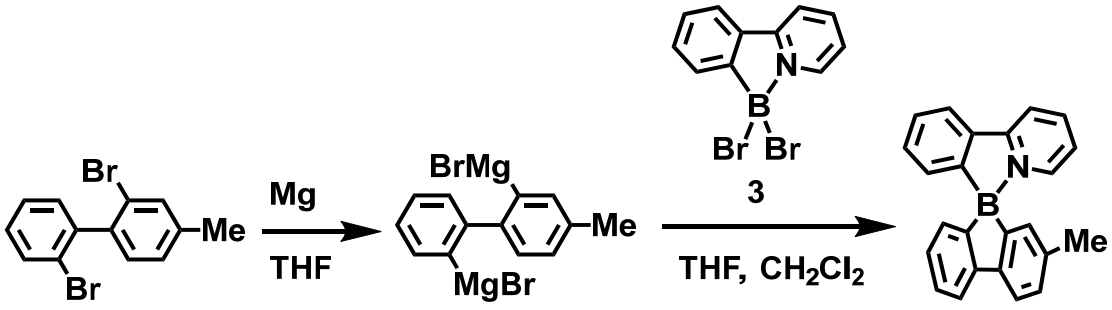

S4 **3d** **1d**

To a suspension of iodine-activated magnesium turnings (107 mg, 4.40 mmol, 8.80 equiv) in anhydrous THF (4 mL), **S4** (652 mg, 2.00 mmol, 4.00 equiv) was added at 0 °C. The suspension was stirred at room temperature for 10 min. After the supernatant becomes cloudy, refluxing for 2 h, then Grignard reagent **3d** was prepared. A flask was charged with pyridine-borane complex **2** (162 mg, 0.500 mmol, 1.00 equiv) in anhydrous THF (5 mL) and CH_2Cl_2 (5 mL). The THF solution of **3d** was transferred via a cannula

at 0 °C. After being stirred at room temperature overnight, saturated NH_4Cl aqueous solution was added to the reaction mixture. The organic layer was separated and the aqueous layer was extracted with $CHCl_3$. The combined organic layer was washed with brine and dried over $MgSO_4$. After removal of the solvent, the crude reaction mixture was purified by column chromatography (hexane and CH_2Cl_2) and GPC to give **1d** as a white solid (29 mg, 0.088 mmol, 18% yield). R_f = 0.44 (silica gel, hexane : CH_2Cl_2 = 3 : 2). **^{1}H NMR (400 MHz, $CDCl_3$)**: δ 8.04 (d, *J* = 8.2 Hz 1H), 7.98-7.93 (m, 2H), 7.84 (d, *J* = 5.5 Hz, 1H), 7.75 (d, *J* = 7.8 Hz, 1H), 7.68 (d, *J* = 7.3 Hz, 1H), 7.41-7.35 (m, 3H), 7.27 (td, *J* = 7.5, 1.4 Hz, 1H), 7.12-7.08 (m, 2H), 7.00 (t, *J* = 7.3 Hz, 1H), 6.85 (d, *J* = 6.8 Hz, 1H), 6.68 (s, 1H), 2.20 (s, 3H); **^{13}C NMR (100 MHz, $CDCl_3$)**: δ 159.8, 158.9, 154.2, 151.1, 148.4, 143.2, 140.5, 137.7, 135.9, 131.1, 130.8, 130.2, 128.1, 127.3, 126.3, 126.2, 121.9, 121.5, 119.2, 119.1, 117.9, 21.5 (Note: Three ipso carbons bound to the quadrupolar boron nucleus were not observed.); **^{11}B NMR (128 MHz, $CDCl_3$)**: δ 2.35; **IR (ATR, *ν*/cm^{-1})**: 3042, 2982, 2913, 2858, 1621, 1482; **HRMS (EI)**: calcd. for $C_{24}H_{19}{}^{10}BN$, 331.1641; Found, 331.1640.

Aza-boraspirobifluorene 1e

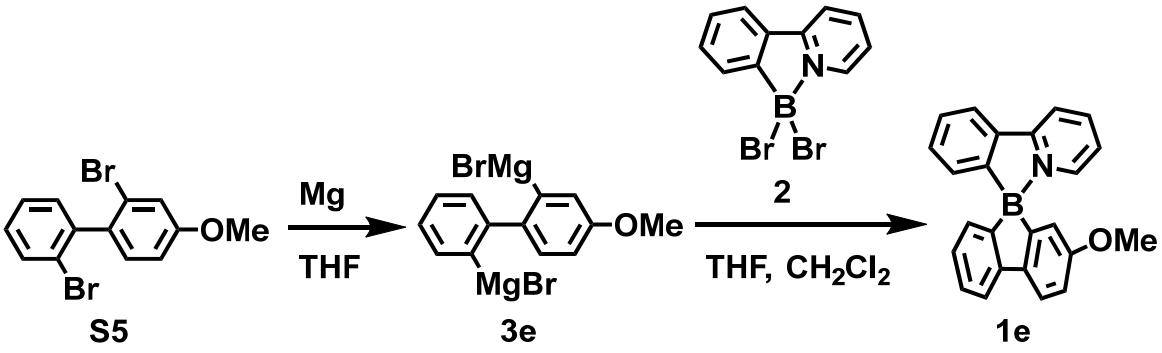

To a suspension of iodine-activated magnesium turnings (107 mg, 4.40 mmol, 8.80 equiv) in anhydrous THF (4 mL), **S5** (684 mg, 2.00 mmol, 4.00 equiv) was added at 0 °C. The suspension was stirred at room temperature for 10 min. After the supernatant becomes cloudy, refluxing for 2 h, then Grignard reagent **3e** was prepared. A flask was charged with pyridine-borane complex **2** (162 mg, 0.500 mmol, 1.00 equiv) in anhydrous THF (5 mL) and CH_2Cl_2 (5 mL). The THF solution of **3e** was transferred via a cannula at 0 °C. After being stirred at room temperature overnight, saturated NH_4Cl aqueous solution was added to the reaction mixture. The organic layer was separated and the aqueous layer was extracted with $CHCl_3$. The combined organic layer was washed with brine and dried over $MgSO_4$. After removal of the solvent, the crude reaction mixture was

purified by column chromatography (hexane and CH_2Cl_2) and GPC to give **1e** as a white solid (70 mg, 0.20 mmol, 40% yield). R_f = 0.27 (silica gel, hexane : CH_2Cl_2=3 : 2). **^{1}H NMR (400 MHz, $CDCl_3$)**: δ 8.04 (dt, *J* = 8.0, 1.0 Hz 1H), 8.01-7.92 (m, 2H), 7.82 (dt, *J* = 5.7, 1.0 Hz, 1H), 7.67-7.63 (m, 2H), 7.40-7.32 (d, 3H), 7.26-7.20 (m, 1H), 7.12 (ddd, *J* = 7.2, 5.8, 1.3 Hz, 1H), 6.92 (td, *J* = 7.0, 1.0 Hz, 1H), 6.79 (d, *J* = 8.3, 2.5 Hz, 2H), 6.38 (d, *J* = 2.5 Hz, 1H), 3.65 (s, 3H); **^{13}C NMR (100 MHz, $CDCl_3$)**: δ 159.0, 159.0, 151.0, 144.0, 143.3, 140.6, 137.7, 131.2, 131.0, 130.1, 127.4, 126.4, 125.6, 121.9, 121.5, 121.1, 118.7, 118.0, 115.9, 112.4, 55.3 (Note: Three ipso carbons bound to the quadrupolar boron nucleus were not observed.); **^{11}B NMR (128 MHz, $CDCl_3$)**: δ 2.17; **IR (ATR, ν/cm^{-1})**: 304, 3005, 2988, 2936, 2903, 2829, 1621, 1485; **HRMS (EI)**: calcd. for $C_{24}H_{19}{}^{10}BNO$, 347.1591; Found, 347.1591.

Aza-boraspirobifluorene 1f

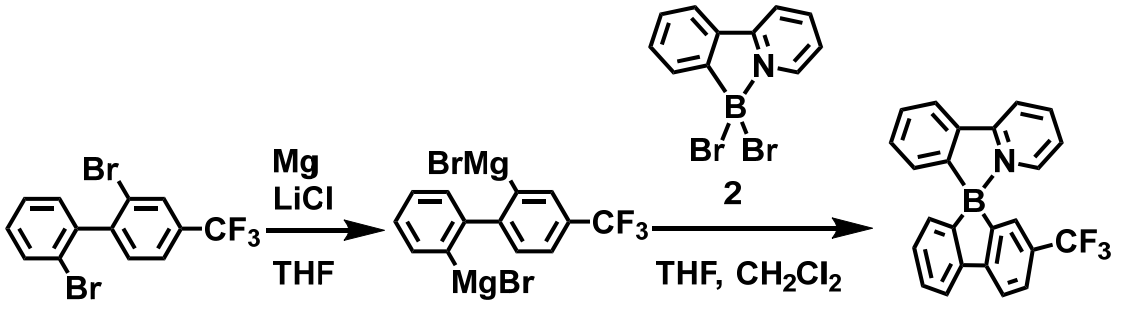

S6 **3f** **1f**

A solution of LiCl in THF was prepared by adding anhydrous THF (10 mL) to LiCl (212 mg, 5.0 mmol, heated to 140 °C under vacuum for 5 h). To a mixture of magnesium turnings (244 mg, 10.0 mmol, 20.0 equiv) and LiCl (10 mL, 0.5 M in THF, 5.0 mmol, 10 equiv), DIBAL-H (40 μL, 1.0 M in THF, 0.04 mmol) was added. After being stirred for 5 min, **S6** (760 mg, 2.00 mmol, 4.00 equiv) was added at 0 °C. After being stirred at 0 °C for 30 min, the Grignard reagent **3f** was prepared. A flask was charged with pyridine-borane complex **2** (162 mg, 0.500 mmol, 1.00 equiv) in anhydrous THF (4 mL), and toluene (1 mL). The THF solution of **3f** was transferred via a cannula at 0 °C. After being stirred at room temperature overnight, saturated NH_4Cl aqueous solution was added to the reaction mixture. The organic layer was separated and the aqueous layer was extracted with $CHCl_3$. The combined organic layer was washed with brine and dried over $MgSO_4$. After removal of the solvent, the crude reaction mixture was purified by column chromatography (hexane and CH_2Cl_2) and GPC to give **1f** as a white solid (28 mg, 0.073 mmol, 15% yield). R_f = 0.35 (silica gel, hexane : CH_2Cl_2=3 : 1).

^{1}H NMR (400 MHz, $CDCl_3$): δ 8.08 (dt, *J* = 8.3, 1.0 Hz 1H), 8.02 (td, *J* = 7.3, 1.5 Hz, 1H), 7.98-7.94 (m, 1H), 7.81-7.75 (m, 3H), 7.50 (dd, *J* = 8.0, 1.0 Hz, 1H), 7.42-7.32 (m, 2H), 7.32-7.25 (m, 1H), 7.16 (ddd, *J* = 7.2, 5.8, 1.3 Hz, 1H), 7.05 (td, *J* = 6.8, 1.0 Hz, 2H), 6.86 (d, *J* = 7.0 Hz, 1H); **^{13}C NMR (100 MHz, $CDCl_3$)**: δ 159.2, 154.5, 149.4, 143.2, 141.0, 137.7, 131.4, 130.9, 130.5, 128.1 (q, J_F = 31.2 Hz), 127.7, 127.6, 126.7 (m), 126.7, 125.3 (q, J_F = 272.5 Hz), 124.8 (q, J_F = 3.6 Hz), 122.1, 121.7, 120.2, 119.1, 118.2 (Note: Three ipso carbons bound to the quadrupolar boron nucleus were not observed.); **^{11}B NMR (128 MHz, $CDCl_3$)**: δ 2.01; **^{19}F NMR (375 MHz, $CDCl_3$)**: δ -59.9; **IR (ATR, ν/cm^{-1})**: 3053, 2986, 2925, 1623, 1484, 1320, 1110; **HRMS (EI)**: calcd. for $C_{24}H_{16}{}^{10}BF_3N$, 385.1359; Found, 385.1362.

Synthesis of aryl pyridine derivatives

2-(2-Bromophenyl)-4-methylpyridine (S7) [6]

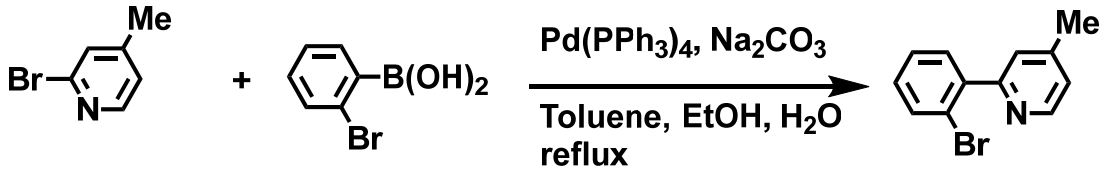

S7

To a mixture of 2-bromophenylboronic acid (552 mg, 2.60 mmol, 1.30 equiv), $Pd(PPh_3)_4$ (69 mg, 60 μmol, 3 mol%) and Na_2CO_3 (1.59 g, 15.0 mmol, 7.50 equiv), 2-bromo-4-methylpyridine (344 mg, 2.00 mmol, 1.00 equiv), toluene (7 mL), ethanol (1.5 mL) and H_2O (7 mL) were added. After being stirred at 110 °C for 18 h, the mixture was cooled to room temperature. Then saturated NH_4Cl aqueous solution was added to the reaction mixture. The organic layer was separated and the aqueous layer was extracted with MTBE. The combined organic layer was washed with brine and dried over Na_2SO_4. After removal of the solvent, the crude reaction mixture was purified by column chromatography (hexane and EtOAc) to give **S7** as a yellow solid (372 mg, 1.50 mmol, 75% yield). R_f = 0.34 (silica gel, hexane : EtOAc = 5 : 1).

^{1}H NMR (400 MHz, $CDCl_3$): δ 8.54 (d, *J* = 5.0 Hz, 1H), 7.64 (dd, *J* = 8.0, 1.0 Hz, 1H), 7.48 (dd, *J* = 7.8, 1.8 Hz, 1H), 7.40-7.34 (m, 2H), 7.25-7.20 (m, 1H), 7.11-7.08 (m, 1H), 2.40 (s, 3H). The data are consistent with those reported in the literature. [6]

2-(2-Bromophenyl)-4-methoxylpyridine (S8)

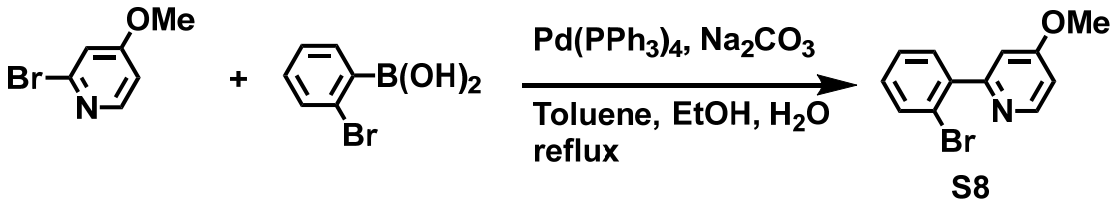

S8

To a mixture of 2-bromophenylboronic acid (552 mg, 2.60 mmol, 1.30 equiv), $Pd(PPh_3)_4$ (69 mg, 60 μmol, 3 mol%) and Na_2CO_3 (1.59 g, 15.0 mmol, 7.50 equiv), 2-bromo-4-methoxypyridine (376 mg, 2.00 mmol, 1.00 equiv), toluene (7 mL), ethanol (1.5 mL) and H_2O (7 mL) were added. After being stirred at 110 °C for 18 h, the mixture was cooled to room temperature. Then saturated NH_4Cl aqueous solution was added to the reaction mixture. The organic layer was separated and the aqueous layer was extracted with MTBE. The combined organic layer was washed with brine and dried over Na_2SO_4. After the removal of the solvent, the crude reaction mixture was purified by column chromatography (hexane and EtOAc) to give **S8** as a yellow solid (301 mg, 1.14 mmol, 57% yield). R_f = 0.25 (silica gel, hexane : EtOAc = 5 : 1).

^{1}H NMR (400 MHz, $CDCl_3$): δ 8.50 (d, *J* = 5.9 Hz, 1H), 7.65 (d, *J* = 7.8 Hz, 1H), 7.50 (dd, *J* = 7.8, 1.4 Hz, 1H), 7.37 (t, *J* = 7.3 Hz 1H), 7.26-7.20 (m, 1H), 7.09 (d, *J* = 2.3 Hz, 1H), 6.81 (dd, *J* = 5.7, 2.5 Hz, 1H) 3.88 (s, 3H); **^{13}C NMR (100 MHz, $CDCl_3$)**: δ 165.6, 160.0, 150.7, 141.4, 133.4, 131.4, 129.8, 127.6, 121.9, 111.0, 108.9, 55.4; **IR (ATR, ν/cm^{-1})**: 3069, 3059, 3018, 2979, 2946, 2935, 2840, 1601, 1567, 1471; **HRMS (EI)**: calcd. for $C_{12}H_{11}{}^{79}BrNO$,264.0019; Found, 264.0018.

2-(2-Bromophenyl)-4-(trifluoromethyl)pyridine (S9)

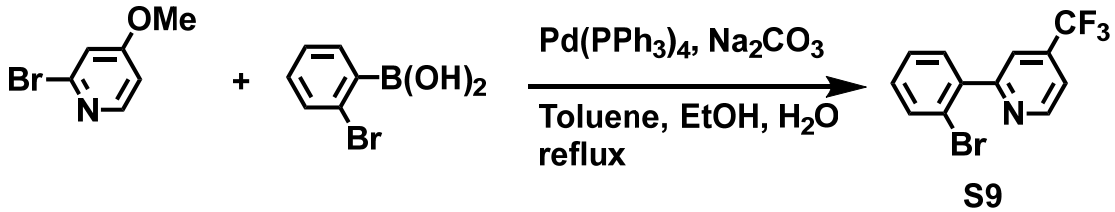

S9

To a mixture of 2-bromophenylboronic acid (552 mg, 2.60 mmol, 1.30 equiv), $Pd(PPh_3)_4$ (69 mg, 60 μmol, 3 mol%) and Na_2CO_3 (1.59 g, 15.0 mmol, 7.50 equiv), 2-bromo-4-(trifluoromethyl)pyridine (452 mg, 2.00 mmol, 1.00 equiv), toluene (7 mL), ethanol (1.5 mL) and H_2O (7 mL) were added. After being stirred at 110 °C for 18 h, the mixture was cooled to room temperature. Then saturated NH_4Cl aqueous solution was added to the reaction mixture. The organic layer was separated and the aqueous layer was

extracted with MTBE. The combined organic layer was washed with brine and dried over Na_2SO_4. After removal of the solvent, the crude reaction mixture was purified by column chromatography (hexane and EtOAc) to give **S9** as a brown oil (463 mg, 1.53 mmol, 77% yield). R_f = 0.51 (silica gel, hexane : EtOAc = 5 : 1).

^{1}H NMR (400 MHz, $CDCl_3$) δ 8.88 (d, *J* = 5.2 Hz, 1H), 7.84 (t, *J*= 0.75 Hz, 1H), 7.69 (dd, *J* = 8.0, 1.0 Hz, 1H), 7.53 (dd, *J* = 7.6, 1.6 Hz, 1H), 7.52-7.48 (m, 1H), 7.42 (td, *J* = 7.5, 1.3 Hz, 1H), 7.32-7.26 (m, 1H); **^{13}C NMR (100 MHz, $CDCl_3$)** δ 159.7, 150.5, 140.1, 138.4 (q, J_F = 33.7 Hz), 133.7, 131.5, 130.6, 127.9, 122.9 (q, J_F = 273.6 Hz), 121.7, 120.7 (q, J_F = 3.9 Hz), 118.2 (q, J_F = 2.9 Hz); **^{19}F NMR (375 MHz, $CDCl_3$)** δ -63.2; **IR (ATR, ν/cm^{-1})**: 3064, 1610, 1402, 1338, 1175; **HRMS (EI)**: calcd. for $C_{12}H_8{}^{79}BrF_3N$, 301.9787; Found, 301.9783.

General procedure for preparation of a solution of 5 [7]

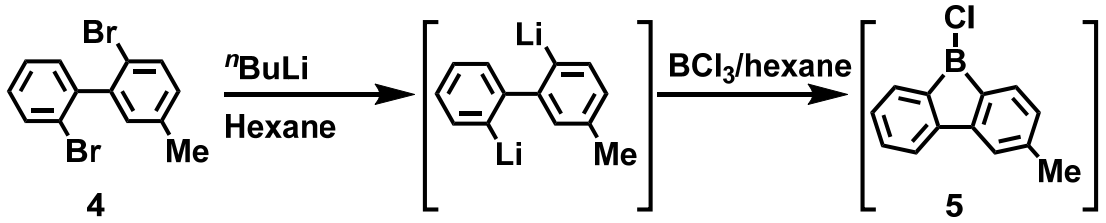

To a solution of **4** (326 mg, 1.00 mmol, 1.00 equiv) in anhydrous hexane (15.6 mL), ^{n}BuLi (1.59 M in hexane, 1.26 mL, 2.00 mmol, 2.00 equiv) was added at 0 °C. The solution was stirred at room temperature for 3 days. After removal of the solvent in vacuo, the remaining white solid was washed with anhydrous hexane (3 × 5 mL). Then a white slurry was made in anhydrous hexane (15.6 mL) by vigorous stirring, and BCl_3 (1.0 M in hexane, 1.0 mL, 1.0 mmol, 1.0 equiv) was added at 0 °C. The mixture was stirred at room temperature overnight. After removal of the solvent in vacuo, a yellow solid was given. The solid was dissolved into 8 mL of anhydrous Et_2O to yield a solution of **5**. Since compound 5 was unstable, it was used in the next step without further purification.

Synthesis of aza-boraspirobifluorenes with substituents on the pyridine ring

Aza-boraspirobifluorene 1g

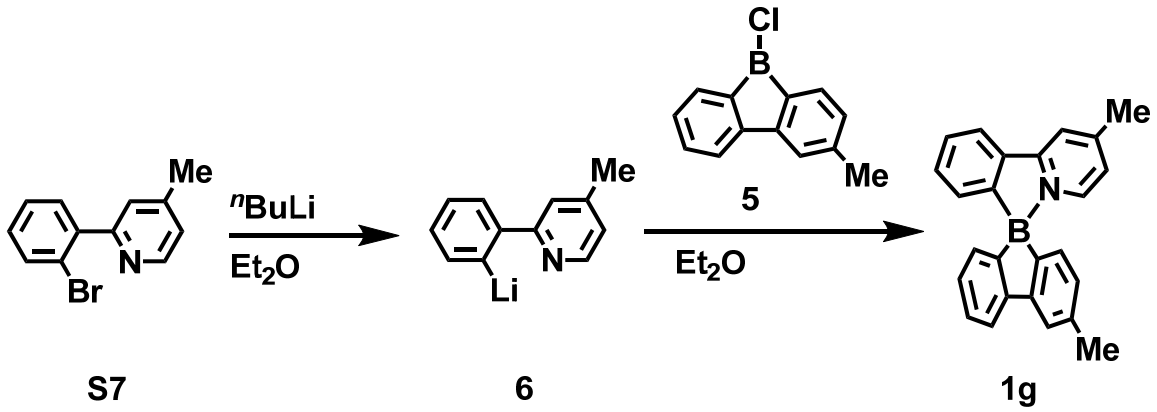

To a solution of **S7** (191 mg, 0.771 mmol, 1.00 equiv) in anhydrous Et_2O (7.1 mL), ^{n}BuLi (1.59 M in hexane, 0.512 mL, 0.814 mmol, 1.06 equiv) was added at -78 °C. After the solution was stirred at this temperature for 1 h, the disappearance of **S7** was confirmed by TLC. Afterward a prepared solution of **5** (*ca.* 1.0 mmol, 1.3 equiv) in anhydrous Et_2O (8 mL) was transferred via a cannula at −78 °C. The solution was stirred at this temperature for 10 min and then at room temperature overnight. Then saturated NH_4Cl aqueous solution was added to the reaction mixture. The organic layer was separated and the aqueous layer was extracted with CH_2Cl_2. The combined organic layer was washed with brine and dried over $MgSO_4$. After removal of the solvent, the crude reaction mixture was purified by column chromatography (Hexane and CH_2Cl_2) and GPC to give **1g** as a white solid (63 mg, 0.18 mmol, 24% yield). R_f = 0.42 (silica gel, hexane : CH_2Cl_2 = 3 : 2).

^{1}H NMR (400 MHz, $CDCl_3$): δ 7.93-7.88 (m, 1H), 7.83 (t, *J* = 0.8 Hz 1H), 7.72 (d, *J* = 7.5 Hz, 1H), 7.66 (d, *J* = 6.0 Hz, 1H), 7.57 (s, 1H), 7.37-7.29 (m, 3H), 7.26-7.20 (m, 1H), 6.97 (td, *J* = 7.1, 1.0 Hz, 1H), 6.91 (dd, *J* = 5.8, 1.0 Hz, 1H), 6.81 (t, *J* = 8.0 Hz,2H), 6.73 (d, *J* = 7.3 Hz, 1H), 2.53 (s, 3H), 2.38 (s, 3H); **^{13}C NMR (100 MHz, $CDCl_3$)**: δ 158.6, 153.0, 151.3, 151.0, 142.5, 137.7, 136.7, 130.9, 130.8, 130.14, 130.10, 127.5, 127.2, 126.5, 126.2, 123.1, 121.3, 120.3, 119.3, 118.3, 22.0, 21.9 (Note: Three ipso carbons bound to the quadrupolar boron nucleus were not observed.); **^{11}B NMR (128 MHz, $CDCl_3$)**: δ 1.74; **IR (ATR, ν/cm^{-1})**: 3044, 2985, 2914, 2861, 1630; **HRMS (EI)**: calcd. for $C_{25}H_{21}{}^{10}BN$, 345.1798; Found, 345.1801.

Aza-boraspirobifluorene 1h

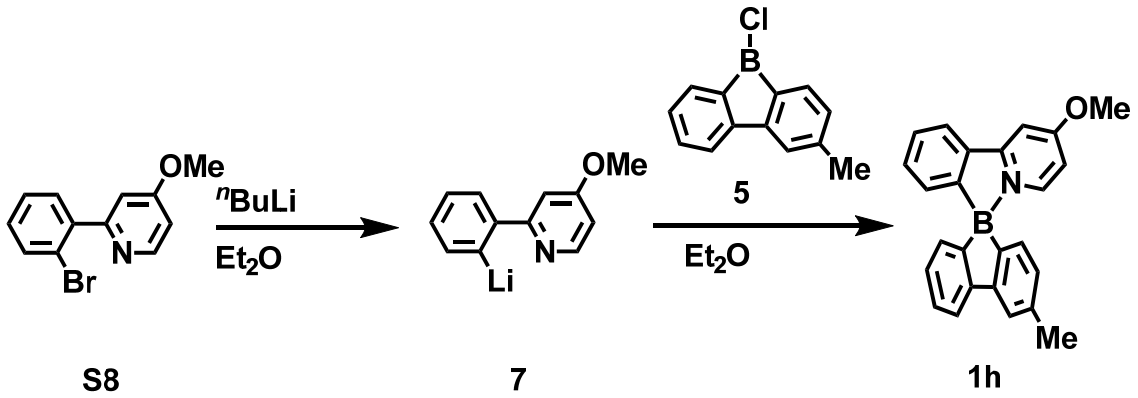

To a solution of **S8** (204 mg, 0.771 mmol, 1.00 equiv) in anhydrous Et_2O (7.1 mL), ^{n}BuLi (1.59 M in hexane, 0.512 mL, 0.814 mmol, 1.06 equiv) was added at -78 °C. After the solution was stirred at this temperature for 1 h, the disappearance of **S8** was confirmed by TLC. Afterward a prepared solution of **5** (*ca.* 1.0 mmol, 1.3 equiv) in anhydrous Et_2O (8 mL) was transferred via a cannula at −78 °C. The solution was stirred at this temperature for 10 min and then at room temperature overnight. Then saturated NH_4Cl aqueous solution was added to the reaction mixture. The organic layer was separated and the aqueous layer was extracted with CH_2Cl_2. The combined organic layer was washed with brine and dried over $MgSO_4$. After removal of the solvent, the crude reaction mixture was purified by column chromatography (Hexane and CH_2Cl_2) and GPC to give **1h** as a white solid (119 mg, 0.329 mmol, 43% yield). R_f = 0.37 (silica gel, hexane : CH_2Cl_2 = 3 : 2).

^{1}H NMR (400 MHz, $CDCl_3$): δ 7.93-7.88 (m, 1H), 7.77 (d, *J* = 7.3 Hz, 1H), 7.67-7.60 (m, 2H), 7.45 (d, *J* = 2.3 Hz, 1H), 7.40-7.24 (m, 4H), 7.03 (t, *J* = 7.3 Hz, 1H), 6.89 (d, *J* = 7.3 Hz 2H), 6.82 (dd, *J* = 7.1, 1.6 Hz, 1H) 6.62 (dd, *J* = 6.6, 2.5 Hz, 1H), 3.99 (s, 3H), 2.44 (s, 3H); **^{13}C NMR (100 MHz, $CDCl_3$)**: δ 159.1, 160.8, 151.2, 150.8, 144.1, 137.7, 136.6, 131.0, 130.8, 130.2, 130.1, 127.4, 127.1, 126.4, 126.1, 121.2, 120.2, 119.2, 109.3, 102.1, 56.3, 21.8 (Note: Three ipso carbons bound to the quadrupolar boron nucleus were not observed.); **^{11}B NMR (128 MHz, $CDCl_3$)**: δ 1.77; **IR (ATR, ν/cm^{-1})**: 3041, 3013, 2941, 2914, 2862, 1626, 1490; **HRMS (EI)**: calcd. for $C_{25}H_{21}{}^{10}BNO$, 361.1747; Found, 361.1749.

Aza-boraspirobifluorene 1i

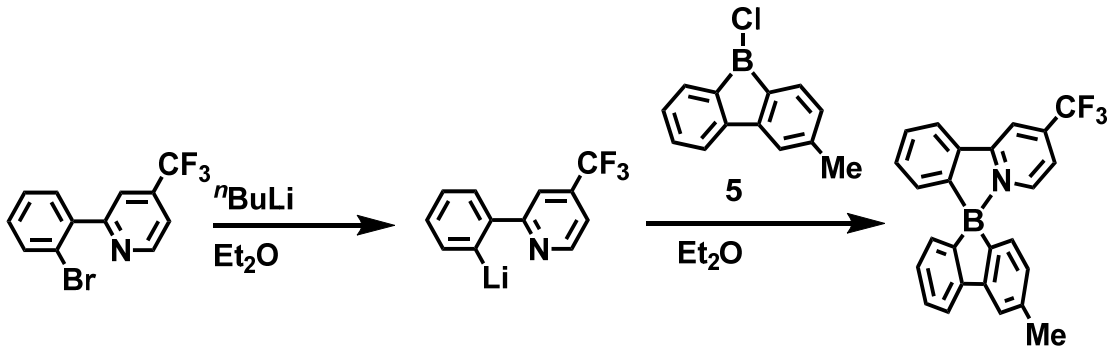

To a solution of **S9** (233 mg, 0.771 mmol, 1.00 equiv) in anhydrous Et_2O (7.1 mL), ^{n}BuLi (1.59 M in hexane, 0.512 mL, 0.814 mmol, 1.06 equiv) was added at -78 °C. After the solution was stirred at this temperature for 1 h, the disappearance of **S9** was confirmed by TLC. Afterward, a solution of **5** (*ca.* 1.0 mmol, 1.3 equiv) in anhydrous Et_2O (8 mL) was transferred via a cannula at −78 °C. The solution was stirred at this temperature for 10 min and then at room temperature overnight. Then saturated NH_4Cl aqueous solution was added to the reaction mixture. The organic layer was separated and the aqueous layer was extracted with CH_2Cl_2. The combined organic layer was washed with brine and dried over $MgSO_4$. After removal of the solvent, the crude reaction mixture was purified by column chromatography (hexane and CH_2Cl_2) and GPC to give **1i** as a yellow solid (102 mg, 0.255 mmol, 33% yield). R_f = 0.57 (silica gel, hexane : CH_2Cl_2 = 3 : 2).

^{1}H NMR (400 MHz, $CDCl_3$) : δ 8.25 (s, 1H), 8.04-7.97 (m, 2H), 7.76 (d, J = 7.3 Hz, 1H), 7.61 (s, 1H), 7.44-7.38 (m, 3H), 7.32-7.25 (m, 2H), 7.00 (t, J = 7.3 Hz 1H), 6.86 (d, J = 7.3 Hz, 1H) 6.81 (d, J = 7.5 Hz, 1H), 6.74 (d, J = 7.3 Hz, 1H) 2.41 (s, 3H); **^{13}C NMR (100 MHz, $CDCl_3$)**: δ 160.3, 151.5, 151.2, 144.6, 142.3 (q, J_F = 34.7 Hz), 137.3, 136.6, 132.2, 131.1, 130.13, 130.09, 127.7, 126.8, 122.2 (q, J_F = 274.5 Hz), 122.1, 120.6, 119.5, 117.7 (q, J_F = 2.9 Hz), 114.5 (q, J_F = 3.8 Hz), 21.8 (Note: Three ipso carbons bound to the quadrupolar boron nucleus were not observed. Two carbon signals are missing.); **^{11}B NMR (128 MHz, $CDCl_3$)**: δ 2.70; **^{19}F NMR (375 MHz, $CDCl_3$)**: δ -63.4; **IR (ATR, ν/cm^{-1})**: 3048, 3019, 2982, 2926, 2868, 1470, 1423, 1342; **HRMS (EI)**: calcd. for $C_{25}H_{18}{}^{10}BF_3N$, 399.1515; Found, 399.1514.

Attempts for improvement of yield of 1d.

Table S1. Summary of our attempts for synthesis of **1d** by use of several organometallic reagents.

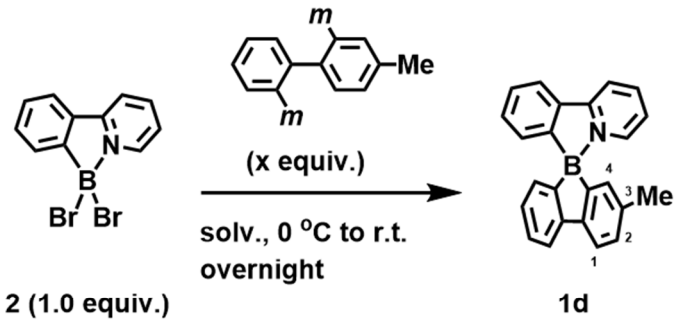

2 (1.0 equiv.) 1d

entry	*m*	x	solv.	yield (%)
1	MgBr	2.0	THF, CH_2Cl_2	trace
2	MgBr	4.0	THF, CH_2Cl_2	18
3	MgBr	6.0	THF, CH_2Cl_2	16
4	MgCl·LiCl	4.0	THF, CH_2Cl_2	trace
5	ZnCl	4.0	THF, CH_2Cl_2	trace
6	Sn^nBu_3	4.0	THF, CH_2Cl_2	trace

3. Isolation of the enantiomers of 1a-f by high performance liquid chromatography (HPLC)

The isolation of the enantiomers was performed on a JASCO LC-2080 assemble coupled with a YMC CHIRAL Amylose-SA (for analytical: L × D: 250 mm × 4.6 mm, particle size: 5 μm; for semi-preparative: L × D: 250 mm × 20 mm, particle size: 5 μm). HPLC charts were recorded with a Photo diode array (PDA) detector. Elution rates were controlled and stabilized at 0.8 mL/min (for analytical) or 8.0 mL/min (for semi-preparative). For all HPLC experiments, the solvents (*n*-hexane, $CHCl_3$, and *i*-PrOH) with HPLC grade were passed through the degasser included in the assemble.

Table S2. Summary of isolation of the enantiomers by HPLC and the analysis by CD spectroscopy for **1a-1i**.

	Eluents: *n*-hexane / $CHCl_3$ / *i*-PrOH	**Fraction 1** Retention time, t_1 /min. (capacity factor, k_1)	%*ee*[a]	[CD(+/-)][b]	**Fraction 2** Retention time, t_2 /min. (capacity factor, k_2)	%*ee*[a]	[CD(+/-)][b]	Sepatation factor, α[c]
1a	93 / 2/ /5	13.7 (2.48)	>99	(-)	18.7 (3.75)	>99	(+)	1.51
1b	86 / 5 / 9	15.0 (2.94)	>99	(-)	17.6 (3.62)	>99	(+)	1.23
1c	93 / 2 / 5	10.6 (1.35)	>99	(-)[c]	12.0 (1.66)	>99	(+)	1.23
1d	93 / 2 / 5	13.1 (2.23)	>99	(-)	20.9 (4.16)	>99	(+)	1.86
1e	86 / 5 / 9	13.9 (2.82)	>99	(-)	16.0 (3.40)	>99	(+)	1.20
1f	93 / 2 / 5	11.3 (1.57)	>99	(-)	14.6 (2.32)	>99	(+)	1.48
1g	93 / 2 / 5	11.6 (2.71)	>99	(-)	13.2 (3.22)	>99	(+)	1.19
1h	93 / 2 / 5	19.2 (3.76)	>99	(-)[d]	24.2 (5.00)	>99	(+)[d]	1.33
1i	93 / 2 / 5	7.55 (1.82)	>99	(-)	8.46 (2.16)	>99	(+)	1.89

[a] To determine %*ee* values, an independent HPLC analysis for each fractions was performed; A chromatogram gave two integration values ($I(t_n)$) around two retention times(t_n); The values were applied into the equation: For fraction 1 : %*ee* = $[I(t_1)-I(t_2)]/[I(t_1)+I(t_2)]$; For fraction 2 : %*ee* = $[I(t_2)-I(t_1)]/[I(t_1)+I(t_2)]$; [b] To determine [CD(+/-)], a sign of $[\theta]$ (/deg·cm^2·dmol^{-1}) value at 320 nm of the CD spectra in CH_2Cl_2 solution of the each sample was used. Spectra were shown in below. [c] $\alpha = k_2/k_1$. [d] at 305 nm. [e] at 335 nm

4. X-ray crystallographic structure of 1a-i

Single crystals of **1a-i** suitable for X-ray crystallographic measurement were obtained by vapor diffusion or by liquid/liquid diffusion of a combination of solvents stated below. X-ray diffraction data for **1a-i** were collected on a Bruker D8 QUEST diffractometer coupled to a Photon III area detector with Mo Kα radiation (λ = 0.7107 Å), from a IμS X-ray source. The diffraction images were processed and scaled using the APEX III software, and finalized using the OLEX2[8] software. A numerical absorption correction (μ) was applied. The structure was solved through intrinsic phasing using SHELXT[9] and refined against F^2 on all data by full-matrix least squares with SHELXL[9] following established refinement strategies. All nonhydrogen atoms were refined anisotropically. All hydrogen atoms bound to carbon were included in the model at geometrically calculated positions and refined using a riding model. ORTEP drawings of **1a-i** are shown in Figures S1-S3 and details of the data quality and a summary of the residual values of the refinements are listed in Tables S3-S5.

Single-crystal X-ray structures that contain the supplementary crystallographic data for this paper can be obtained free of charge from the Cambridge Crystallographic Data Centre at www.ccdc.cam.ac.uk/data_request/cif.

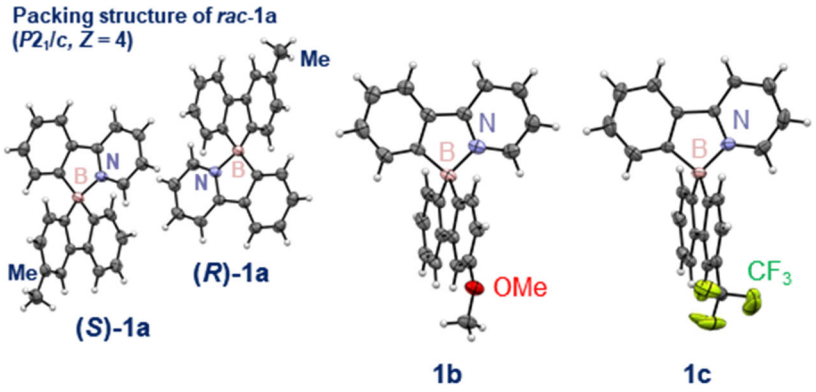

Figure S1. ORTEP drawing of **1a-1c**. Hydrogen atoms were omitted for clarity.

Table S3. Crystal data and structure refinement for **1a-1c**

Compound	**1a**	**1b**	**1c**
CCDC No.	2203027	2203028	2203029
Solvent system	Toluene / Hexane	Toluene / Hexane	Toluene / Hexane
Color	Colorless	Colorless	Colorless
Formula	$C_{24}H_{18}BN$	$C_{24}H_{18}BNO$	$C_{24}H_{15}BF_3N$
F_w	331.23	347.20	385.20
Crystal size /mm	0.02 x 0.02 x 0.02	0.02 x 0.02 x 0.02	0.02 x 0.02 x 0.0.2
Crystal system	monoclinic	monoclinic	monoclinic
Space group	$P2_1/c$ (No. 14)	$P2_1/c$ (No. 14)	$P2_1/c$ (No. 14)
a /Å	12.2016(13)	12.929(2)	13.3393(5)
b /Å	9.8758(12)	9.6055(19)	9.3980(3)
c /Å	14.9890(18)	15.347(3)	15.5279(5)
α /°	90	90	90
β /°	103.647(4)	108.252(4)	110.4660(10)
γ /°	90	90	90
V /Å^3	1755.2(4)	1810.0(5)	1823.7(5)
Z	4	4	4
D_c /g cm^{-3}	1.253	1.274	1.403
No. of reflections measured	21468	16138	23835
No. of unique reflections	20780	15581	23000
No. observations ($I > 2\sigma(I)$)	3258	2723	3967
R	0.0607	0.0665	0.0742
R_w	0.1586	0.1929	0.1756
GOF on F^2	1.080	1.087	1.181

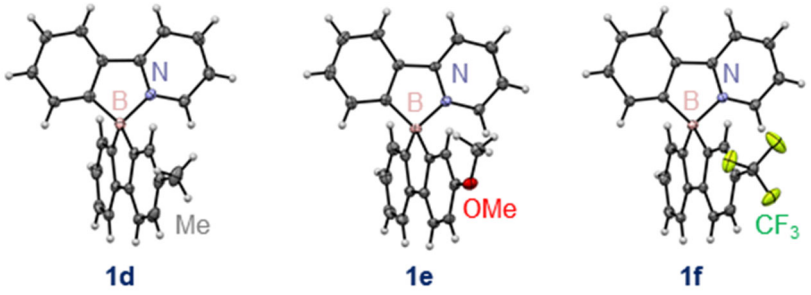

Figure S2. ORTEP drawing of **1d-1f**. Hydrogen atoms were omitted for clarity.

Table S4. Crystal data and structure refinement for **1d-1f**

Compound	**1d**	**1e**	**1f**
CCDC No.	2215757	2203030	2203032
Solvent system	Toluene / Hexane	Toluene / Hexane	Toluene / Hexane
Color	Colorless	Colorless	Colorless
Formula	$C_{24}H_{18}BN$	$C_{24}H_{18}BNO$	$C_{24}H_{15}BF_3N$
F_w	331.23	347.20	385.20
Crystal size /mm	0.02 x 0.02 x 0.02	0.58 x 0.35 x 0.26	0.45 x 0.28 x 0.25
Crystal system	Orthorhombic	Triclinic	Orthorhombic
Space group	$P2_12_12_1$ (No. 19)	P-1 (No. 1)	$P2_12_12_1$ (No. 19)
a /Å	11.1612(9)	11.9380(5)	9.1093(2)
b /Å	17.6966(14)	12.7143(5)	11.4141(3)
c /Å	9.0820(7)	14.2807(6)	17.6390(4)
α /°	90	109.1900(10)	90
β /°	90	103.259(2)	90
γ /°	90	108.8850(10)	90
V /Å^3	1793.83	1793.52	1834.01
Z	4	2	4
D_c /g cm^{-3}	1.226	1.286	1.395
No. of reflections measured	20719	41845	36680
No. of unique reflections	20668	41838	36578
No. observations ($I > 2\sigma(I)$)	3501	6084	4630
R	0.0902	0.0488	0.0742
R_w	0.2448	0.1426	0.1756
GOF on F^2	1.083	1.019	1.181

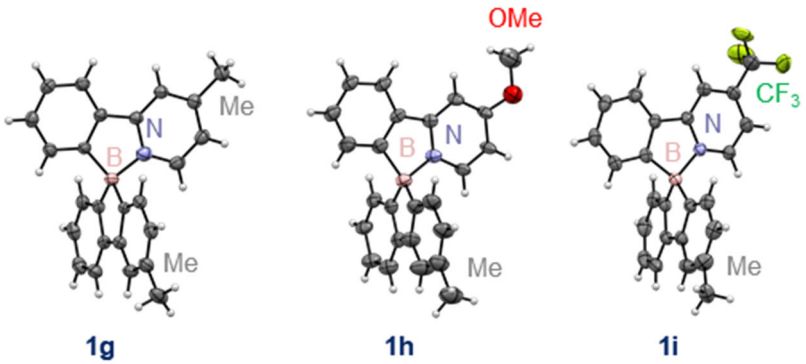

Figure S3. ORTEP drawing of **1g-1i**. Hydrogen atoms were omitted for clarity.

Table S5. Crystal data and structure refinement for **1g-1i**

Compound	**1g**	**1h**	**1i**
CCDC No.	2203031	2203033	2176259
Solvent system	Toluene / Hexane	Toluene / Hexane	Toluene / Hexane
Color	Colorless	Colorless	Colorless
Formula	$C_{25}H_{20}BN$	$C_{24}H_{18}BNO$	$C_{24}H_{15}BF_3N$
F_w	345.05	347.22	385.18
Crystal size /mm	0.05 x 0.05 x 0.05	0.03 x 0.02 x 0.02	0.02 x 0.02 x 0.0.2
Crystal system	monoclinic	monoclinic	monoclinic
Space group	$P2_1/c$ (No. 14)	$P2_1/c$ (No. 14)	$P2_1/c$ (No. 14)
a /Å	18.386(4)	12.1041(15)	9.1093(2)
b /Å	8.564(2)	8.6562(9)	9.3980(3)
c /Å	12.291(3)	36.508(4)	1.5279(5)
α /°	90	90	90
β /°	107.445(7)	92.703(4)	110.466(1)
γ /°	90	90	90
V /Å^3	1846.3(7)	3820.8(8)	1823.75(11)
Z	4	4	4
D_c /g cm^{-3}	1.241	1.253	1.403
No. of reflections measured	15534	41857	23835
No. of unique reflections	14991	40071	23000
No. observations ($I > 2\sigma(I)$)	2647	5249	3967
R	0.0623	0.0723	0.0742
R_w	0.1563	0.1943	0.0950
GOF on F^2	1.0590	1.0710	1.1810

4. First-order kinetic plots of racemization of 1a-i

A solution of [CD(+) $320_{CH_2Cl_2}$]-**1a-i** (3 mg) in DMSO (3 mL) was heated at the specific temperatures (25, 135, 140 and 145 ºC). At different intervals, an aliquot of the sample solution was transferred *via* syringe to another glassware to remove the solvent in *vacuo*, then the residue was dissolved into a solvent mixture of *n*-hexane, $CHCl_3$, and *i*-PrOH to be subjected to HPLC analysis. The %*ee* values were determined by the ratio of integration value calculated on an HPLC chart. The initial (t = 0 s) and certain (t /s) %*ee* were as in ee_0 and ee_t, respectively. The slope of first-order plots ($\ln(ee_0/ee_t)$ vs. t /s)) [10,11] gave the rate constant of racemization (k_{rac}). The activation parameters of the racemization reaction was determined by Eyring-Polanyi plots.[12]

Table S6. Summary and comparison of the kinetic parameter of **1a-i**.

	k_{rac} (145 ºC) 10^{-5} /s^{-1}	$\Delta G^{\ddagger}$ (145 ºC) /kcal·mol^{-1}	$\Delta H^{\ddagger}$ /kcal·mol^{-1}	$\Delta S^{\ddagger}$ /cal·mol^{-1}·K^{-1}
1a	5.76	33.4	28.4	-12.0
1b	11.3	32.9	29.6	-7.80
1c	0.984	34.9	33.9	-2.40
1d	4.00	33.7	26.8	-16.6
1e	4.04	33.7	31.6	-5.00
1f	1.84	34.4	27.1	-17.4
1g	2.70	33.4	28.4	-12.0
1h	1.77	34.4	30.7	-8.90
1i	114	31.0	23.5	-17.8

Table S7. Kinetic profile of racemization of **1a** by HPLC charts at 135 °C.

***t* (s)**	***ee* (%)**	**ln(ee_0/ee_t)**
0	100	0
3600	90.7	0.09778925
7200	84.1	0.173449034
10800	76.7	0.265633603
14400	70.3	0.35234149
18000	64.3	0.441237374

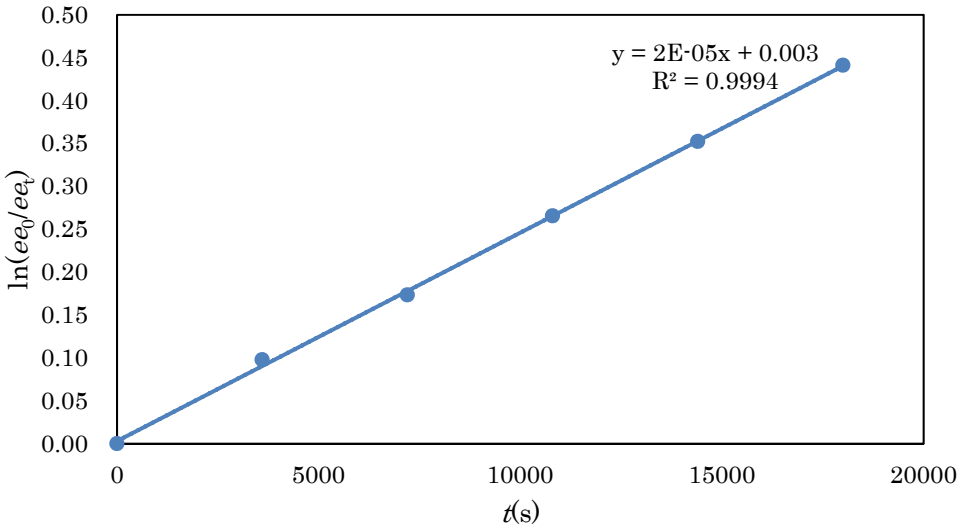

Figure S4. The plot of ln(ee_0/ee_t) vs time of **1a** at 135 °C.

$k_{racemization}$ (135 °C) = 2.43×10^{-5}

$k_{enantiomerization}$ (135 °C) = 1.22×10^{-5}

$\Delta G^{\neq}_{enantiomerization}$ (135 °C) = 33.3 ± 0.2 kcal/mol

Table S8. Kinetic profile of racemization of **1a** by HPLC charts at 140 °C.

***t* (s)**	***ee* (%)**	**ln(ee_0/ee_t)**
0	100	0
3600	87.5	0.133165745
7200	75.8	0.277652537
10800	65.8	0.418155289
14400	57.1	0.560015868
18000	50.2	0.688637365

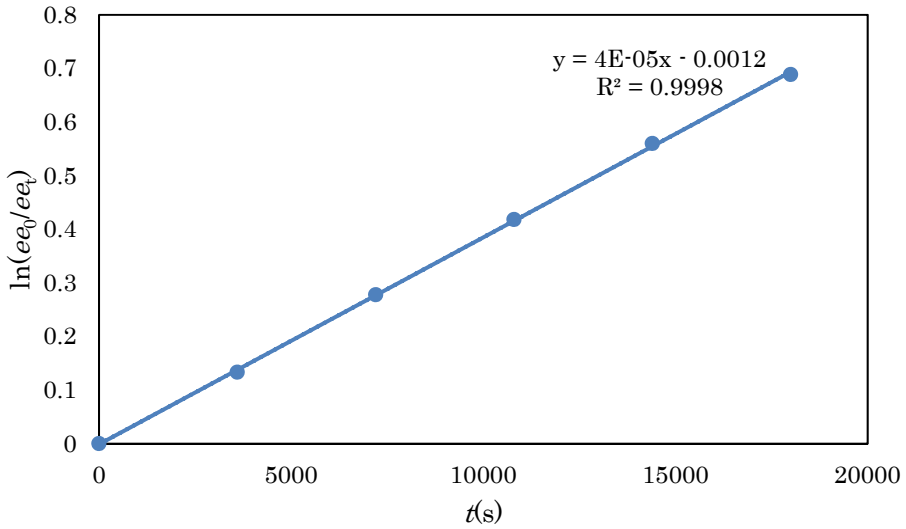

Figure S5. The plot of ln(ee_0/ee_t) vs time of **1a** at 140 °C.

$k_{racemization}$ (140 °C) = 3.86×10^{-5}

$k_{enantiomerization}$ (140 °C) = 1.93×10^{-5}

$\Delta G^{\neq}_{enantiomerization}$ (140 °C) = 33.4 ± 0.2 kcal/mol

Table S9. Kinetic profile of racemization of **1a** by HPLC charts at 145 °C.

***t* (s)**	***ee* (%)**	**ln(ee_0/ee_t)**
0	100	0
3600	80.3	0.219699489
7200	65.8	0.417973007
10800	53.3	0.629233855
14400	43.5	0.831949583
18000	35.3	1.0408907

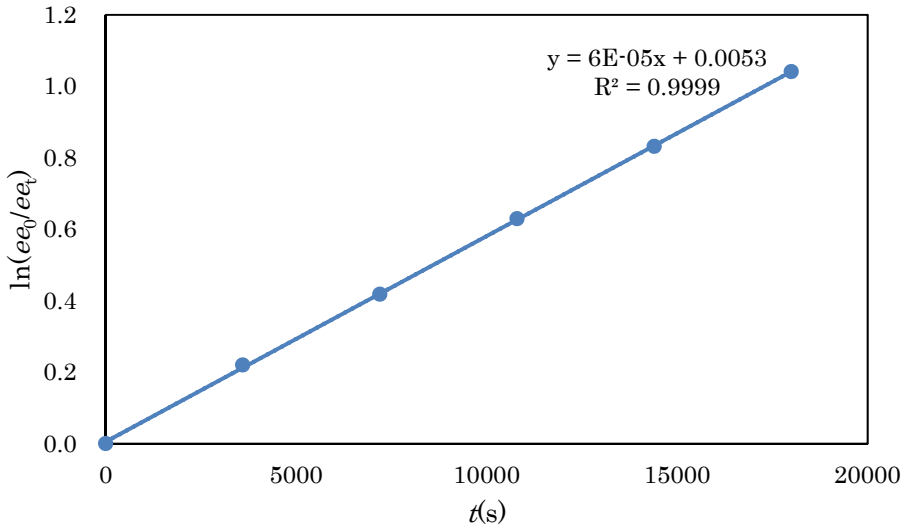

Figure S6. The plot of ln(ee_0/ee_t) vs time of **1a** at 145 °C.

$k_{racemization}$ (145 °C) = 5.76×10^{-5}

$k_{enantiomerization}$ (145 °C) = 2.88×10^{-5}

$\Delta G^{\neq}_{enantiomerization}$ (145 °C) = 33.4 ± 0.2 kcal/mol

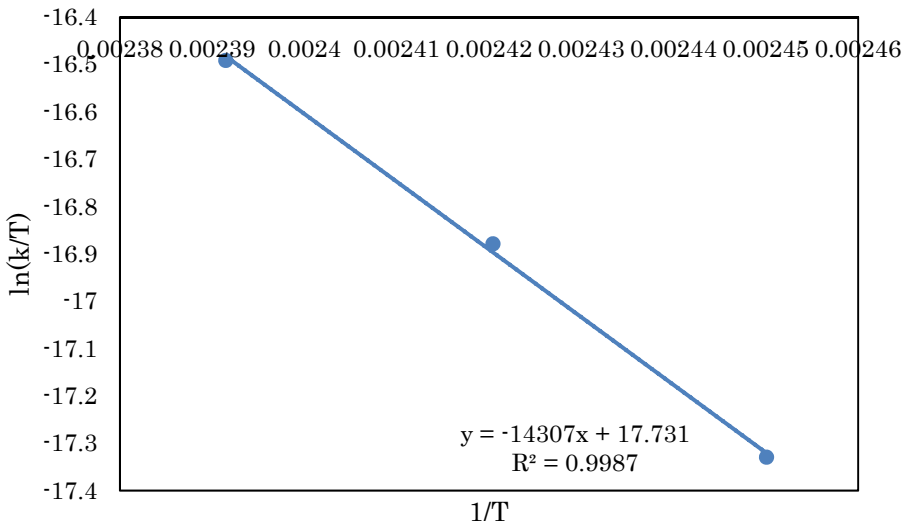

Figure S7. Eyring-Polanyi plots of **1a.**

$\Delta H^{\neq}_{\text{enantiomerization}}$ = 28.4 ± 0.1 kcal/mol

$\Delta S^{\neq}_{\text{enantiomerization}}$ = -12.0 ± 0.3 cal/mol·K

Table S10. Kinetic profile of racemization of **1b** by HPLC charts at 135 ºC.

***t* (s)**	***ee* (%)**	**ln(ee_0/ee_t)**
0	100	0
3600	85.3	0.158667532
7200	72.1	0.327116142
10800	61.0	0.49423075
14400	51.3	0.667284521
18000	43.9	0.822663786

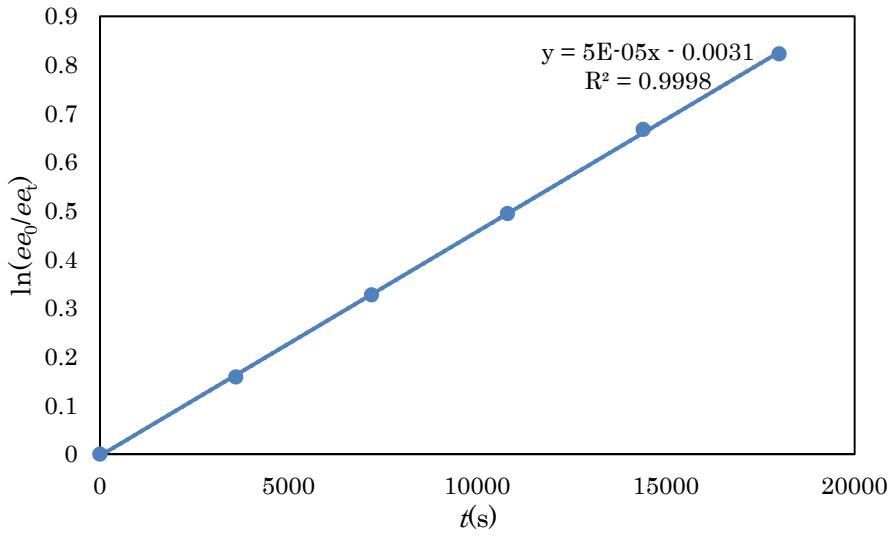

Figure S9. The plot of ln(ee_0/ee_t) vs time of **1b** at 135 ºC.

$k_{racemization}$ (135 ºC) = 4.61×10^{-5}

$k_{enantiomerization}$ (135 ºC) = 2.30×10^{-5}

$\Delta G^{\neq}_{enantiomerization}$ (135 ºC) = 32.81 ± 0.06 kcal/mol

Table S11. Kinetic profile of racemization of **1b** by HPLC charts at 140 °C.

***t* (s)**	***ee* (%)**	**ln(ee_0/ee_t)**
0	100	0
3600	76.3	0.270471036
7200	58.4	0.538162563
10800	45.6	0.78478013
14400	35.3	1.042250859
18000	27.2	1.300190062

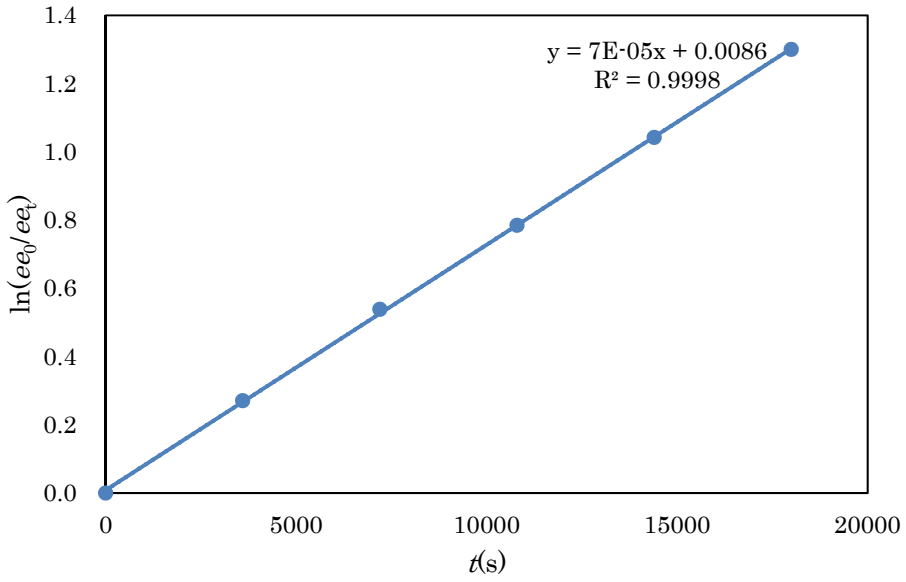

Figure S10. The plot of ln(ee_0/ee_t) vs time of **1b** at 140 °C.

$k_{racemization}$ (140 °C) = 7.19×10^{-5}

$k_{enantiomerization}$ (140 °C) = 3.60×10^{-5}

$\Delta G^{\neq}_{enantiomerization}$ (140 °C) = 32.85 ± 0.06 kcal/mol

Table S12. Kinetic profile of racemization of **1b** by HPLC charts at 145 °C.

***t* (s)**	***ee* (%)**	**ln(ee_0/ee_t)**
0	100	0
3600	65.5	0.423792025
7200	43.5	0.832455226
10800	29.4	1.225809499
14400	19.5	1.634345548

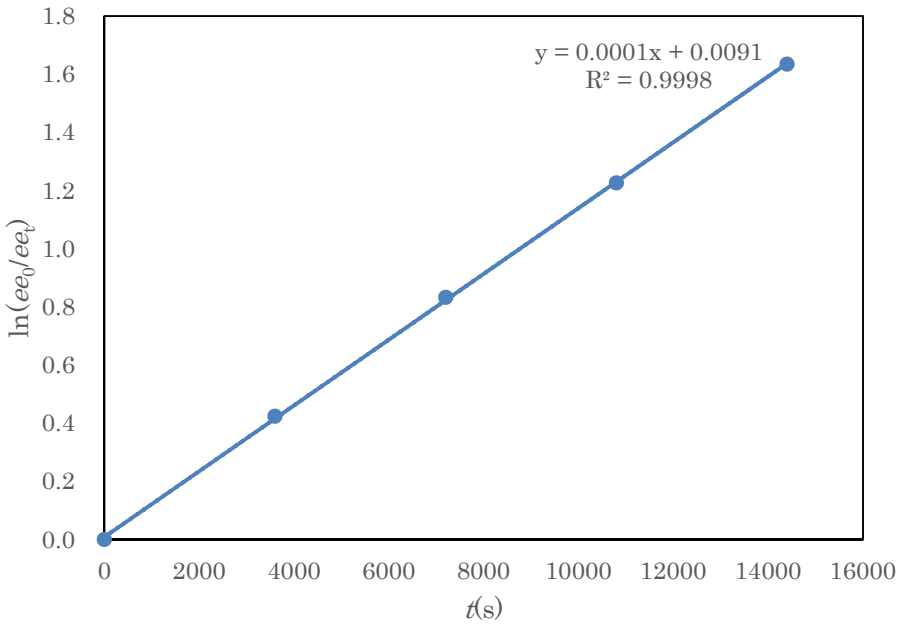

Figure S7. The plot of ln(ee_0/ee_t) vs time of **1b** at 145 °C.

$k_{racemization}$ (145 °C) = 1.13×10^{-4}

$k_{enantiomerization}$ (145 °C) = 5.65×10^{-5}

$\Delta G^{\neq}_{enantiomerization}$ (145 °C) = 32.9 ± 0.06 kcal/mol

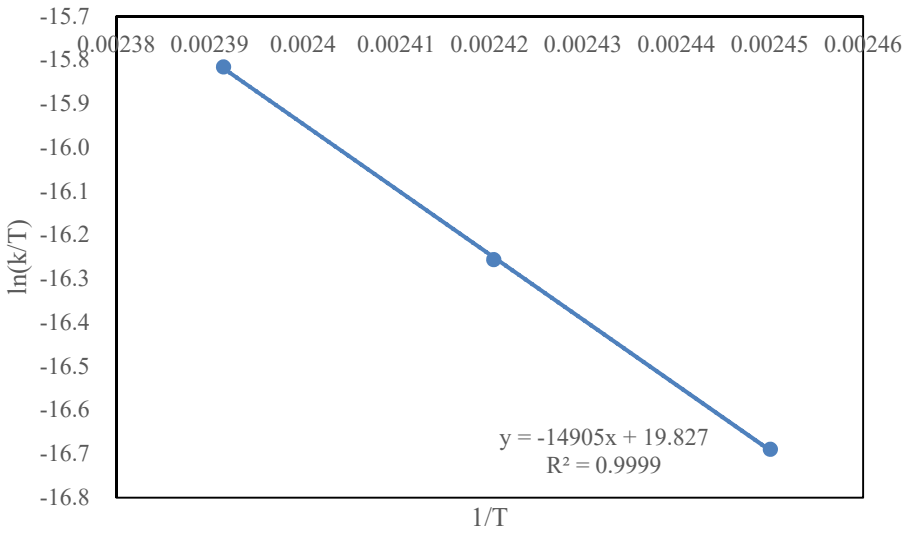

Figure S8. Eyring-Polanyi plots of **1b**.

$\Delta H^{\neq}_{\text{enantiomerization}}$ = 29.62 ± 0.04 kcal/mol

$\Delta S^{\neq}_{\text{enantiomerization}}$ = -7.8 ± 0.1 cal/mol·K

Table S13. Kinetic profile of racemization of **1c** by HPLC charts at 135 °C.

***t* (s)**	***ee* (%)**	**ln(ee_0/ee_t)**
0	100	0
3600	98.5	0.015397942
7200	97.0	0.030459207
10800	95.9	0.041843349
14400	94.8	0.053358584
18000	93.8	0.06400533

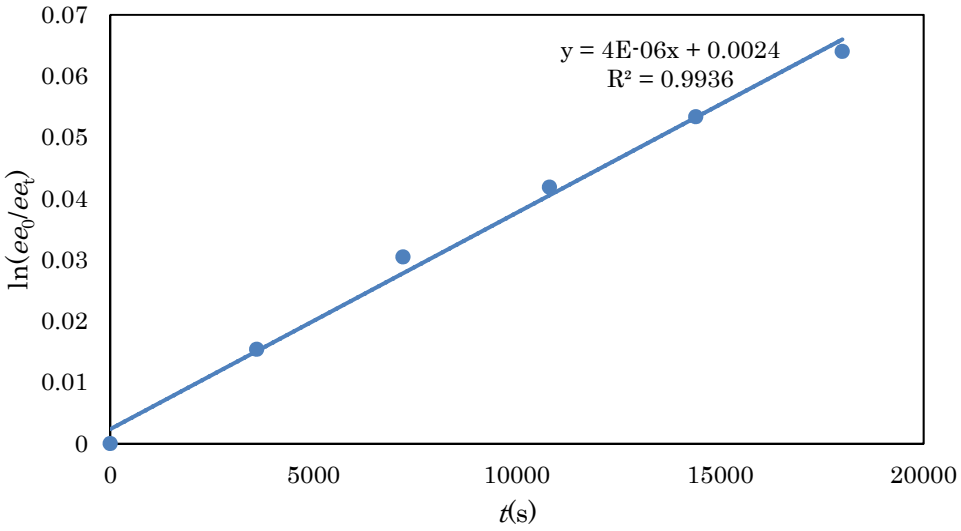

Figure S9. The plot of ln(ee_0/ee_t) vs time of **1c** at 135 °C.

$k_{racemization}$ (135 °C) = 3.53×10^{-6}

$k_{enantiomerization}$ (135 °C) = 1.77×10^{-6}

$\Delta G^{\neq}_{enantiomerization}$ (135 °C) = 34.9 ± 0.2 kcal/mol

Table S14. Kinetic profile of racemization of **1c** by HPLC charts at 140 °C.

***t* (s)**	***ee* (%)**	**ln(ee_0/ee_t)**
0	100	0
7200	95.7	0.044223607
10800	93.7	0.065605757
14400	91.4	0.089574659
18000	89.7	0.108610235

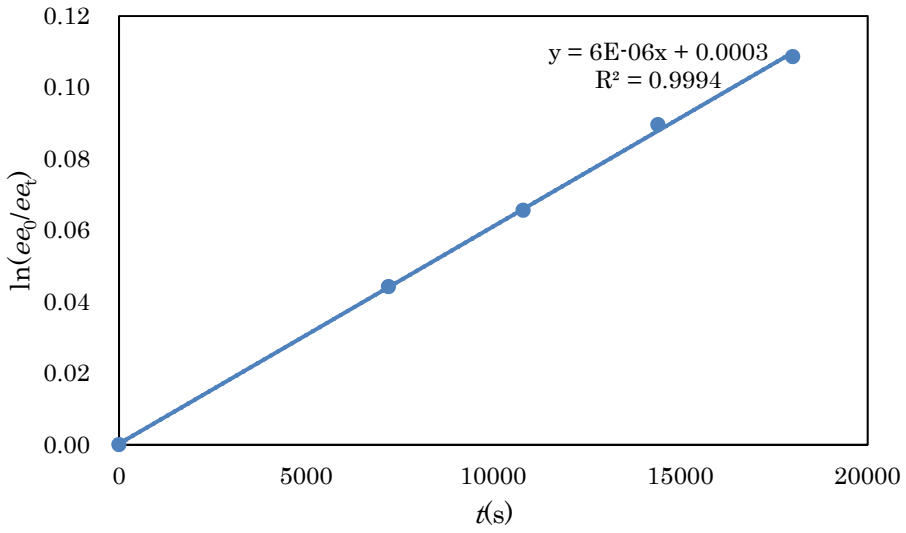

Figure S10. The plot of ln(ee_0/ee_t) vs time of **1c** at 140 °C**.**

$k_{racemization}$ (140 °C) = 6.08 × 10^{-6}

$k_{enantiomerization}$ (140 °C) = 3.04 × 10^{-6}

$\Delta G^{\neq}_{enantiomerization}$ (140 °C) = 34.9 ± 0.2 kcal/mol

Table S15. Kinetic profile of racemization of **1c** by HPLC charts at 145 °C.

***t* (s)**	***ee* (%)**	**ln(ee_0/ee_t)**
0	100	0
3600	95.7	0.043513112
7200	91.6	0.08771708
10800	89.2	0.11449096
14400	86.4	0.14588163
18000	83.4	0.181114286

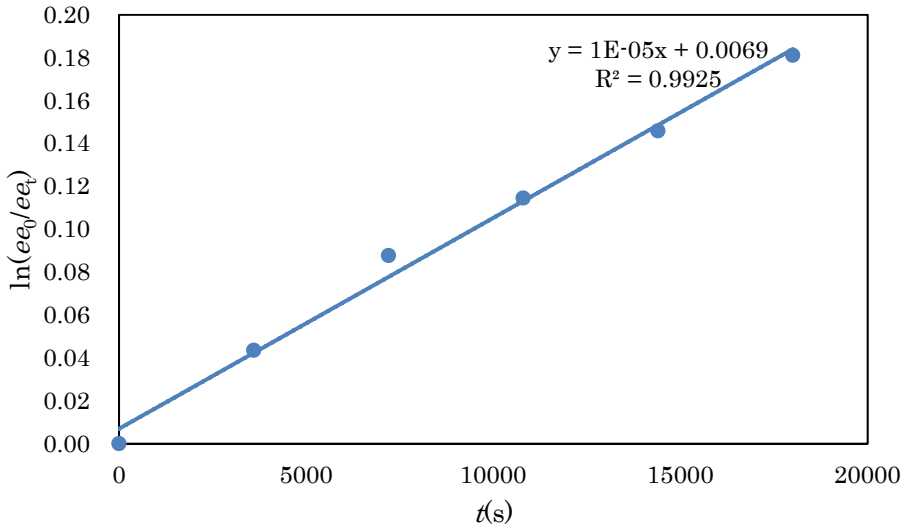

Figure S11. The plot of ln(ee_0/ee_t) vs time of **1c** at 145 °C.

$k_{racemization}$ (145 °C) = 9.84 × 10^{-6}

$k_{enantiomerization}$ (145 °C) = 4.92 × 10^{-6}

$\Delta G^{\neq}_{enantiomerization}$ (145 °C) = 34.9 ± 0.2 kcal/mol

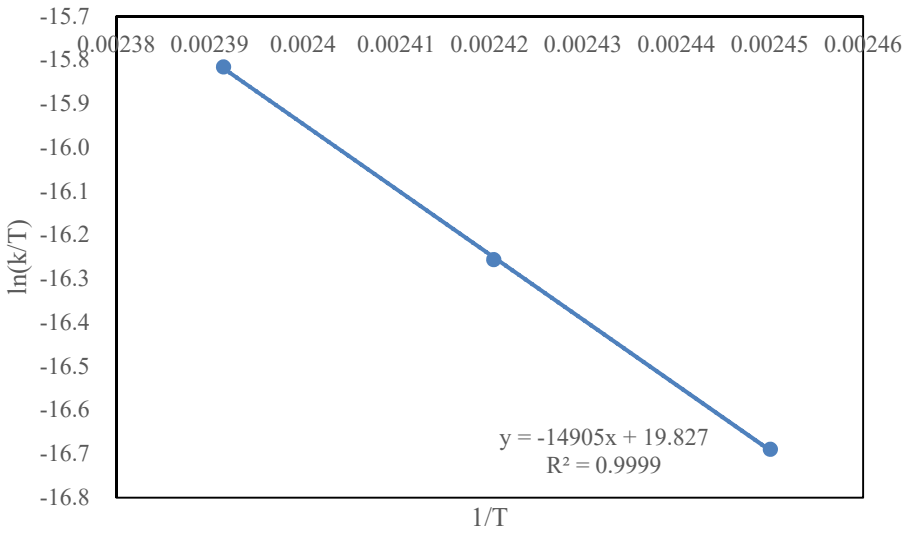

Figure S12. Eyring-Polanyi plots of **1c**.

$\Delta H^{\neq}_{\text{enantiomerization}}$ = 33.9 ± 0.2 kcal/mol

$\Delta S^{\neq}_{\text{enantiomerization}}$ = -2.4 ± 0.3 cal/mol·K

Table S16. Kinetic profile of racemization of **1d** by HPLC charts at 135 °C.

***t* (s)**	***ee* (%)**	**ln(ee_0/ee_t)**
0	100	0
3600	93.2	0.070916148
7200	86.4	0.145789069
10800	81.8	0.20035519
14400	77.1	0.259937212
18000	72.4	0.322881017

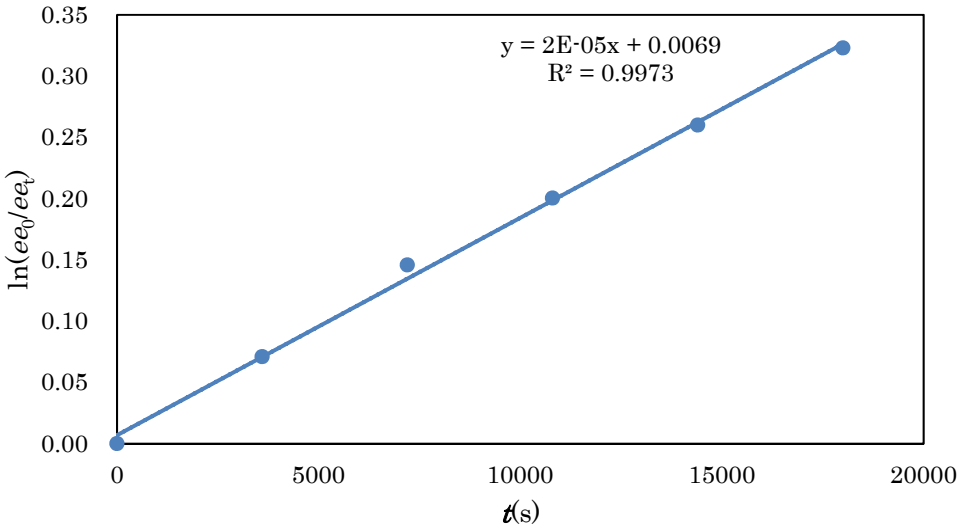

Figure S13. The plot of ln(ee_0/ee_t) vs time of **1d** at 135 °C.

$k_{racemization}$ (135 °C) = 1.77×10^{-5}

$k_{enantiomerization}$ (135 °C) = 8.87×10^{-6}

$\Delta G^{\neq}_{enantiomerization}$ (135 °C) = 33.60 ± 0.2 kcal/mol

Table S17. Kinetic profile of racemization of **1d** by HPLC charts at 140 °C.

***t* (s)**	***ee* (%)**	**ln(ee_0/ee_t)**
0	100	0
3600	90.6	0.098715973
7200	82.2	0.195990553
10800	74.9	0.288615842
14400	68.0	0.384956847
18000	62.8	0.464451073

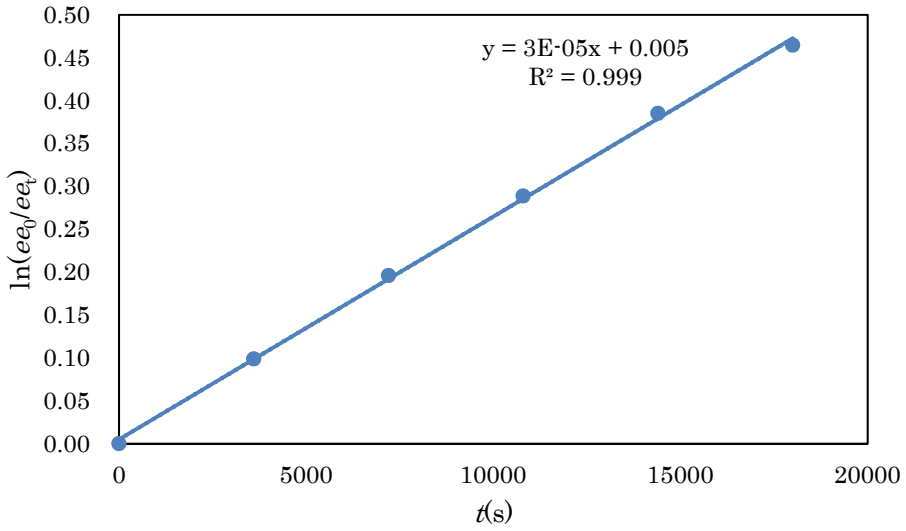

Figure S14. The plot of ln(ee_0/ee_t) vs time of **1d** at 140 °C.

$k_{racemization}$ (140 °C) = 2.60×10^{-5}

$k_{enantiomerization}$ (140 °C) = 1.30×10^{-5}

$\Delta G^{\neq}_{enantiomerization}$ (140 °C) = 33.7 ± 0.2 kcal/mol

Table S18. Kinetic profile of racemization of **1d** by HPLC charts at 145 °C.

***t* (s)**	***ee* (%)**	**ln(ee_0/ee_t)**
0	100	0
3600	83.6	0.178552668
7200	74.5	0.294639553
10800	63.9	0.447944726
14400	55.6	0.587526699
18000	48.0	0.733802522

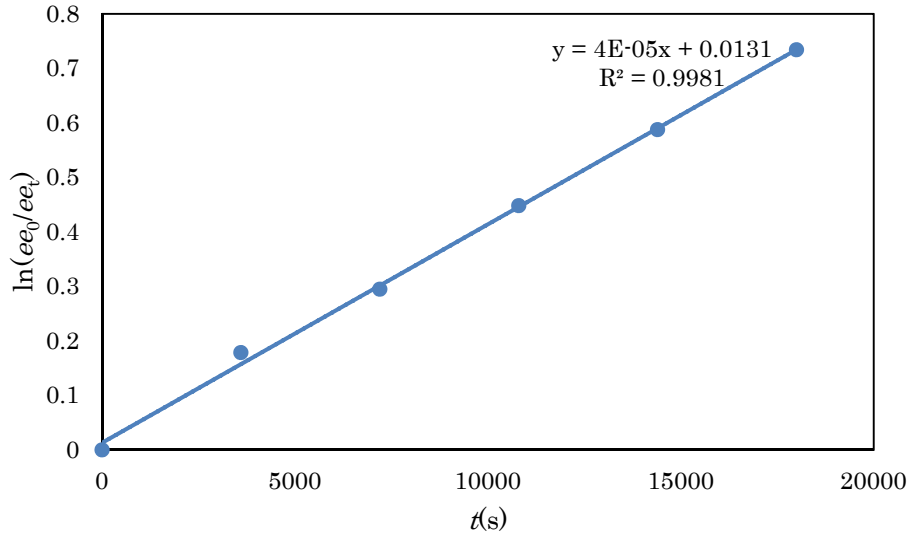

Figure S15. The plot of ln(ee_0/ee_t) vs time of **1d** at 145 °C.

$k_{racemization}$ (145 °C) = 4.00×10^{-5}

$k_{enantiomerization}$ (145 °C) = 2.00×10^{-5}

$\Delta G^{\neq}_{enantiomerization}$ (145 °C) = 33.8 ± 0.2 kcal/mol

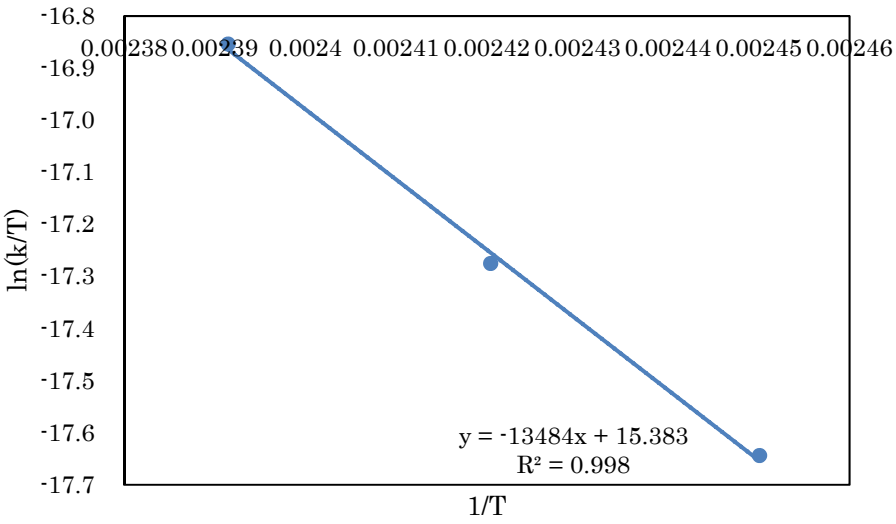

Figure S16. Eyring-Polanyi plots of **1d**.

$\Delta H^{\neq}_{\text{enantiomerization}}$ = 26.8 ± 0.1 kcal/mol

$\Delta S^{\neq}_{\text{enantiomerization}}$ = -16.6 ± 0.4 cal/mol·K

Table S19. Kinetic profile of racemization of **1e** by HPLC charts at 135 °C.

***t* (s)**	***ee* (%)**	**ln(ee_0/ee_t)**
0	98.0	0
3600	93.3	0.048773834
10800	83.1	0.165159313
14400	78.0	0.227629183
18000	74.6	0.273145205

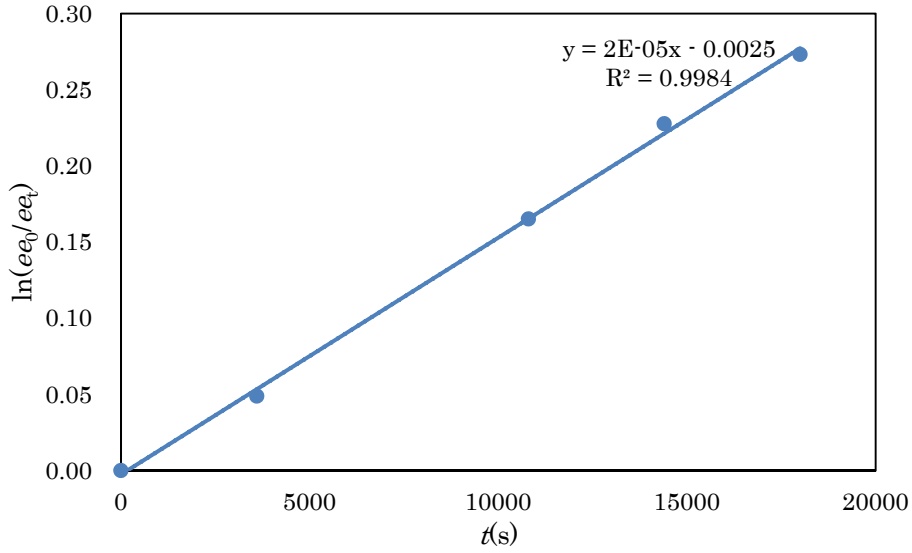

Figure S17. The plot of ln(ee_0/ee_t) vs time of **1e** at 135 °C.

$k_{racemization}$ (135 °C) = 1.55×10^{-5}

$k_{enantiomerization}$ (135 °C) = 7.77×10^{-6}

$\Delta G^{\neq}_{enantiomerization}$ (135 °C) = 33.7 ± 0.2 kcal/mol

Table S20. Kinetic profile of racemization of **1e** by HPLC charts at 140 °C.

***t* (s)**	***ee* (%)**	**ln(ee_0/ee_t)**
0	97.976	0
3600	89.73	0.087917389
7200	82.334	0.173938406
14400	66.598	0.386048004
18000	61.89	0.459363935

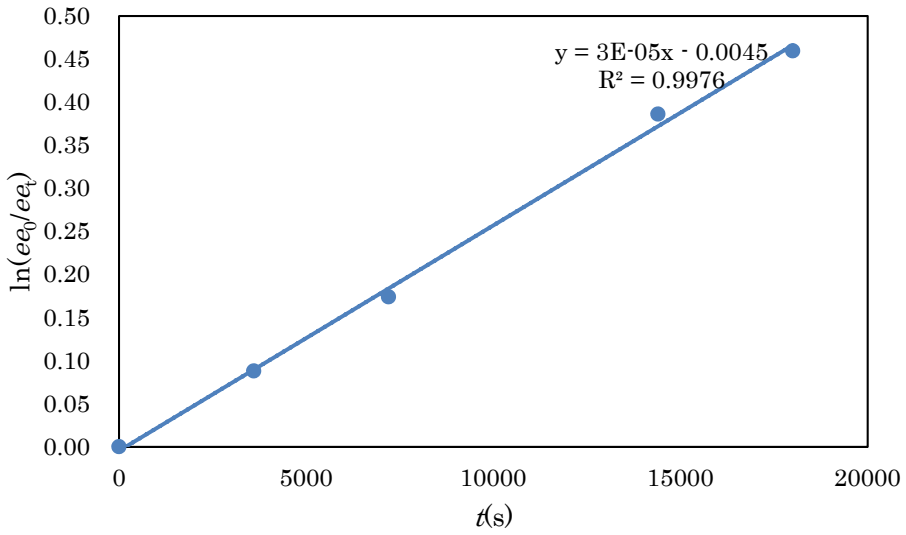

Figure S18. The plot of ln(ee_0/ee_t) vs time of **1e** at 140 °C.

$k_{racemization}$ (140 °C) = 2.62×10^{-5}

$k_{enantiomerization}$ (140 °C) = 1.31×10^{-5}

$\Delta G^{\neq}_{enantiomerization}$ (140 °C) = 33.7 ± 0.2 kcal/mol

Table S21. Kinetic profile of racemization of **1e** by HPLC charts at 145 °C.

***t* (s)**	***ee* (%)**	**ln(ee_0/ee_t)**
0	97.98	0
3600	86.28	0.12707837
10800	63.60	0.432171975
14400	55.92	0.560800453
18000	47.26	0.728973644

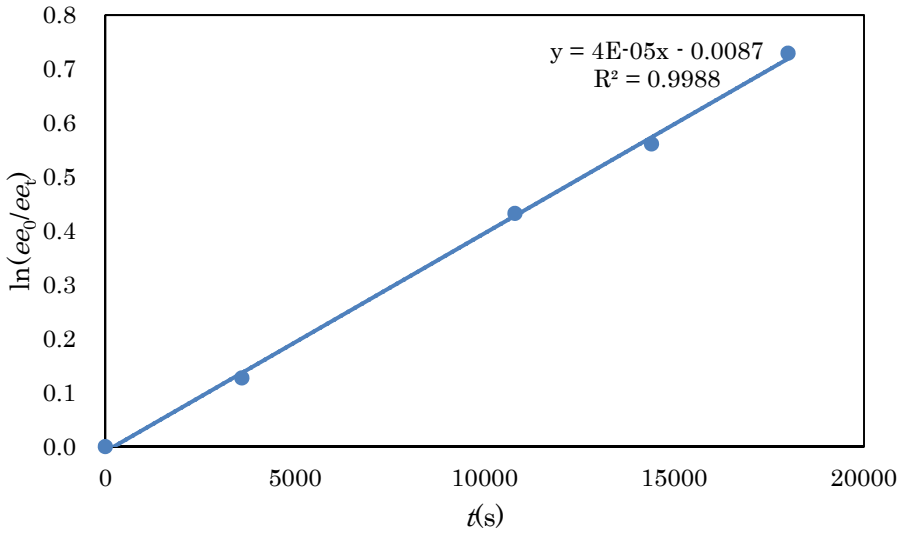

Figure S19. The plot of ln(ee_0/ee_t) vs time of **1e** at 145 °C.

$k_{racemization}$ (145 °C) = 4.04×10^{-5}

$k_{enantiomerization}$ (145 °C) = 2.02×10^{-5}

$\Delta G^{\neq}_{enantiomerization}$ (145 °C) = 33.7 ± 0.2 kcal/mol

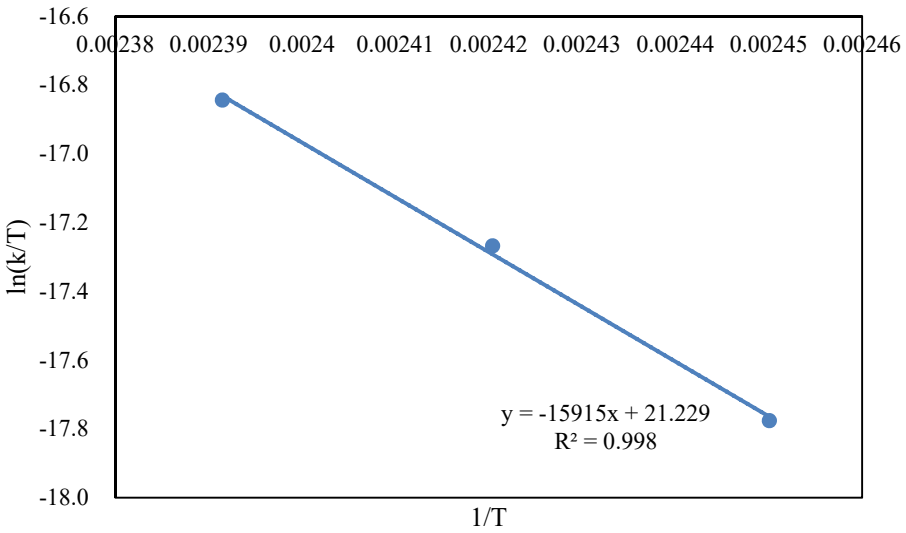

Figure S20. Eyring-Polanyi plots of **1e**.

$\Delta H^{\neq}_{\text{enantiomerization}}$ = 31.6 ± 0.2 kcal/mol

$\Delta S^{\neq}_{\text{enantiomerization}}$ = -5.0 ± 0.4 cal/mol·K

Table S22. Kinetic profile of racemization of **1f** by HPLC charts at 135 °C.

***t* (s)**	***ee* (%)**	**ln(ee_0/ee_t)**
0	100	**0**
3600	97.2	**0.028399475**
7200	95.352	**0.047594879**
10800	91.448	**0.089399681**
14400	88.986	**0.116691132**
18000	86.756	**0.142070605**

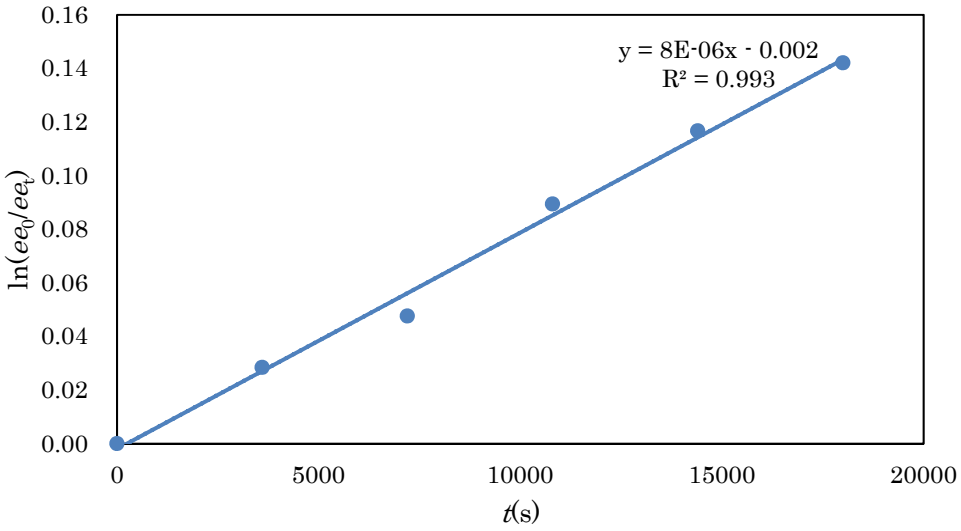

Figure S21. The plot of ln(ee_0/ee_t) vs time of **1f** at 135 °C.

$k_{racemization}$ (135 °C) = 8.07 × 10^{-6}

$k_{enantiomerization}$ (135 °C) = 4.04 × 10^{-6}

$\Delta G^{\neq}_{enantiomerization}$ (135 °C) = 34.21 ± 0.09 kcal/mol

Table S23. Kinetic profile of racemization of **1f** by HPLC charts at 140 °C.

***t* (s)**	***ee* (%)**	**ln(ee_0/ee_t)**
0	100	0
3600	95.7	0.044349041
7200	91.3	0.09121657
10800	87.1	0.137631214
14400	83.8	0.176689447
18000	79.9	0.224043957

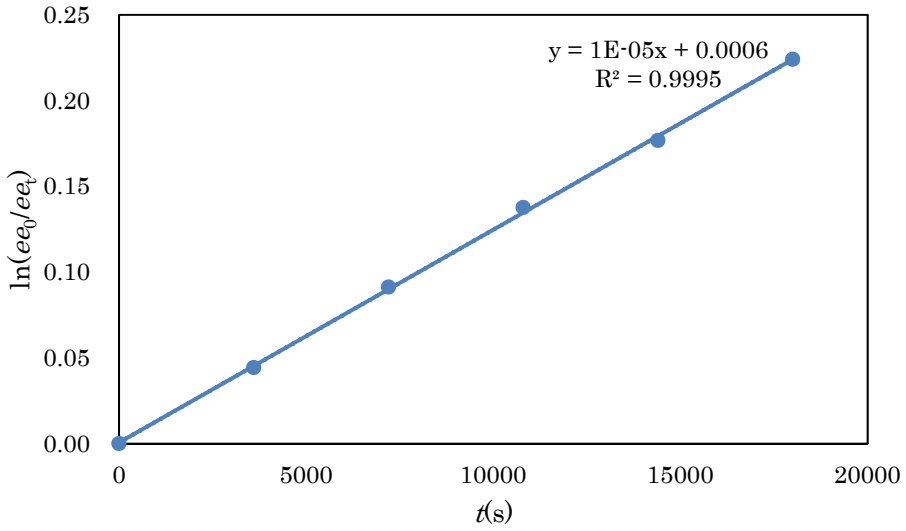

Figure S22. The plot of ln(ee_0/ee_t) vs time of **1f** at 140 °C.

$k_{racemization}$ (140 °C) = 1.24×10^{-5}

$k_{enantiomerization}$ (140 °C) = 6.20×10^{-6}

$\Delta G^{\neq}_{enantiomerization}$ (140 °C) = 34.30 ± 0.09 kcal/mol

Table S24. Kinetic profile of racemization of **1f** by HPLC charts at 145 °C..

***t* (s)**	***ee* (%)**	**ln(ee_0/ee_t)**
0	100	0
3600	92.2	0.081709095
7200	86.9	0.139905953
10800	81.9	0.200013134
14400	76.4	0.269449304
18000	71.3	0.338975367

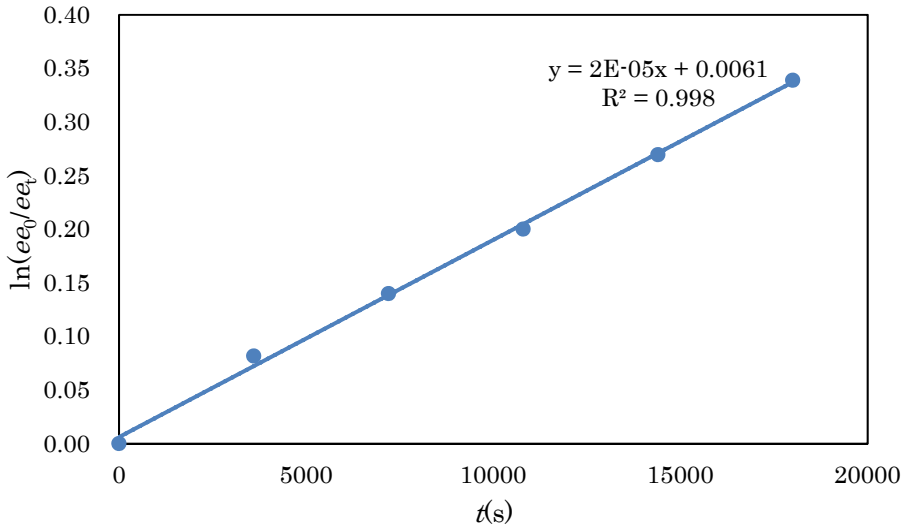

Figure S23. The plot of ln(ee_0/ee_t) vs time of **1f** at 145 °C.

$k_{racemization}$ (145 °C) = 1.84×10^{-5}

$k_{enantiomerization}$ (145 °C) = 9.20×10^{-6}

$\Delta G^{\neq}_{enantiomerization}$ (145 °C) = 34.39 ± 0.09 kcal/mol

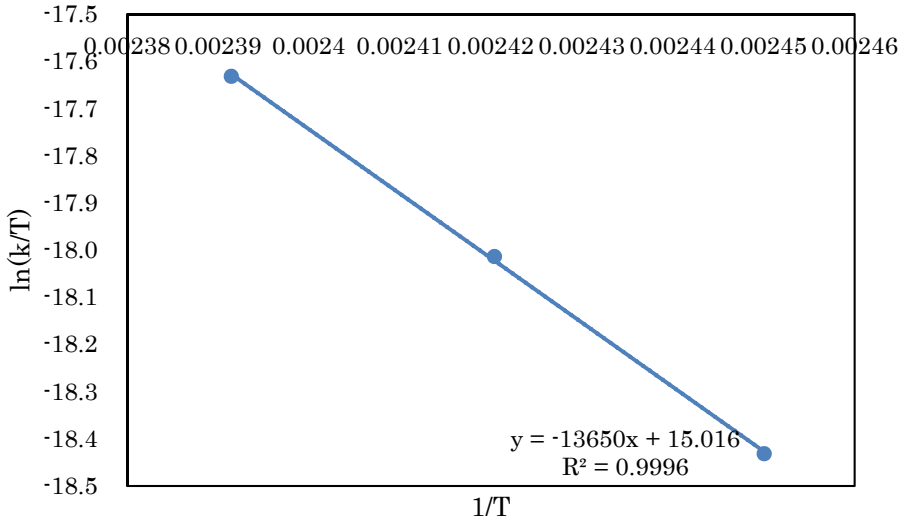

Figure S24. Eyring-Polanyi plots of **1f**.

$\Delta H^{\neq}_{\text{enantiomerization}}$ = 27.12 ± 0.6 kcal/mol

$\Delta S^{\neq}_{\text{enantiomerization}}$ = -17.4 ± 0.2 cal/mol·K

Table S25. Kinetic profile of racemization of **1g** by HPLC charts at 135 °C.

***t* (s)**	***ee* (%)**	**ln(ee_0/ee_t)**
0	100	0
3600	96.4	0.036892226
7200	91.7	0.087105927
10800	88.4	0.123660273
14400	84.6	0.16685774
18000	81.8	0.200819595

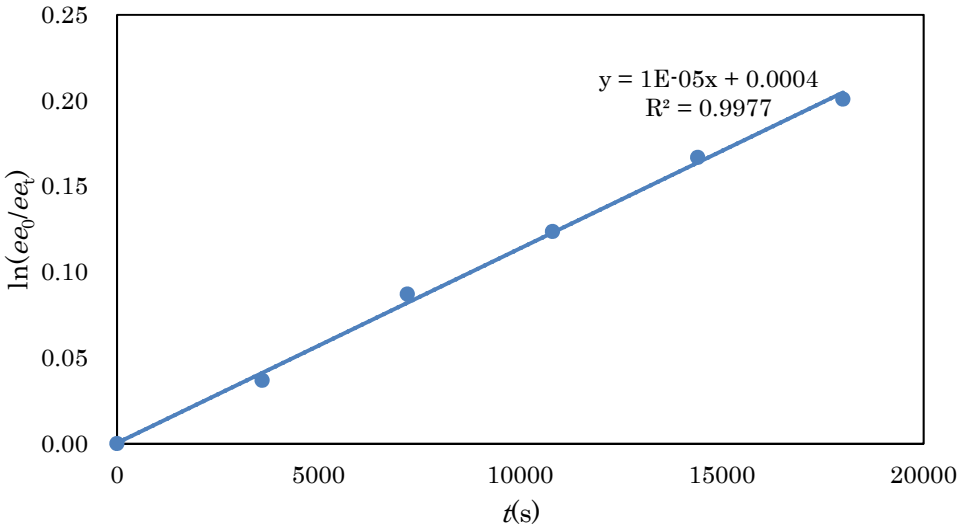

Figure S25. The plot of ln(ee_0/ee_t) vs time of **1g** at 135 °C.

$k_{racemization}$ (135 °C) = 1.14×10^{-6}

$k_{enantiomerization}$ (135 °C) = 6.68×10^{-6}

$\Delta G^{\neq}_{enantiomerization}$ (135 °C) = 34.1 ± 0.2 kcal/mol

Table S26. Kinetic profile of racemization of **1g** by HPLC charts at 140 °C.

***t* (s)**	***ee* (%)**	**ln(ee_0/ee_t)**
0	100	0
3600	94.1	0.060599622
7200	88.6	0.121241509
10800	83.2	0.183370106
14400	78.6	0.240671268
18000	73.4	0.30911002

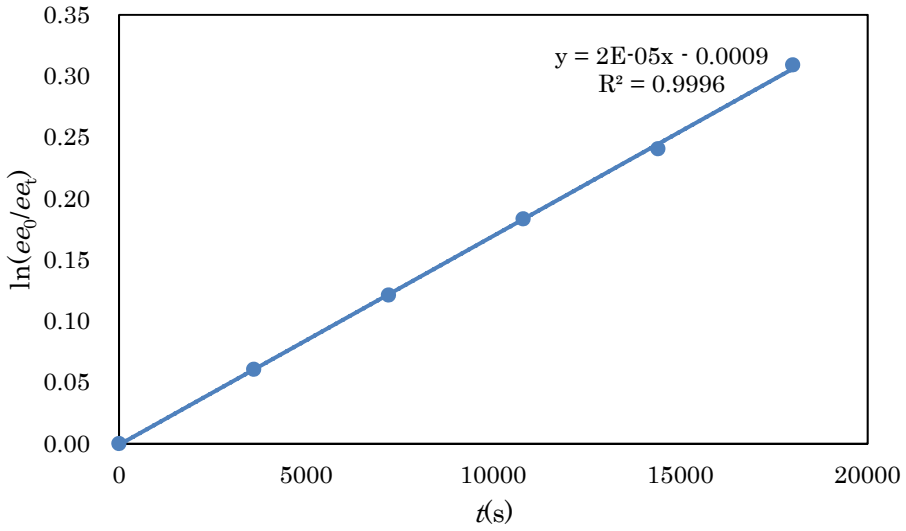

Figure S26. The plot of ln(ee_0/ee_t) vs time of **1g** at 140 °C.

$k_{racemization}$ (140 °C) = 1.70×10^{-5}

$k_{enantiomerization}$ (140 °C) = 8.52×10^{-6}

$\Delta G^{\neq}_{enantiomerization}$ (140 °C) = 34.0 ± 0.2 kcal/mol

Table S27. Kinetic profile of racemization of **1g** by HPLC charts at 145 °C.

***t* (s)**	***ee* (%)**	**ln(ee_0/ee_t)**
0	100	0
3600	90.3	0.102564428
7200	81.7	0.202287557
10800	74.6	0.293244179
14400	67.6	0.392213302
18000	61.4	0.488542416

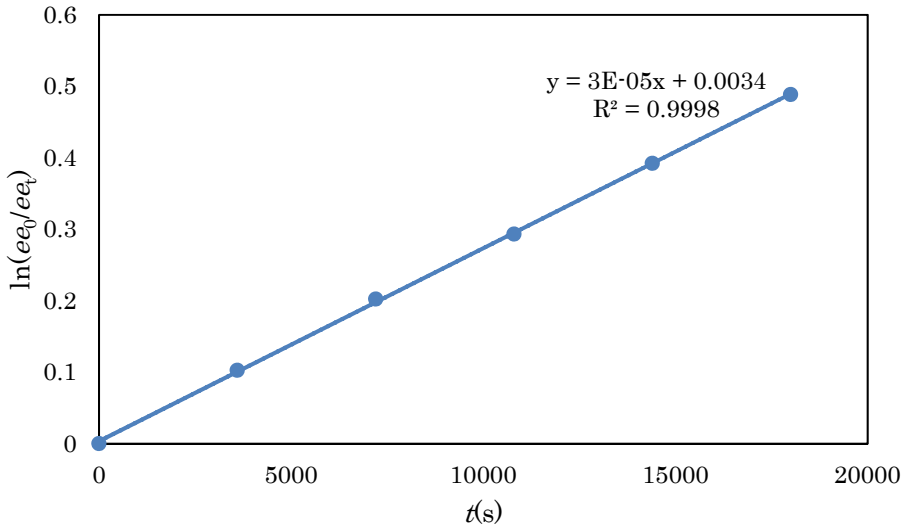

Figure S27. The plot of ln(ee_0/ee_t) vs time of **1g** at 145 °C.

$k_{racemization}$ (145 °C) = 2.70×10^{-5}

$k_{enantiomerization}$ (145 °C) = 1.35×10^{-6}

$\Delta G^{\neq}_{enantiomerization}$ (145 °C) = 34.1 ± 0.2 kcal/mol

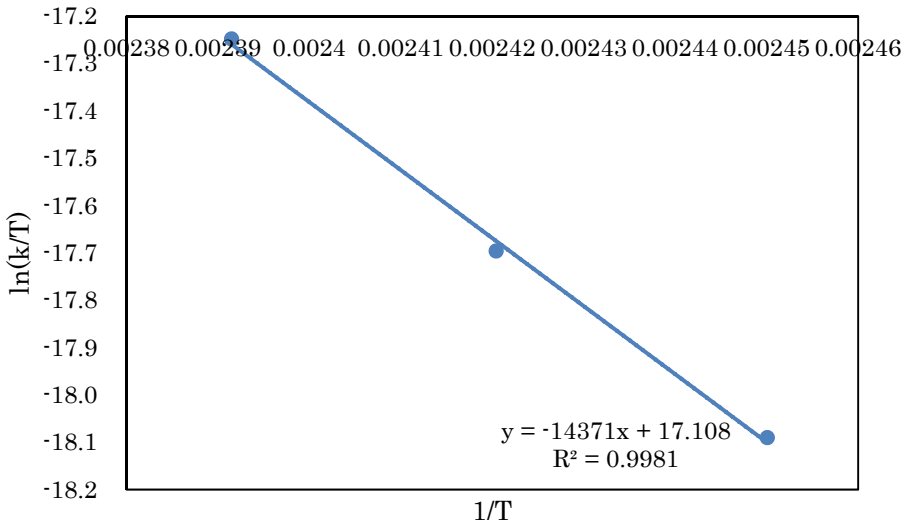

Figure S28. Eyring-Polanyi plots of **1g**.

$\Delta H^{\neq}_{\text{enantiomerization}}$ = 28.4 ± 0.1 kcal/mol

$\Delta S^{\neq}_{\text{enantiomerization}}$ = -12.0 ± 0.3 cal/mol·K

Table S28. Kinetic profile of racemization of **1h** by HPLC charts at 135 °C.

***t* (s)**	***ee* (%)**	**ln(ee_0/ee_t)**
0	100	0
3600	97.6	0.02388294
10800	94.8	0.05337968
14400	90.4	0.101058671
18000	88.2	0.125563223

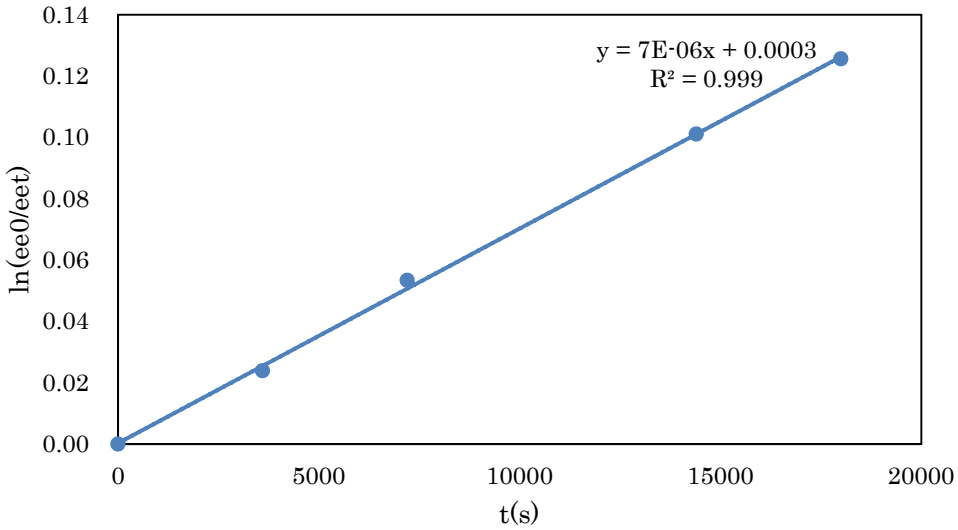

Figure S29. The plot of ln(ee_0/ee_t) vs time of **1g** at 135 °C.

$k_{racemization}$ (135 °C) = 7.00×10^{-6}

$k_{enantiomerization}$ (135 °C) = 3.50×10^{-6}

$\Delta G^{\neq}_{enantiomerization}$ (135 °C) = 34.3 ± 0.5 kcal/mol

Table S29. Kinetic profile of racemization of **1h** by HPLC charts at 140 °C.

***t* (s)**	***ee* (%)**	**ln(ee_0/ee_t)**
0	100	0
3600	97.6	0.048182349
7200	96.0	0.084316829
10800	94.4	0.118963732
14400	92.6	0.160192227
18000	91.4	0.188645511

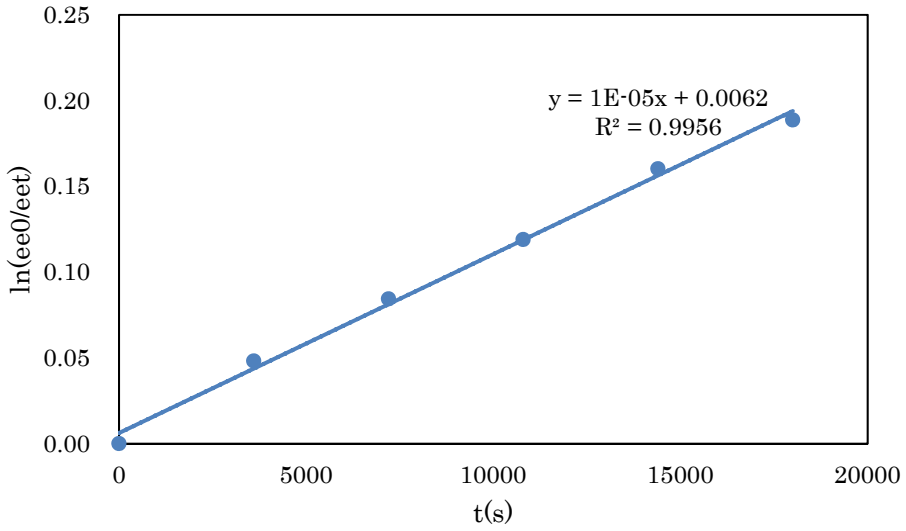

Figure S30. The plot of ln(ee_0/ee_t) vs time of **1h** at 140 °C.

$k_{racemization}$ (140 °C) = 1.04×10^{-5}

$k_{enantiomerization}$ (140 °C) = 5.21×10^{-6}

$\Delta G^{\neq}_{enantiomerization}$ (140 °C) = 34.4 ± 0.5 kcal/mol

Table S30. Kinetic profile of racemization of **1h** by HPLC charts at 145 °C.

***t* (s)**	***ee* (%)**	**ln(ee_0/ee_t)**
0	100	0
3600	93.0	0.072420167
7200	86.9	0.140458185
10800	81.6	0.203316415
14400	77.0	0.260897341
18000	72.5	0.321583624

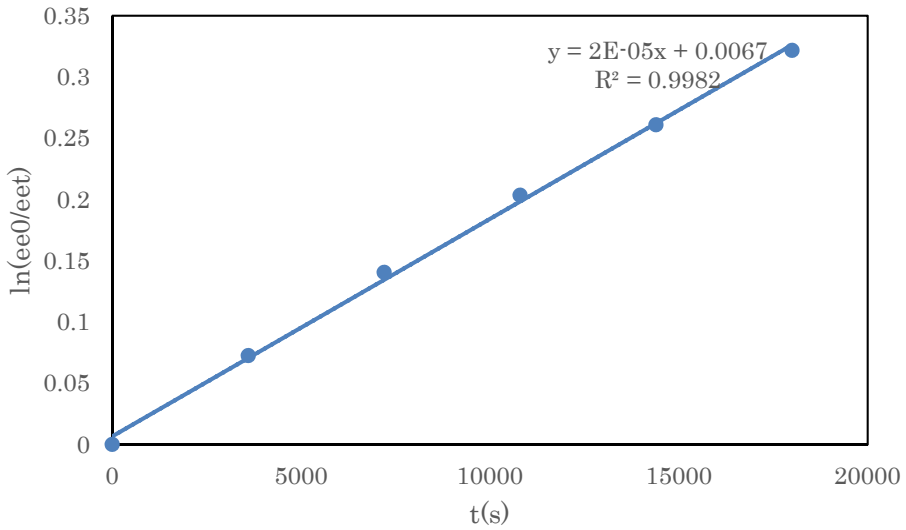

Figure S31. The plot of ln(ee_0/ee_t) vs time of **1h** at 145 °C.

$k_{racemization}$ (145 °C) = 1.77×10^{-5}

$k_{enantiomerization}$ (145 °C) = 8.87×10^{-6}

$\Delta G^{\neq}_{enantiomerization}$ (145 °C) = 34.4 ± 0.5 kcal/mol

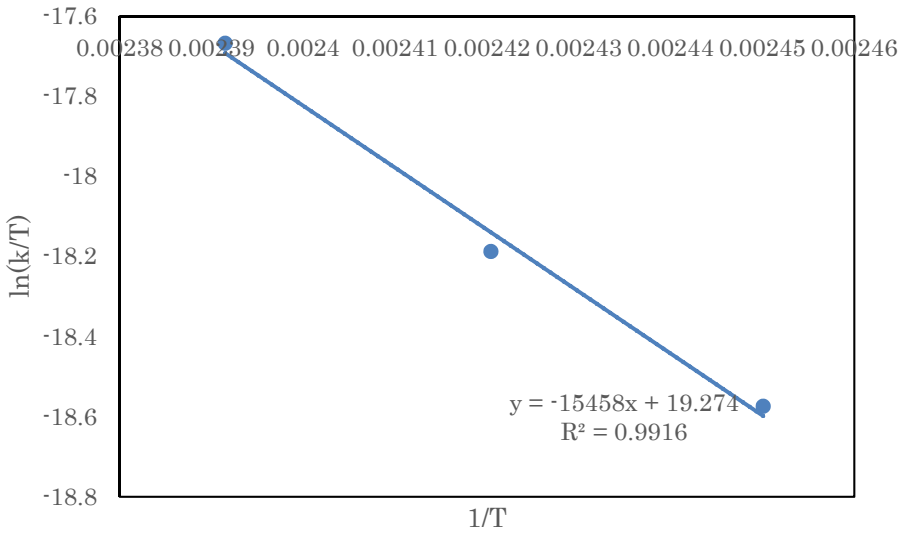

Figure S32. Eyring-Polanyi plots of **1h**.

$\Delta H^{\neq}_{\text{enantiomerization}}$ = 30.7 ± 0.3 kcal/mol

$\Delta S^{\neq}_{\text{enantiomerization}}$ = -8.9 ± 0.8 cal/mol·K

Table S31. Kinetic profile of racemization of **1i** by HPLC charts at 135 ºC.

***t* (s)**	***ee* (%)**	**ln(ee_0/ee_t)**
0	98.2	0
600	77.2	0.24069737
1200	57.1	0.542900506
1800	38.5	0.936413212
2400	27.1	1.287625158
3000	19.1	1.636965902
3600	13.8	1.961760359

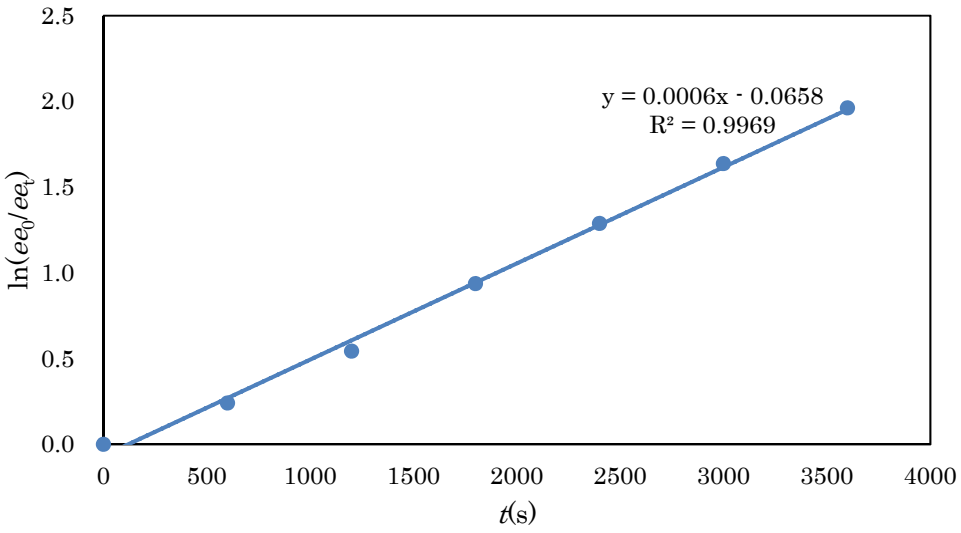

Figure S33. The plot of ln(ee_0/ee_t) vs time of **1i** at 135 ºC.

$k_{racemization}$ (135 ºC) = 5.58×10^{-4}

$k_{enantiomerization}$ (135 ºC) = 2.79×10^{-4}

$\Delta G^{\neq}_{enantiomerization}$ (135 ºC) = 30.8 ± 0.1 kcal/mol

Table S32. Kinetic profile of racemization of **1i** by HPLC charts at 140 °C.

***t* (s)**	***ee* (%)**	**ln(ee_0/ee_t)**
0	98.9	0
600	68.3	0.370978418
1200	41.4	0.870857562
1800	25.4	1.360291399
2400	16.0	1.824622079
3000	9.4	2.348952042
3600	5.9	2.818701574

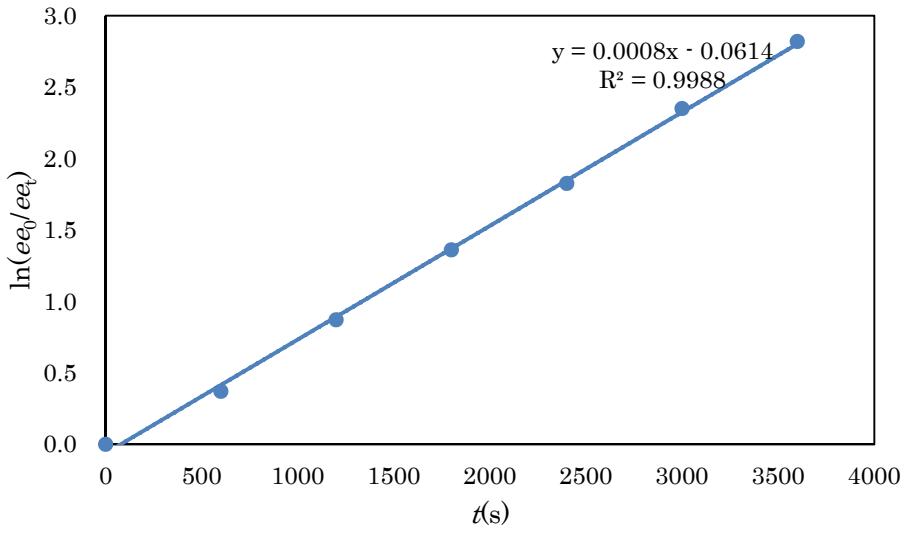

Figure S34. The plot of ln(ee_0/ee_t) vs time of **1i** at 140 °C.

$k_{racemization}$ (140 °C) = 7.90×10^{-4}

$k_{enantiomerization}$ (140 °C) = 3.95×10^{-4}

$\Delta G^{\neq}_{enantiomerization}$ (140 °C) = 30.9 ± 0.1 kcal/mol

Table S33. Kinetic profile of racemization of **1i** by HPLC charts at 145 °C.

***t* (s)**	***ee* (%)**	**ln(ee_0/ee_t)**
0	98.7	0
600	56.2	0.563784375
1200	26.9	1.299384327
1800	12.7	2.048078001
2400	6.1	2.77673187
3000	3.1	3.461771336
3600	1.8	3.98211672

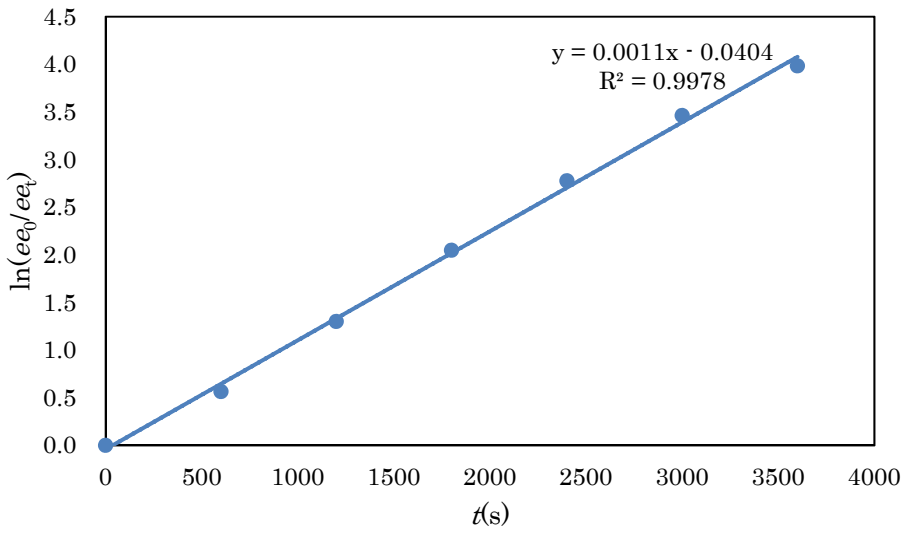

Figure S35. The plot of ln(ee_0/ee_t) vs time of **1i** at 145 °C.

$k_{racemization}$ (145 °C) = 1.14×10^{-3}

$k_{enantiomerization}$ (145 °C) = 5.72×10^{-4}

$\Delta G^{\neq}_{enantiomerization}$ (145 °C) = 31.0 ± 0.1 kcal/mol

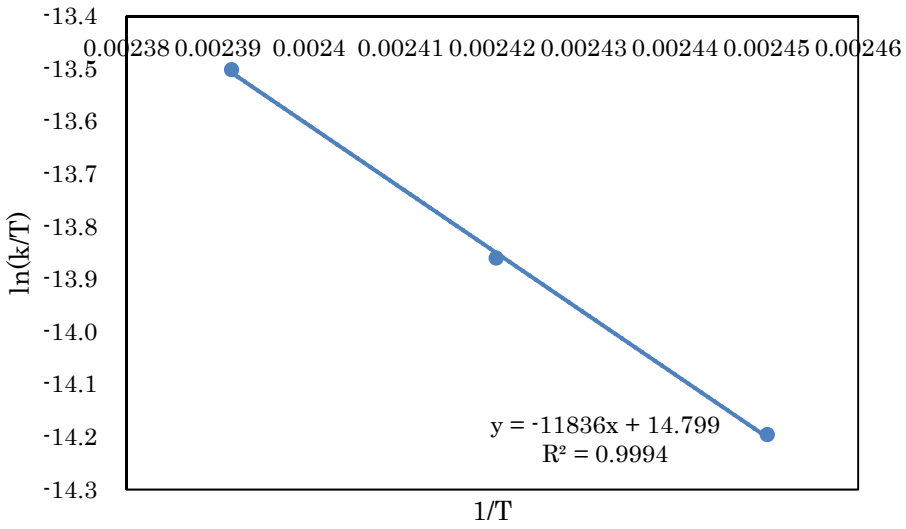

Figure S36. Eyring-Polanyi plots of **1i**.

$\Delta H^{\neq}_{\text{enantiomerization}}$ = 23.51 ± 0.07 kcal/mol

$\Delta S^{\neq}_{\text{enantiomerization}}$ = -17.8 ± 0.2 cal/mol·K

5. Optical absorption, emission, and circular dichroism spectra measurements

The solvents (CH_2Cl_2) with the spectroscopic grade were used for all spectroscopic experiments. UV/vis absorption and photoluminescence (PL) spectra were measured with a SHIMADZU UV-3150PC spectrophotometer, and a SHIMADZU RF-6000 spectrofluorometer, respectively. The circular dichroism (CD) spectra were recorded on a JASCO J-820.

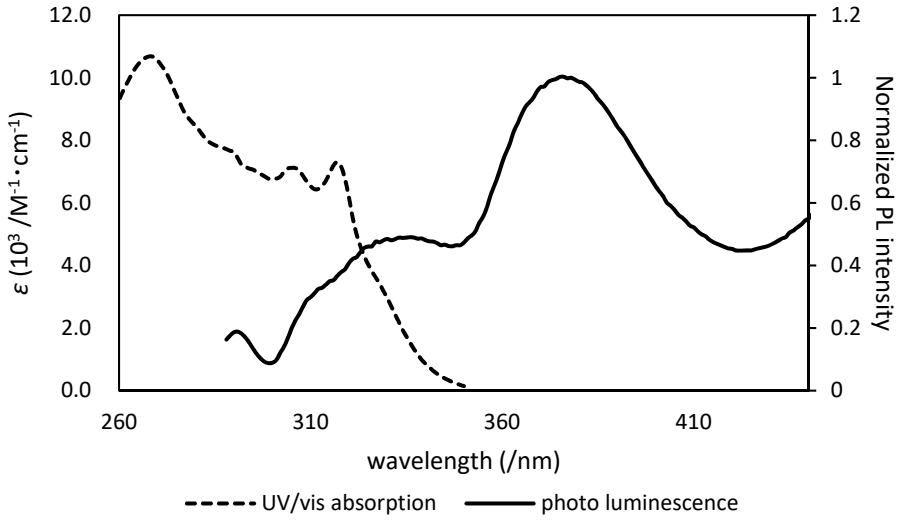

Figure S37. UV / vis absorption and normalized photoluminescence spectra of **1a**.

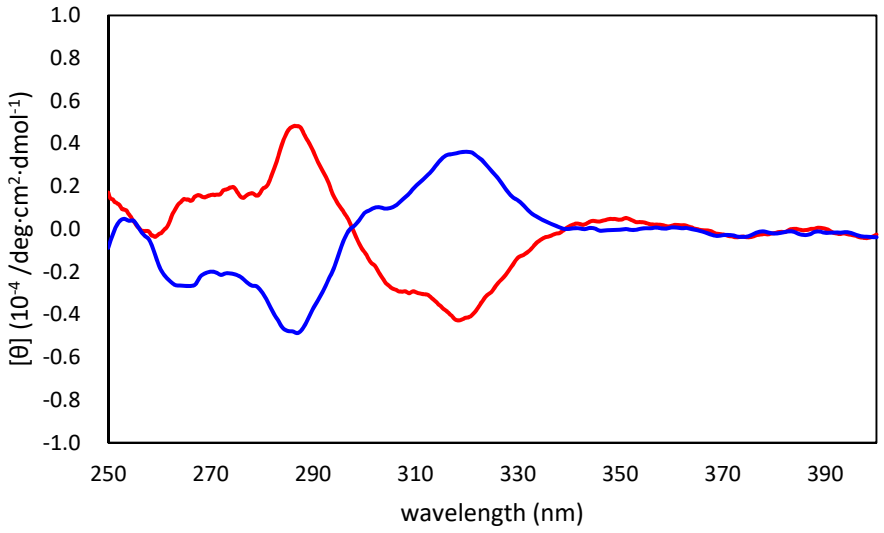

Figure S38. CD spectra of **1a**.

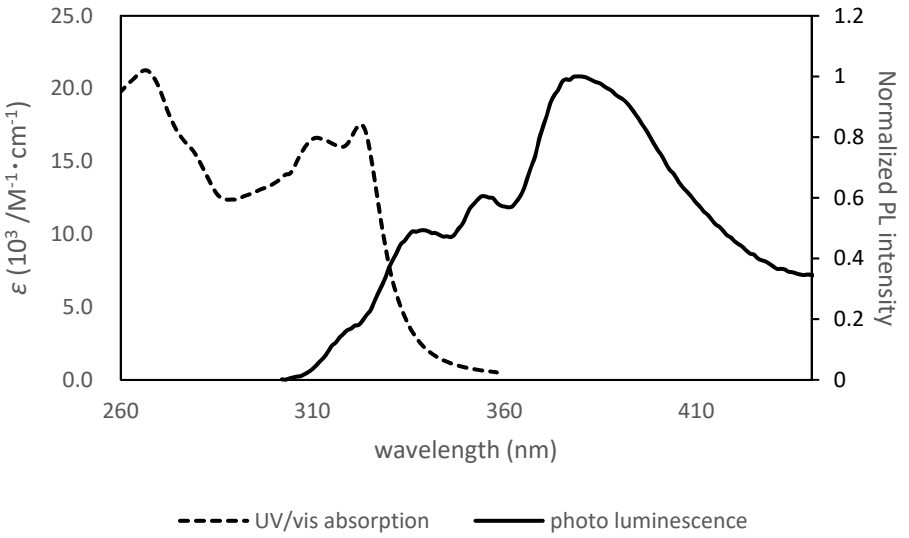

Figure S39. UV / vis absorption and normalized photoluminescence spectra of **1b**.

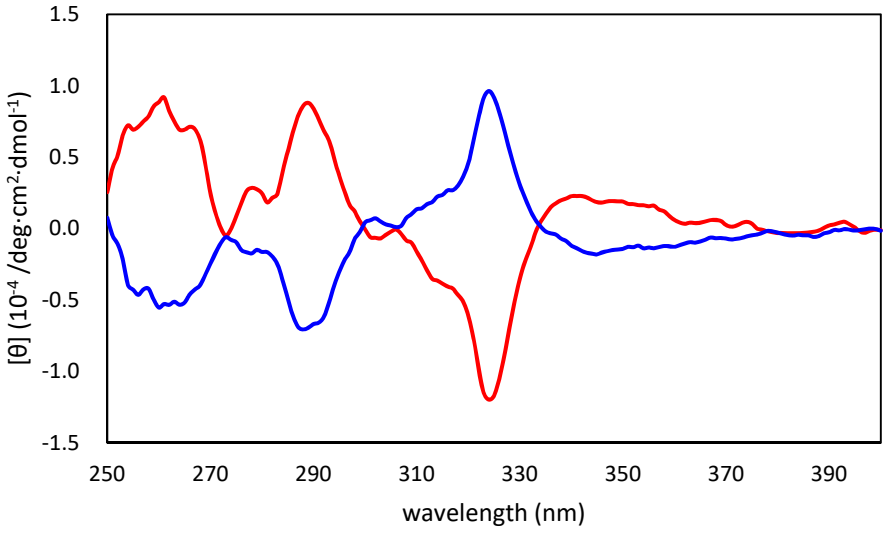

Figure S40. CD spectra of **1b**.

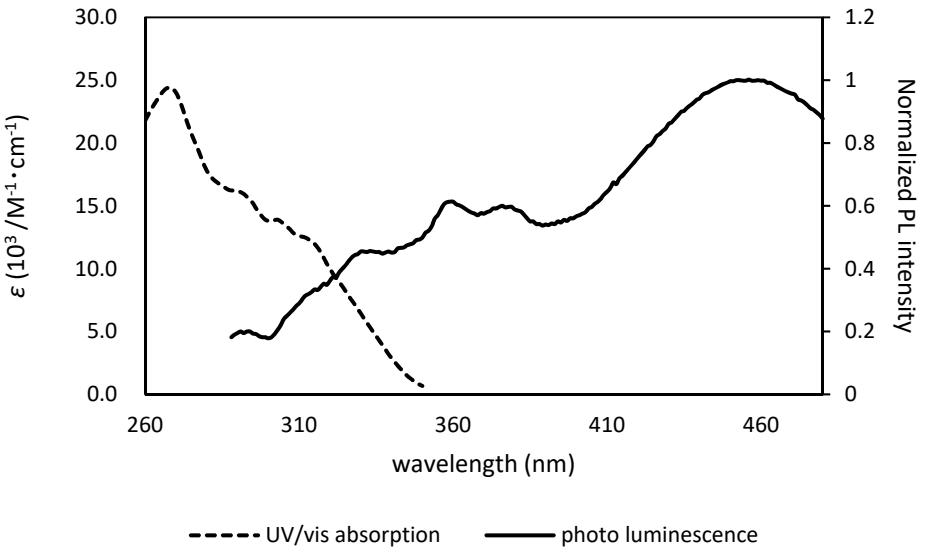

Figure S41. UV / vis absorption and normalized photoluminescence spectra of **1c**.

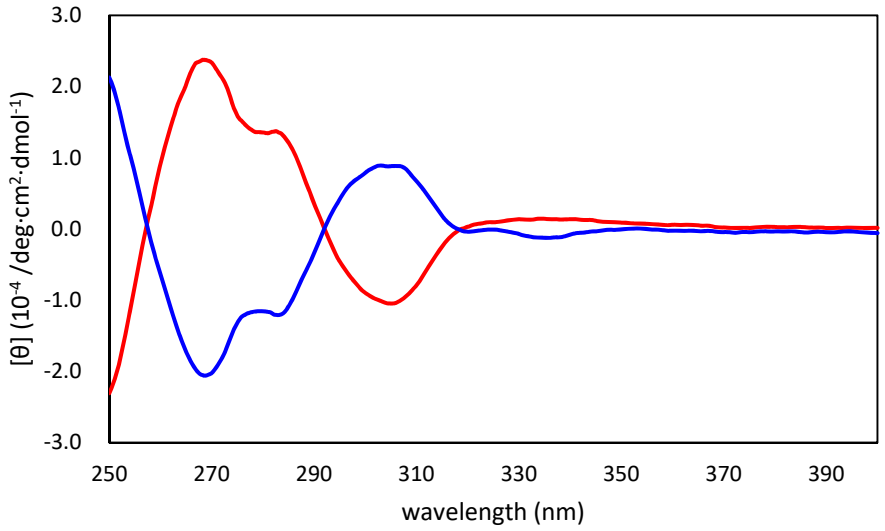

Figure S42. CD spectra of **1c**.

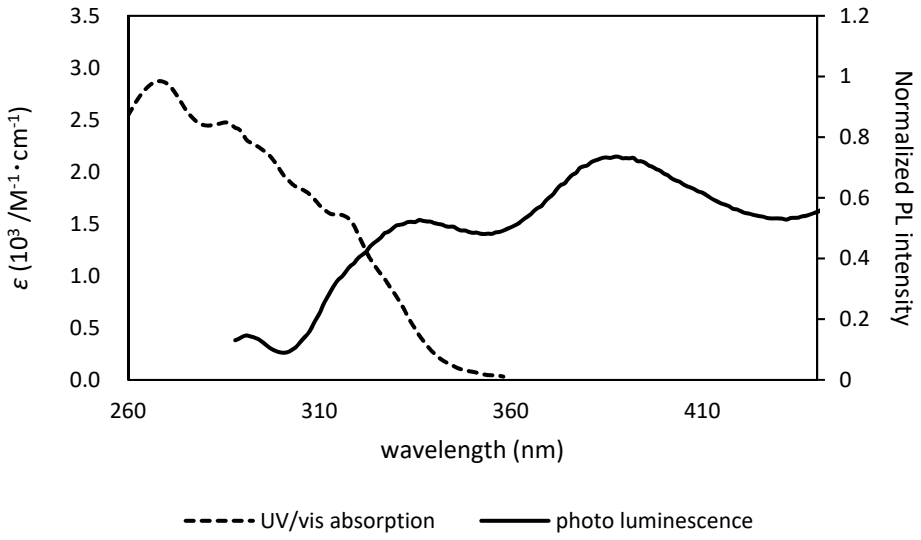

Figure S43. UV / vis absorption and normalized photoluminescence spectra of **1d**.

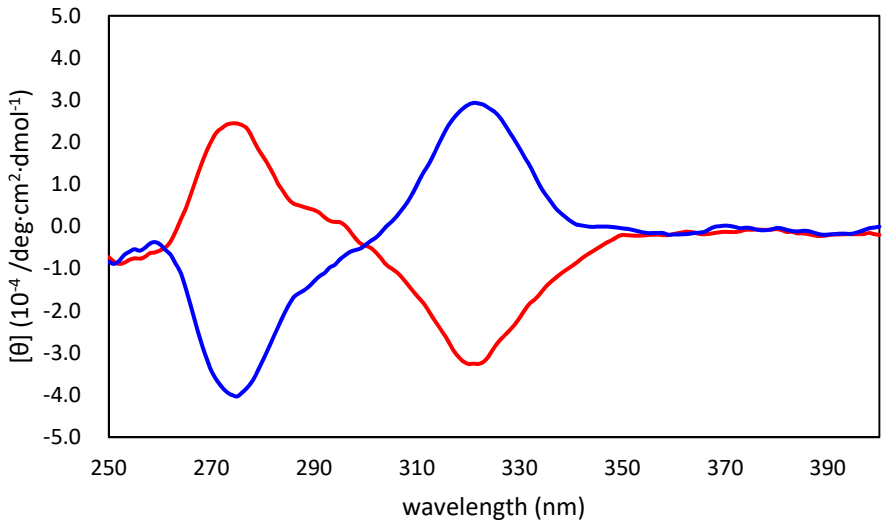

Figure S44. CD spectra of **1d**.

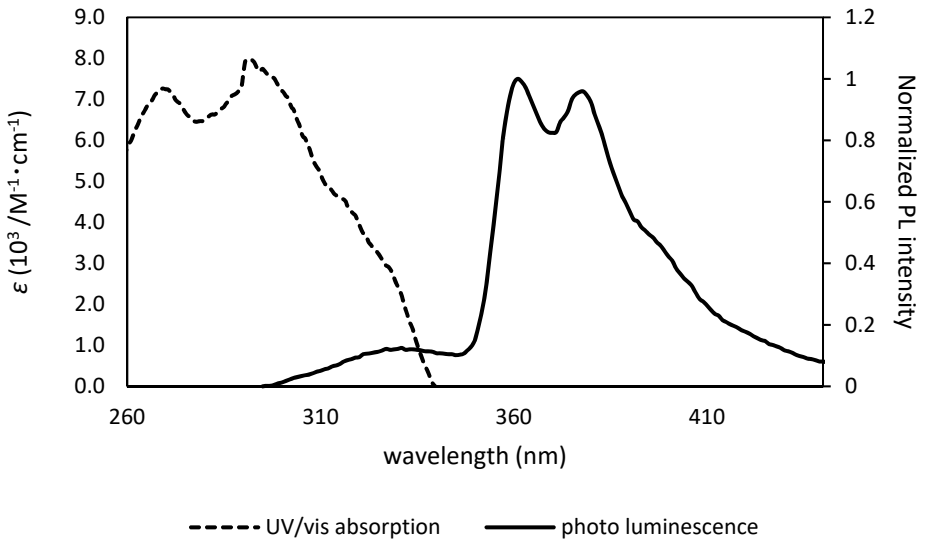

Figure S45. UV / vis absorption and normalized photoluminescence spectra of **1e**.

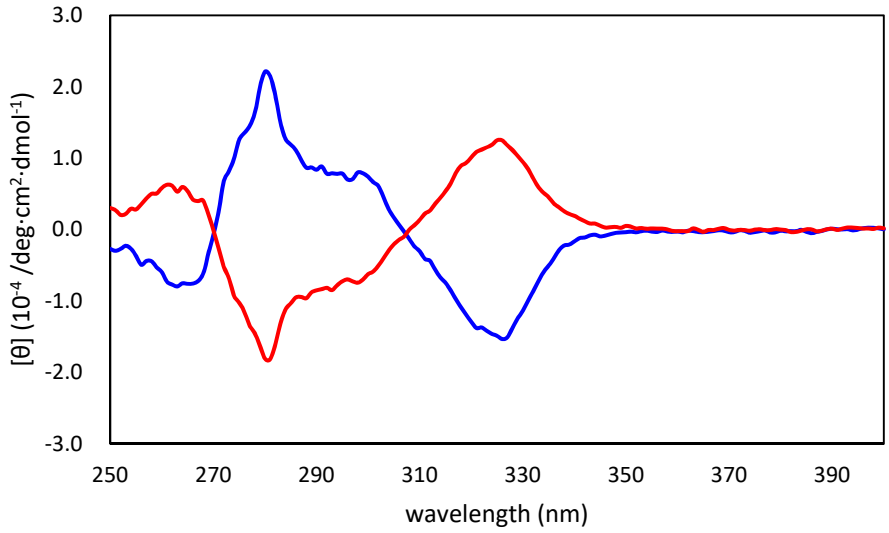

Figure S46. CD spectra of **1e**.

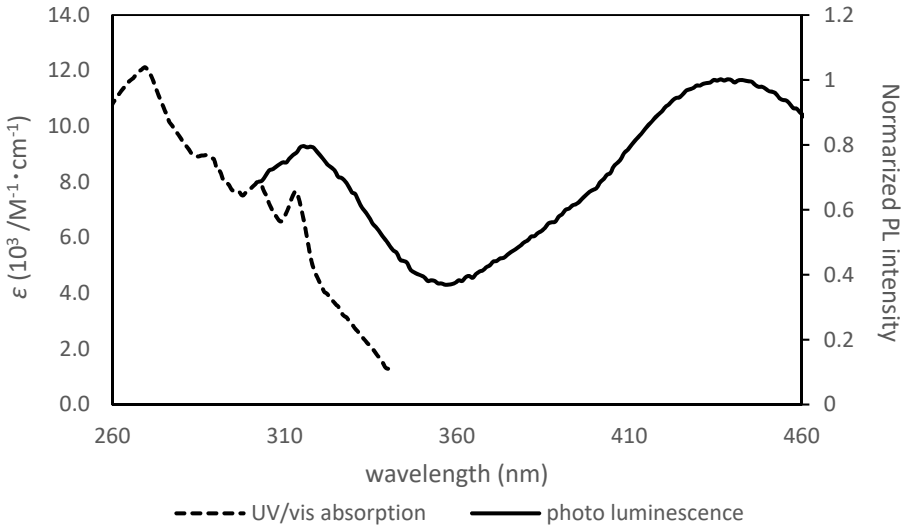

Figure S47. UV / vis absorption and normalized photoluminescence spectra of **1f**.

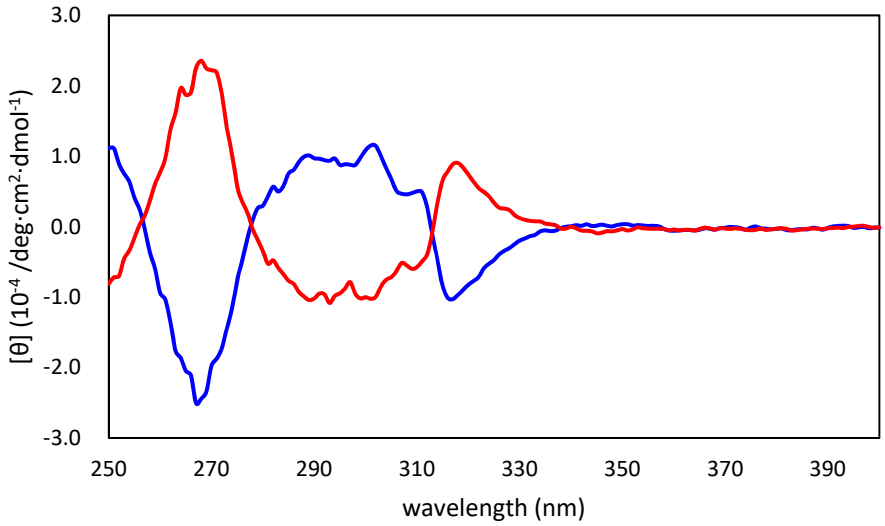

Figure S48. CD spectra of **1f**.

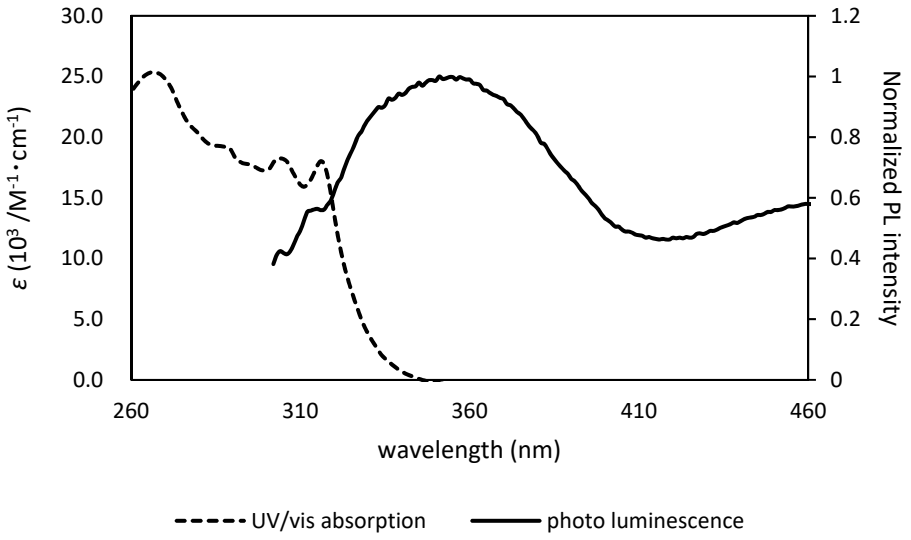

Figure S49. UV / vis absorption and normalized photoluminescence spectra of **1g**.

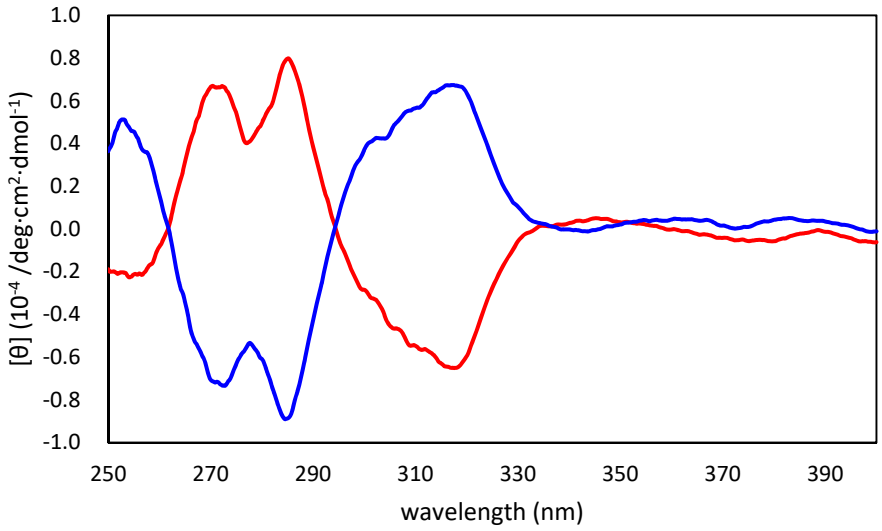

Figure S50. CD spectra of **1g**.

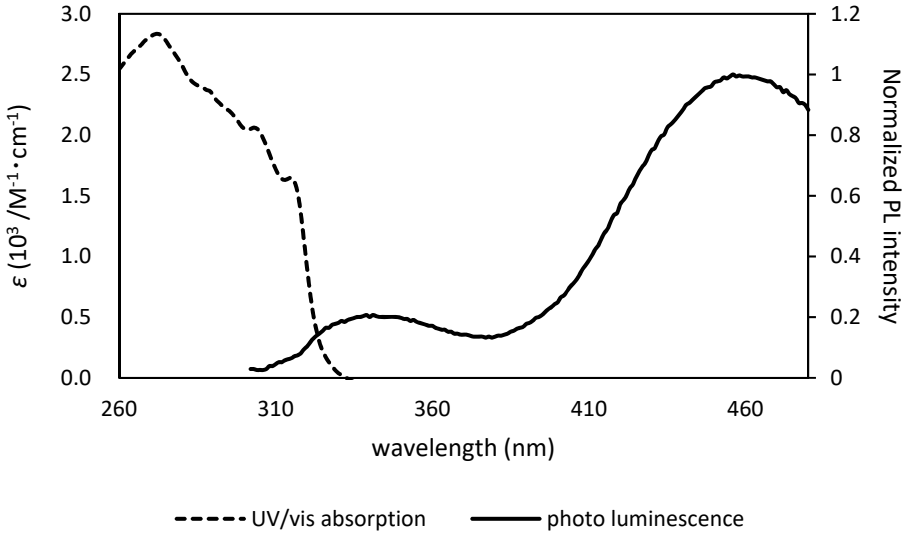

Figure S51. UV / vis absorption and normalized photoluminescence spectra of **1h**.

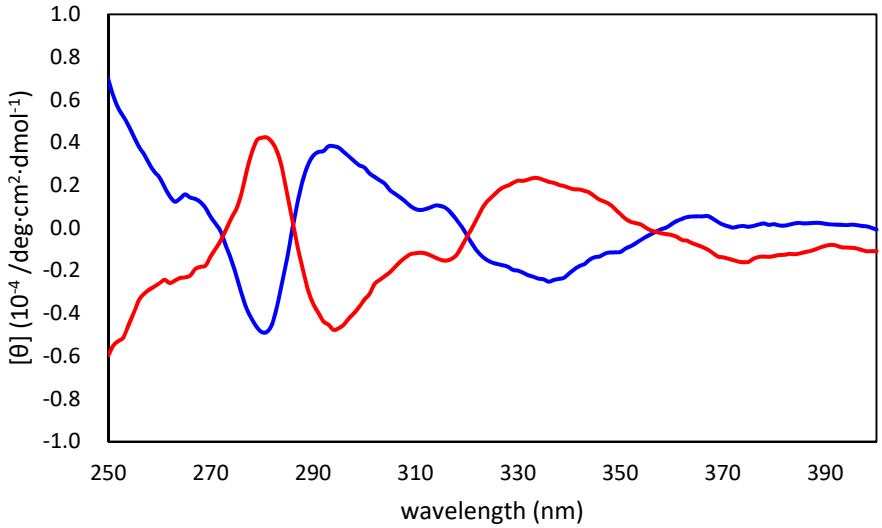

Figure S52. CD spectra of **1h**.

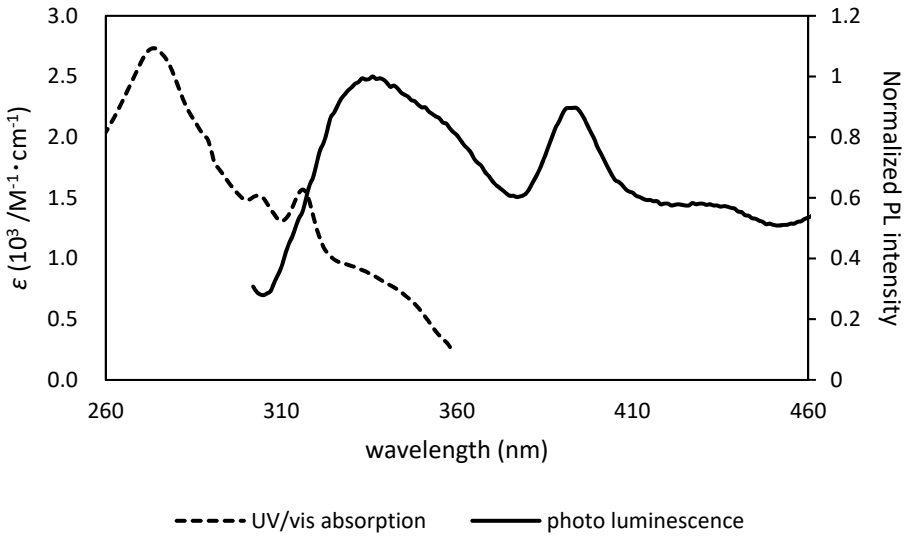

Figure S53. UV / vis absorption and normalized photoluminescence spectra of **1i**.

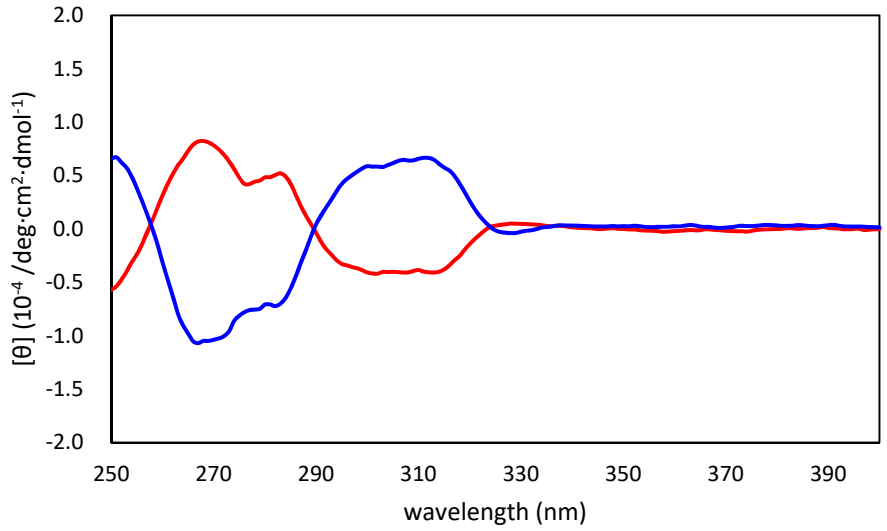

Figure S54. CD spectra of **1i**.

6. Theoretical calculations

All calculations were carried out with Gaussian 16 Rev. B. Program package.[13] Geometry optimizations and energy calculations for the ground-state structures and the transition states were carried out with the DFT methods using Becker's three-parameter hybrid functional B3LYP[14] and the standard 6-31G(d)[15] basis sets. Theoretical ECD spectra were simulated at the time-dependent DFT (TD-DFT)[16] method in Minnesota functional M06-2X[17] with a 6-31+G(d,p)[15] basis set. Frequency calculations at the optimized structures were performed by using the same functional and 6-311+G(d,p)[15] basis sets as in the geometry optimization to estimate the zero-point energy corrections and to identify whether the obtained structures are the stable structures (without imaginary frequency) or the transition states (with sole imaginary frequency). The connection of the transition state with the reactant and product was examined by the intrinsic reaction coordinate (IRC)[18] technique.

Optimized geometry of (*S*)-1d (GS-(*S*))

(This geometry was used to simulate ECD spectra)

C 0.621530 0.196940 -2.466690
H -0.428940 0.423310 -2.599350
C 1.496770 0.046800 -3.527690
C 2.837360 -0.245210 -3.254190
C 3.261850 -0.377730 -1.940920
C 2.334910 -0.215750 -0.906370
N 1.037000 0.067680 -1.199390
B 0.126610 0.215340 0.142860
C 1.299810 -0.064620 1.202630
C 2.521730 -0.301380 0.538350
C 3.710380 -0.573370 1.225510
C 3.678900 -0.609860 2.613990
C 2.476220 -0.377320 3.294540
C 1.298740 -0.107590 2.598380
H 1.138200 0.156050 -4.542430
H 3.543550 -0.367590 -4.067420
H 4.294310 -0.603100 -1.707850
H 0.379380 0.069820 3.146660
H 4.641090 -0.752880 0.697170
H 2.465700 -0.408270 4.379050

H 4.584660 -0.817920 3.172010
C -1.239150 -2.173550 0.058520
C -2.482400 -2.828160 0.040480
C -3.644070 -2.049460 0.068360
C -3.583450 -0.655260 0.117620
C -2.341110 -0.023660 0.134300
C -2.039460 1.422950 0.180980
C -0.641970 1.644420 0.181560
C -2.934030 2.493690 0.224250
C -0.168520 2.953300 0.227620
C -2.437890 3.798070 0.264620
C -1.061970 4.030170 0.265970
H -0.333030 -2.776030 0.042950
H 0.900220 3.150470 0.241430
C -2.558550 -4.336930 0.022420
H -0.686610 5.047540 0.302660
H -4.503410 -0.079420 0.140770
H -4.006110 2.323740 0.228610
H -4.612620 -2.540260 0.053150
H -3.126580 4.635680 0.298710
H -1.825480 -4.766010 -0.666770
H -2.352820 -4.755640 1.014080
H -3.549280 -4.683570 -0.280780
C -1.150460 -0.786390 0.103280

Calculated geometry of TS-1

C -4.442250 0.385460 1.220650
H -4.956100 0.508390 2.172500
C -4.850560 1.110840 0.101520
N -3.430690 -0.493620 1.212970
C -4.165030 0.911830 -1.096980
H -5.684940 1.801660 0.168780
C -2.760680 -0.666020 0.061300
C -3.101670 0.014940 -1.118120
H -4.452070 1.447000 -1.997430
C -1.715370 -1.736950 0.014970

H -2.538880 -0.167360 -2.027240
C -0.312570 -1.523470 -0.132580
C -2.242070 -3.035980 0.021370
B 0.505170 -0.189760 0.070390
C 0.449700 -2.684640 -0.418630
C -1.439490 -4.151800 -0.201710
H -3.308930 -3.161520 0.178530
C 0.105620 1.347030 0.109280
C 2.099780 -0.133720 0.095460
C -0.084470 -3.968160 -0.463760
H 1.502060 -2.568820 -0.633430
H -1.876820 -5.146230 -0.201010
C 1.288180 2.090010 -0.174310
C -1.064370 2.073330 0.351950
C 3.120710 -1.055600 0.338270
C 2.475960 1.208420 -0.178570
H 0.555000 -4.815730 -0.692700
C 1.271410 3.473500 -0.312740
C -1.081920 3.471150 0.248780
H -1.971030 1.572800 0.657070
C 4.481750 -0.703660 0.242750
H 2.885130 -2.071220 0.643820
C 3.809520 1.573920 -0.304550
C 0.071300 4.165240 -0.109070
H 2.179850 4.020610 -0.549390
H -2.001680 4.012580 0.450330
C 4.805710 0.609400 -0.104360
C 5.556190 -1.732470 0.506740
H 4.091170 2.599180 -0.528890
H 0.048590 5.247420 -0.205140
H 5.851230 0.894830 -0.192640
H 5.393400 -2.243200 1.462420
H 5.571330 -2.506060 -0.270780
H 6.549310 -1.275810 0.536410

Calculated geometry of Int-1

C 3.558290 2.630680 -1.249130
H 4.281750 3.044890 -1.946590
C 2.846070 3.469580 -0.393410
C 1.945480 2.885660 0.491440
C 1.787220 1.504930 0.473950
C 2.524550 0.739790 -0.442240
N 3.412080 1.305750 -1.279530
B -0.243800 -0.668490 -0.261080
C 1.142040 -1.379690 -0.294460
C 2.389680 -0.740250 -0.497750
C 3.544290 -1.505270 -0.703400
C 3.492770 -2.894850 -0.688760
C 2.280090 -3.541120 -0.455730
C 1.127290 -2.788330 -0.252150
H 3.004100 4.541100 -0.417280
H 1.381810 3.492250 1.191390
H 1.123780 1.021620 1.180930
H 0.184950 -3.301580 -0.090680
H 4.483550 -0.991980 -0.868580
H 2.232240 -4.624340 -0.432980
H 4.397960 -3.470920 -0.846230
C -1.473640 -1.600560 1.970570
C -2.645540 -1.595980 2.750820
C -3.730370 -0.839570 2.304800
C -3.677810 -0.096680 1.115560
C -2.517090 -0.116390 0.359570
C -2.210400 0.579630 -0.917280
C -0.877670 0.302810 -1.320880
C -3.036150 1.386020 -1.688600
C -0.405020 0.836760 -2.517470
C -2.536310 1.922800 -2.882950
C -1.234720 1.650630 -3.298610
H -0.616680 -2.177940 2.308280
H 0.607300 0.628090 -2.848050
C -2.719070 -2.393660 4.030710
H -0.866680 2.069310 -4.228610

H -4.542650 0.482010 0.808080
H -4.056010 1.599850 -1.386300
H -4.640480 -0.822540 2.896550
H -3.174180 2.553340 -3.493190
H -2.642160 -3.467870 3.833070
H -1.901700 -2.131700 4.709540
H -3.660120 -2.219100 4.556270
C -1.398010 -0.879630 0.784040

Calculated geometry of TS-2

C 3.462140 -1.744400 -1.031560
H 3.746080 -2.720190 -0.641490
C 3.642350 -1.447630 -2.381960
N 2.947850 -0.887360 -0.141510
C 3.258930 -0.185810 -2.832510
H 4.067950 -2.184970 -3.054960
C 2.575930 0.328030 -0.577410
C 2.718700 0.715520 -1.918550
H 3.375790 0.091500 -3.876260
C 2.035350 1.299110 0.429530
H 2.403850 1.706560 -2.228580
C 0.713840 1.213690 0.929510
C 2.869070 2.354440 0.821040
B -0.352710 0.125390 0.569510
C 0.290360 2.224470 1.818310
C 2.435380 3.317340 1.731740
H 3.874470 2.411070 0.412870
C -0.387310 -1.421660 0.825630
C -1.773040 0.436620 -0.029530
C 1.138000 3.249420 2.235920
H -0.729080 2.199300 2.194920
H 3.104220 4.117230 2.036210
C -1.671860 -1.897490 0.438030
C 0.525010 -2.314090 1.390040
C -2.366060 1.609900 -0.484220
C -2.497370 -0.783670 -0.097770

H 0.781090 3.998180 2.937420
C -2.019880 -3.232500 0.599310
C 0.175510 -3.662270 1.556740
H 1.512540 -1.965160 1.673550
C -3.676380 1.608080 -1.005620
H -1.814140 2.547230 -0.437530
C -3.786180 -0.807560 -0.608890
C -1.083290 -4.113820 1.161800
H -2.999940 -3.598400 0.304690
H 0.885670 -4.358280 1.994140
C -4.363300 0.392330 -1.057790
C -4.311860 2.889270 -1.491910
H -4.354800 -1.731960 -0.668140
H -1.346780 -5.159950 1.293860
H -5.373870 0.374500 -1.459290
H -4.393320 3.626670 -0.684630
H -3.718020 3.352910 -2.288220
H -5.317210 2.714360 -1.884830

Calculated geometry of GS-(*R*)
C -10.84677 0.196940 -2.466690
H -9.796300 0.423310 -2.599350
C -11.72201 0.046800 -3.527690
C -13.06260 -0.245210 -3.254190
C -13.48709 -0.377730 -1.940920
C -12.56015 -0.215750 -0.906370
N -11.26224 0.067680 -1.199390
B -10.35185 0.215340 0.142860
C -11.52505 -0.064620 1.202630
C -12.74697 -0.301380 0.538350
C -13.93562 -0.573370 1.225510
C -13.90414 -0.609860 2.613990
C -12.70146 -0.377320 3.294540
C -11.52398 -0.107590 2.598380
H -11.36344 0.156050 -4.542430
H -13.76879 -0.367590 -4.067420

H -14.51955 -0.603100 -1.707850
H -10.60462 0.069820 3.146660
H -14.86633 -0.752880 0.697170
H -12.69094 -0.408270 4.379050
H -14.80990 -0.817920 3.172010
C -8.986090 -2.173550 0.058520
C -7.742840 -2.828160 0.040480
C -6.581170 -2.049460 0.068360
C -6.641790 -0.655260 0.117620
C -7.884130 -0.023660 0.134300
C -8.185780 1.422950 0.180980
C -9.583270 1.644420 0.181560
C -7.291210 2.493690 0.224250
C -10.05672 2.953300 0.227620
C -7.787350 3.798070 0.264620
C -9.163270 4.030170 0.265970
H -9.892210 -2.776030 0.042950
H -11.12546 3.150470 0.241430
C -7.666690 -4.336930 0.022420
H -9.538630 5.047540 0.302660
H -5.721830 -0.079420 0.140770
H -6.219130 2.323740 0.228610
H -5.612620 -2.540260 0.053150
H -7.098660 4.635680 0.298710
H -8.399760 -4.766010 -0.666770
H -7.872420 -4.755640 1.014080
H -6.675960 -4.683570 -0.280780
C -9.074780 -0.786390 0.103280

References and Notes

(1) N. Ishida, T. Moriya, T. Goya and M. Murakami, *J. Org. Chem.*, 2010, **75**, 8709–8712.

(2) X. Cheng, G.-H. Hou, J.-H. Xie and Q.-L. Zhou, *Org. Lett.,* 2004, **6**, 2381–2383.

(3) M. Shimizu, I. Nagao, Y. Tomioka, T. Kadowaki and T. Hiyama, *Tetrahedron*, 2011, **67**, 8014–8026..

(4) R. Wada, S. Kaga, Y. Kawai, K. Futamura, T. Murai and F. Shibahara, *Tetrahedron,* 2021, **83**, 131978.

(5) S. Xu, X. Shangguan, H. Li, Y. Zhang and J. Wang, *J. Org. Chem.*, 2015, **80**, 7779–7784 .

(6) X. Mu, H. Zhang, P. Chen and G. Liu, *Chem. Sci.*, 2014, **5**, 275–280.

(7) (a) Y. Shoji, N. Tanaka, S. Muranaka, N. Shigeno, H. Sugiyama, K. Takenouchi, F. Hajjaj and T. Fukushima, *Nat. Commun.*, 2016, **7**, 12704; (b) Y. Shimizu, Y. Shoji, D. Hashizume, Y. Nagata, and T. Fukushima *Chem. Commun.,* 2018, **54**, 12314-12317; (c) Y. Shoji, N. Shigeno, K. Takenouchi, M. Sugimoto and T. Fukushima, *Chem. Eur. J.,* 2018, **24**, 13223–13230.

(8) Olex2: (a) O. V. Dolomanov, A. J. Blake, N. R. Champness and M. J. Schröder, M. *J. Appl. Cryst.,* 2003, **36**, 1283-1284; (b) O. V. Dolomanov, L. J. Bourhis, R. J. Gildea, J. A. K. Howard, and H. Puschmann, H. *J. Appl. Cryst.,* 2009, **42**, 339-341.

(9) SHELX: G. M. Sheldrick, *Acta Cryst.,* **2015**, *A71*, 3-8.

(10) First-order kinetic analysis: C. H. Bamford, and C. F. H. Tipper, *Comprehensive Chemical Kinetics*, *vol. 1, The practice of kinetics,* Elsevier B.V., Amsterdam, 1969.

(11) First-order kinetic analysis for racemization: (a) T. Turányi, A. S. Tomlin, M. F. Boehm and J. L. Bada, *Proc. Natl. Acad. Sci. USA*, 1984, **81**, 5263; (b) L. Canoira, M.-J. García-Martínez, J. F. Llamas, J. E. Ortíz and T. D. Torres, *Int. J. Chem. Kinet.*, 2003, **35**, 576-591.

(12) Eyring-Planyi plot: (a) H. Eyring and M. Polanyi *Über Einfache Gasreaktionen. Z. Phys. Chem. B,* 1931, **12**, 279–311; (b) H. Eyring, *J. Chem. Phys.,* 1935, **3**, 107–115.

(13) Gaussian 16, Revision B.01, M. J. Frisch, G. W. Trucks, H. B. Schlegel, G. E. Scuseria, M. A. Robb; J. R. Cheeseman; G. Scalmani, V. Barone, G. A. Petersson, H. Nakatsuji, X. Li, M. Caricato, A. V. Marenich, J. Bloino, B. G. Janesko, R. Gomperts, B. Mennucci, H. P. Hratchian, J. V. Ortiz, A. F. Izmaylov, J. L. Sonnenberg, D. Williams-Young, F. Ding, F. Lipparini, F. Egidi, J. Goings, B. Peng, A. Petrone, T. Henderson, D. Ranasinghe, V. G. Zakrzewski, J. Gao, N. Rega, G. Zheng, W. Liang, M. Hada, M. Ehara, K. Toyota, R. Fukuda, J. Hasegawa, M. Ishida, T. Nakajima, Y. Honda, O. Kitao, H. Nakai, T. Vreven, K. Throssell, J. A.

Montgomery Jr., J. E. Peralta, F. Ogliaro, M. J. Bearpark, J. J. Heyd, E. N. Brothers, K. N. Kudin, V. N. Staroverov, T. A. Keith, R. Kobayashi, J. Normand, K. Raghavachari, A. P. Rendell, J. C. Burant, S. S. Iyengar, J. Tomasi, M. Cossi, J. M. Millam, M. Klene, C. Adamo, R. Cammi, J. W. Ochterski, R. L. Martin, K. Morokuma, O. Farkas, J. B. Foresman, D. J. Fox, Gaussian, Inc., Wallingford CT, 2016.

(14) B3LYP: (a) K. Kim and K. D. Jordan, *J. Phys. Chem.,* 1994, **98**, 10089–10094; (b) P. J. Stephens, F. J. Devlin, C. F. Chabalowski and M. J. Frisch *J. Phys. Chem.,* 1994, **98**, 11623–11627.

(15) 6-31G, 6-311G: (a) R. Ditchfield, W. J. Hehre and J. A. Pople, *J. Chem. Phys.,* 1971, **54**, 724-728; (b) W. J. Hehre, R. Ditchfield and J. A. Pople, *J. Chem. Phys.,* 1972, **56**, 2257-2260.

(16) TD-DFT: C. Adamo and D. Jacquemin *Chem. Soc. Rev.*, 2013, **42**, 845-856.

(17) M06-2X: (a) Y. Zhao and D. Truhlar, *Theor. Chem. Acc.,* 2008, **120**, 215−241; (b) B. Chan, A. T. B. Gilbert, P. M. W. Gill and L. Radom, *J. Chem. Theory Comput.,* 2014, **10**, 3777-3783.

(18) IRC: K. Fukui, *Acc. Chem. Res.,* 1981, **14**, 363-368.

NMR Spectra

^{1}H NMR Spectrum of 4 (400 MHz, $CDCl_3$, rt)

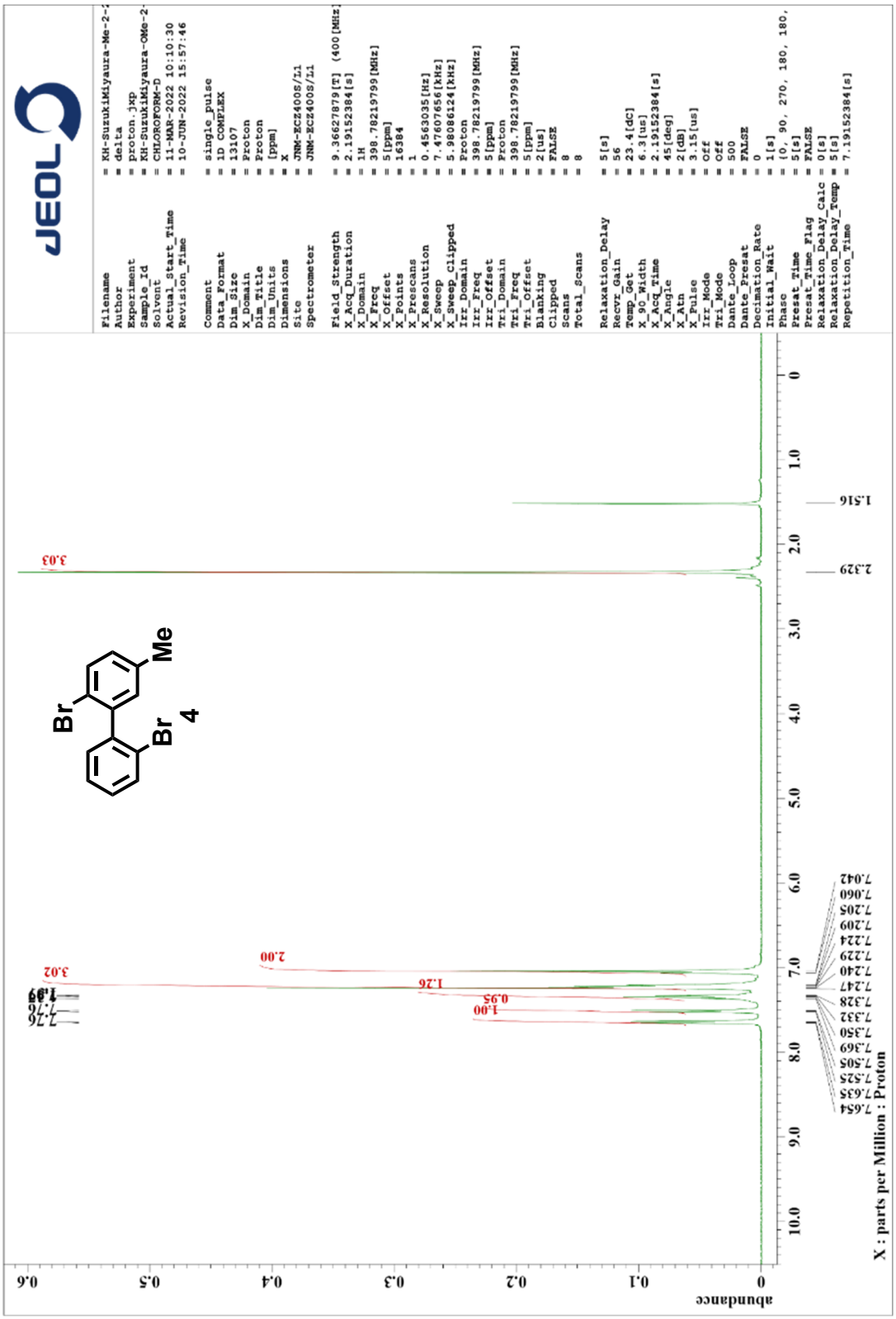

^{13}C NMR Spectrum of 4 (100 MHz, $CDCl_3$, rt)

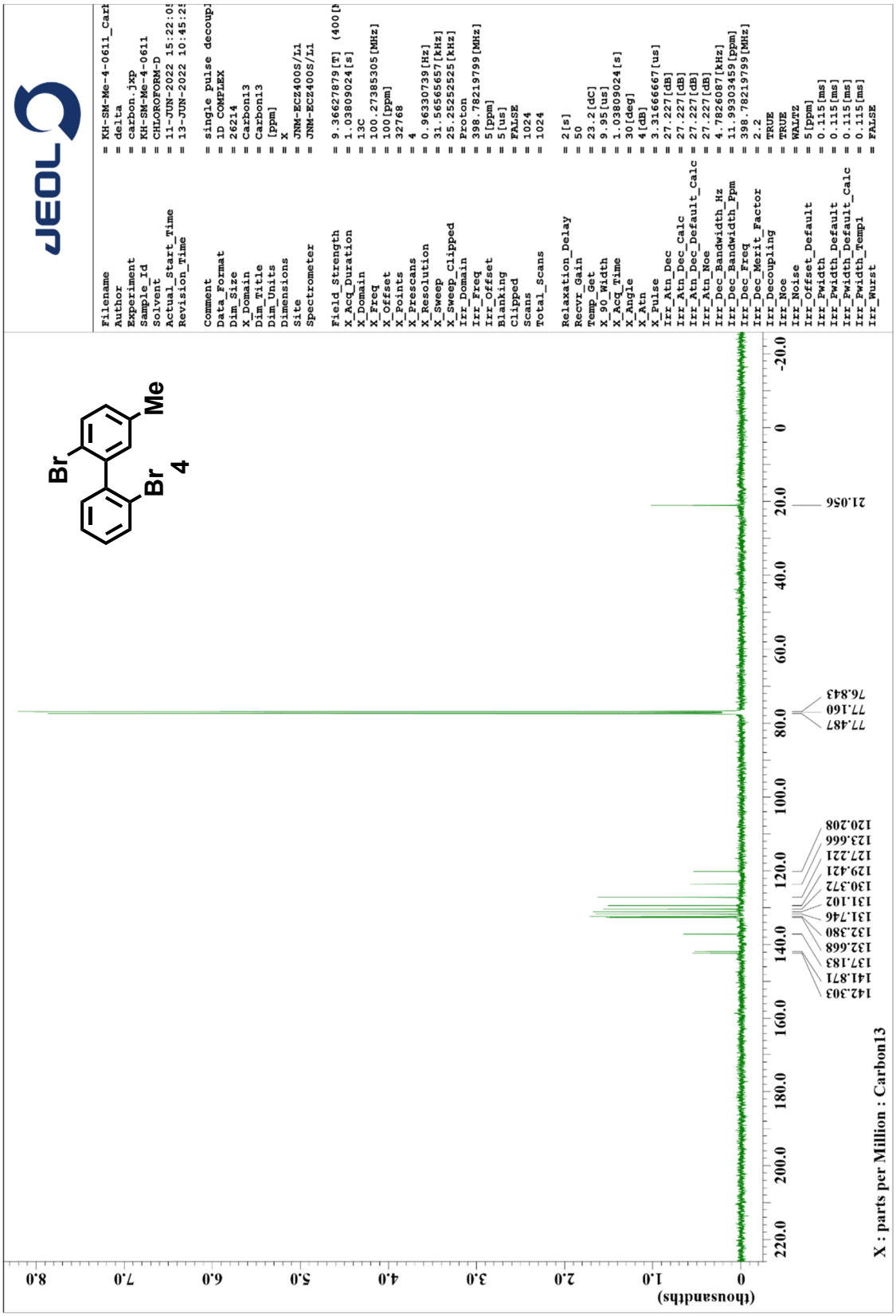

^{1}H NMR Spectrum of S3 (400 MHz, $CDCl_3$, rt)

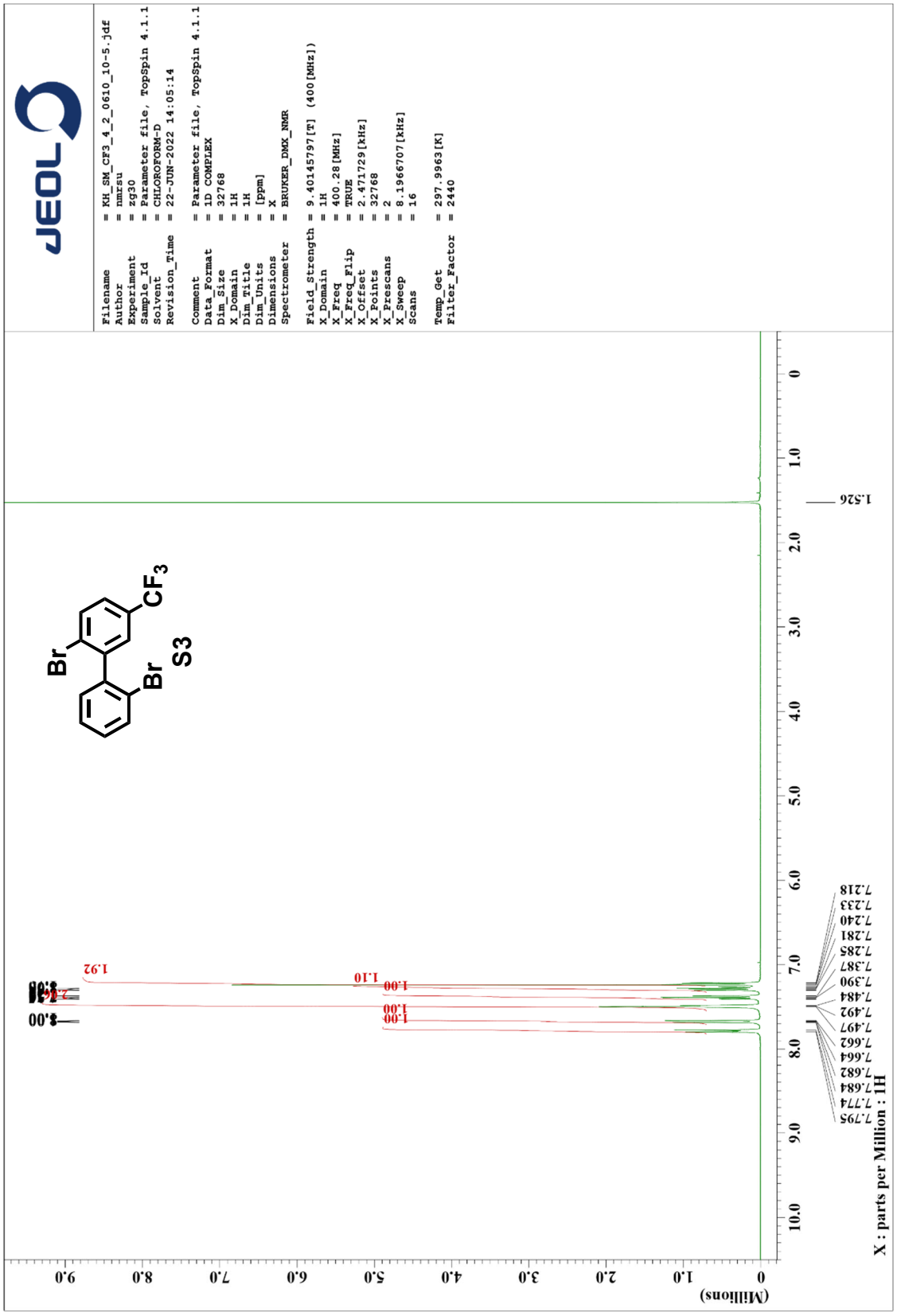

^{13}C NMR Spectrum of S3 (100 MHz, $CDCl_3$, rt)

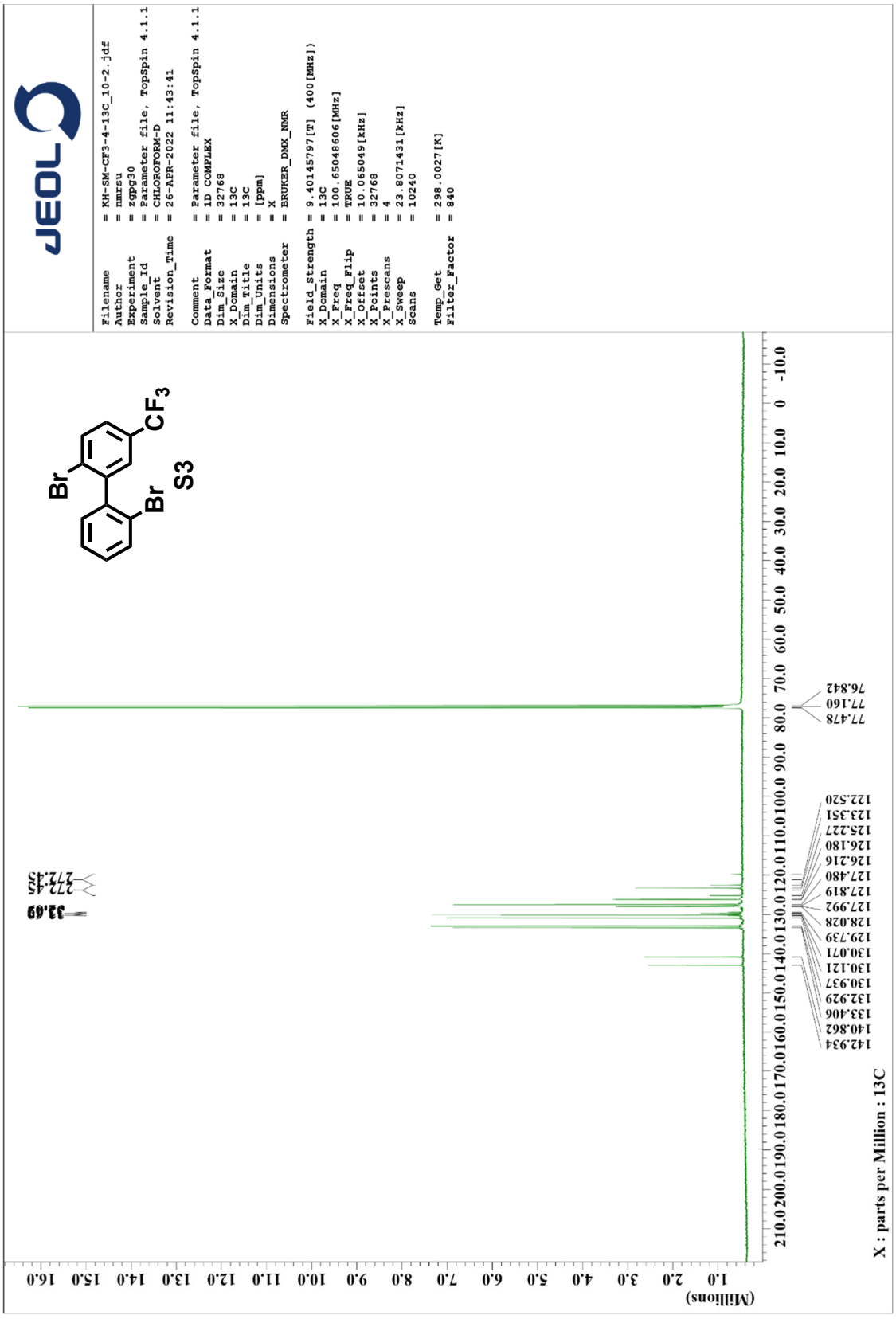

^{19}F NMR Spectrum of S3 (375 MHz, $CDCl_3$, rt)

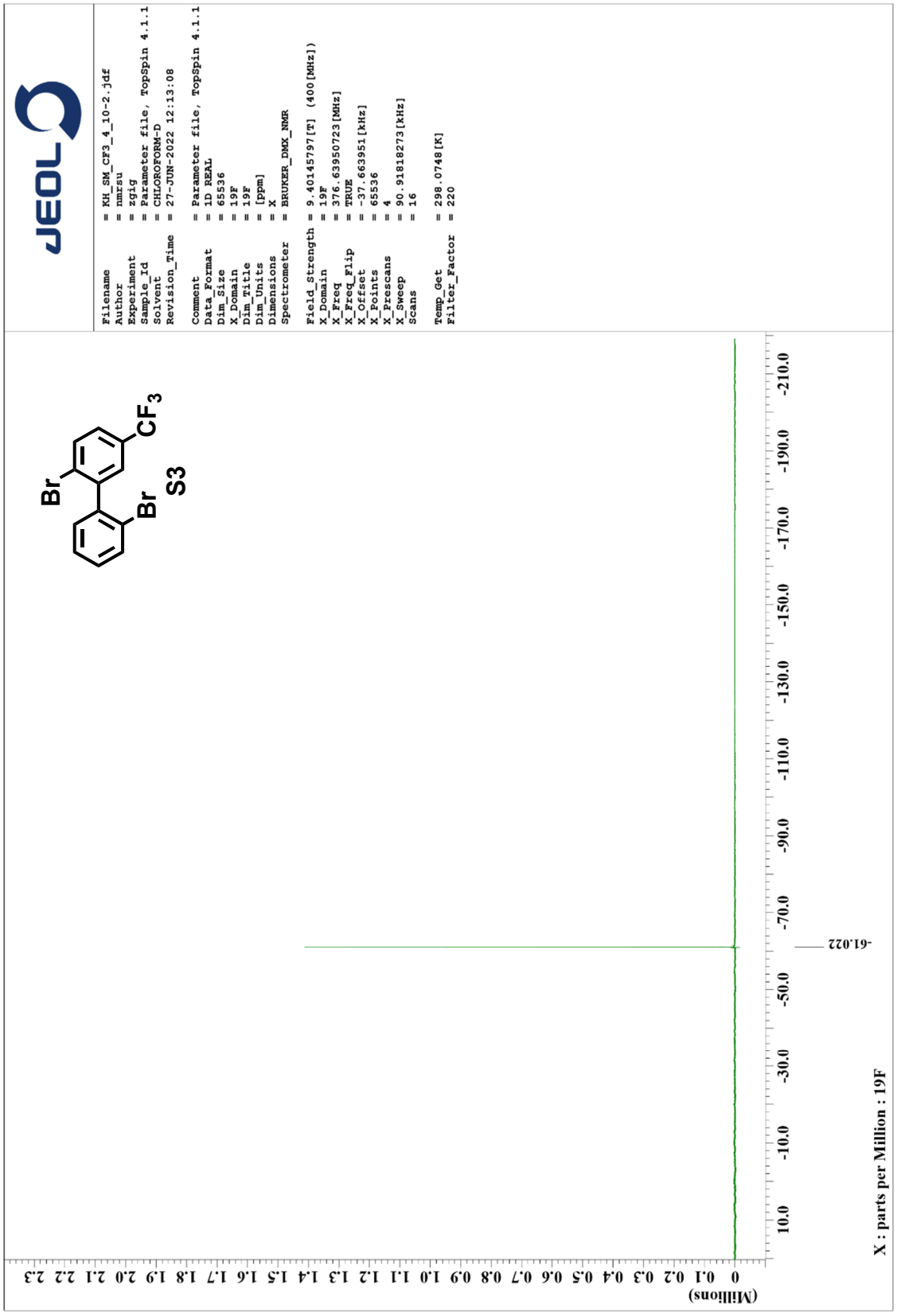

^{1}H NMR Spectrum of 1a (400 MHz, $CDCl_3$, rt)

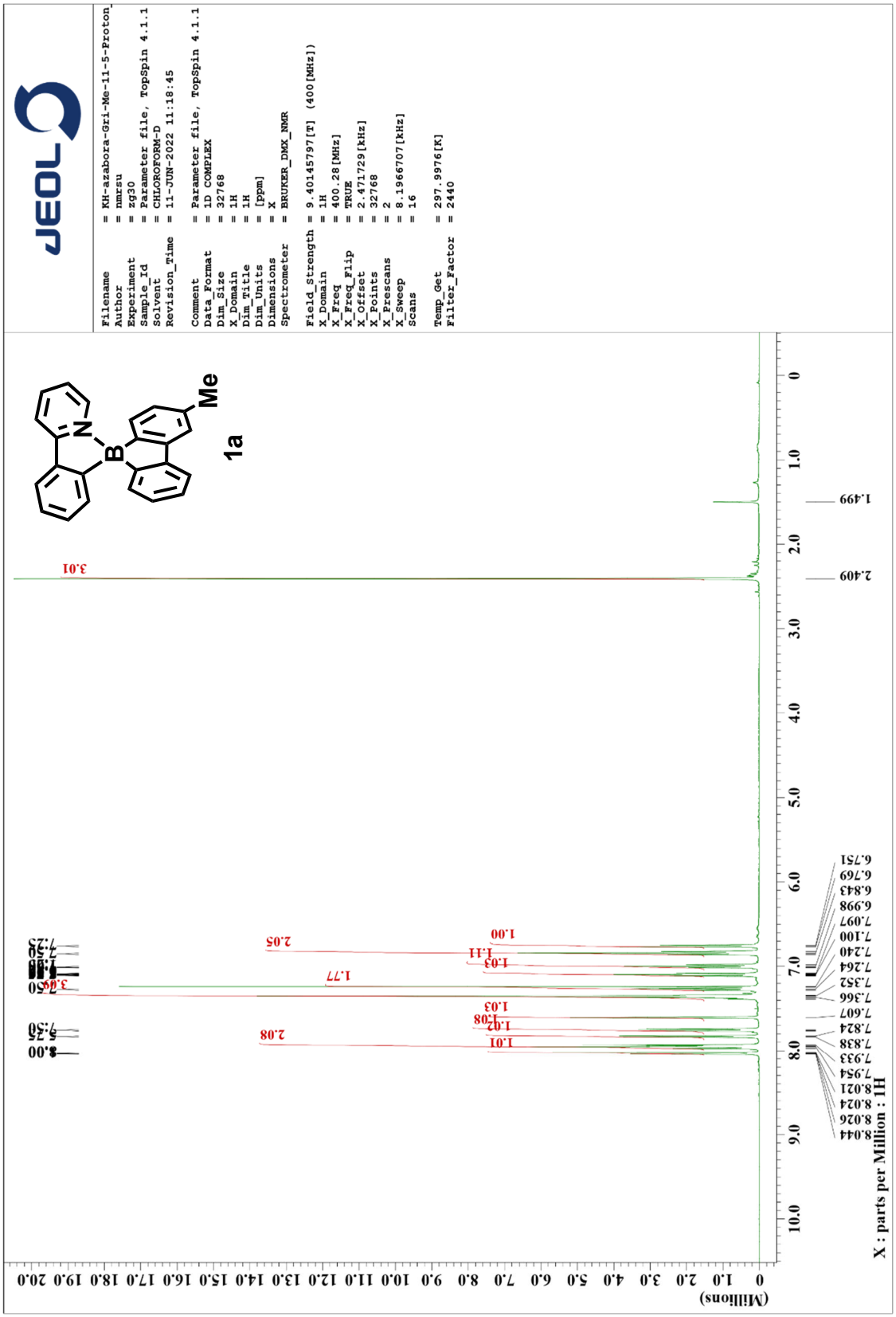

^{13}C NMR Spectrum of 1a (100 MHz, $CDCl_3$, rt)

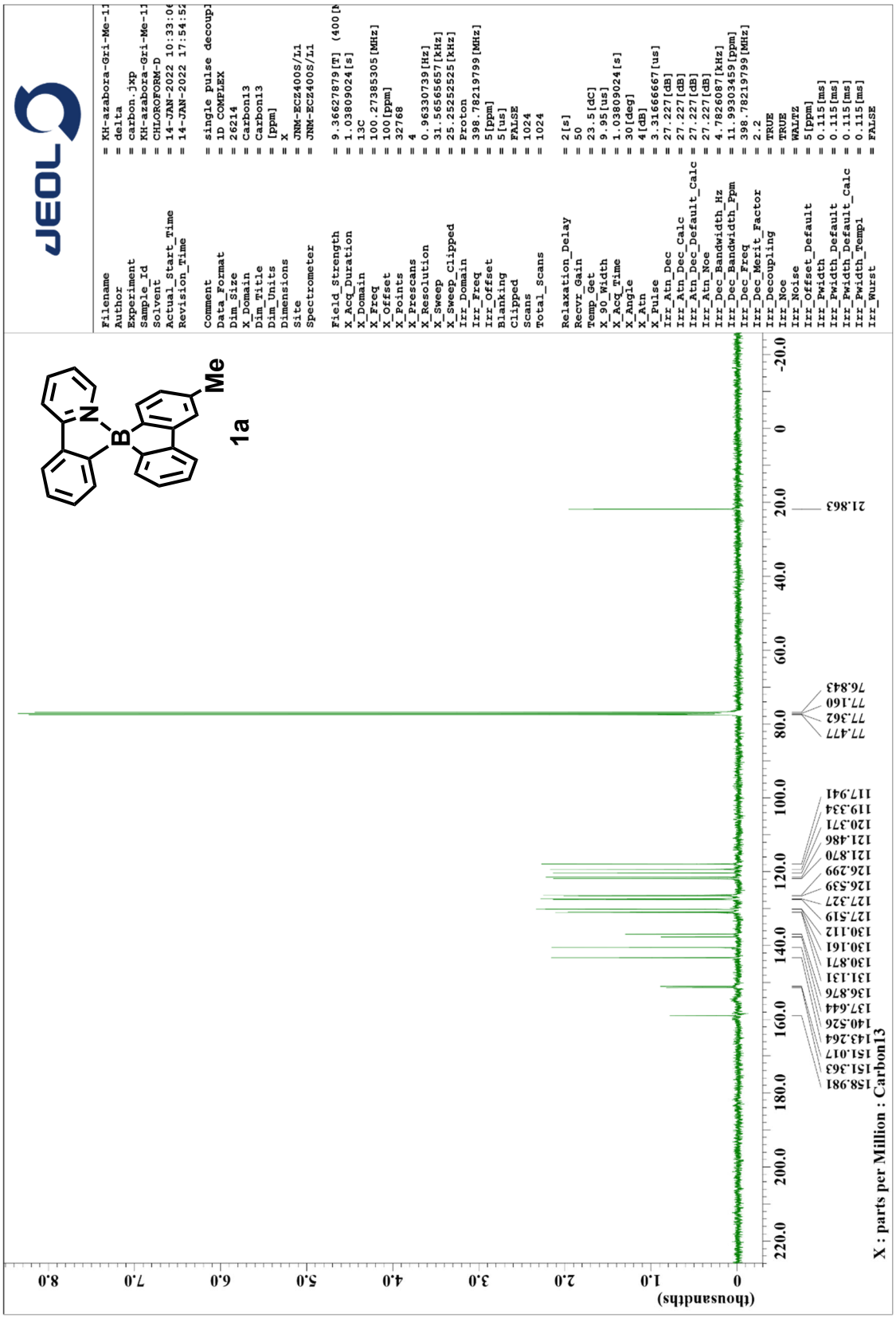

^{11}B NMR Spectrum of 1a (128 MHz, $CDCl_3$, rt)

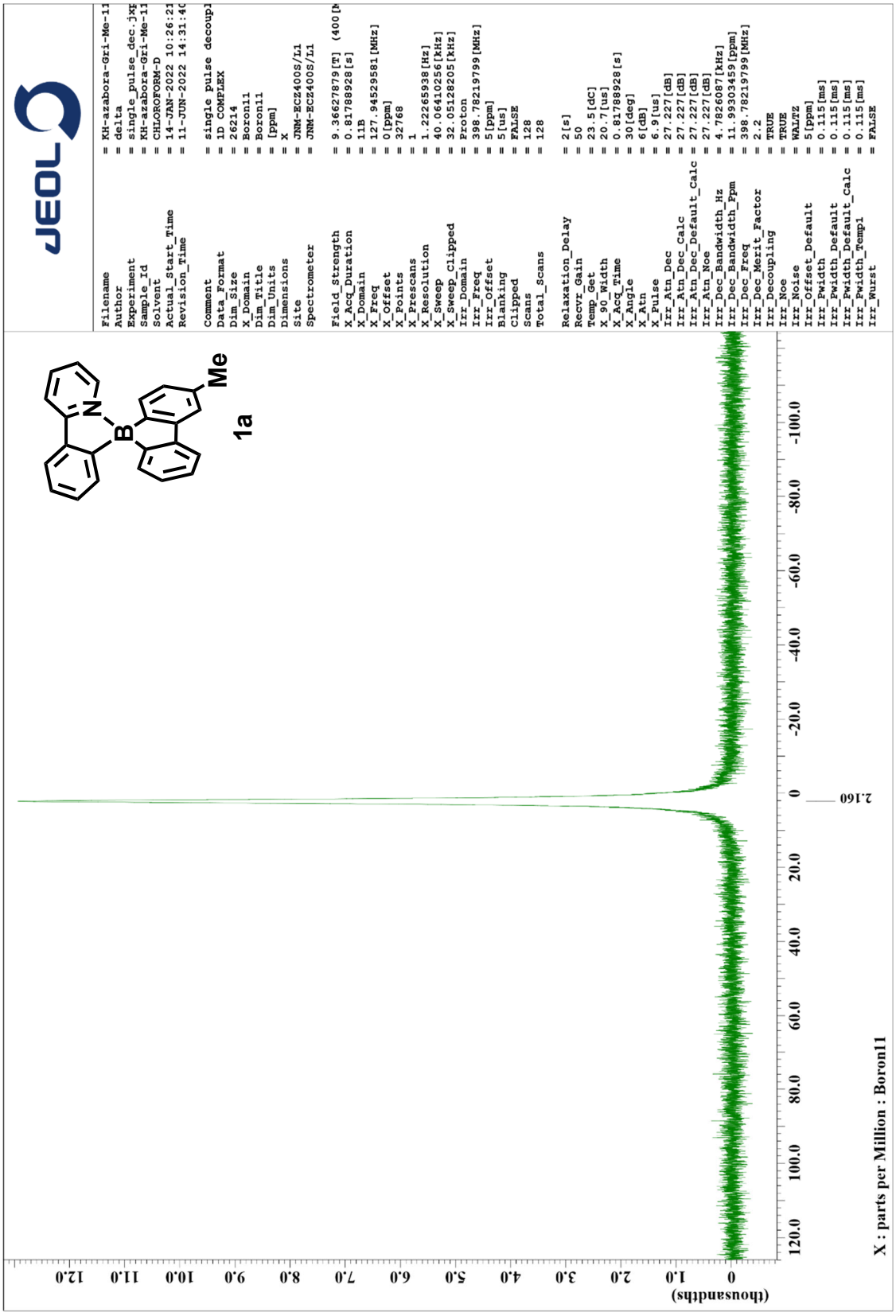

^{1}H NMR Spectrum of 1b (400 MHz, $CDCl_3$, rt)

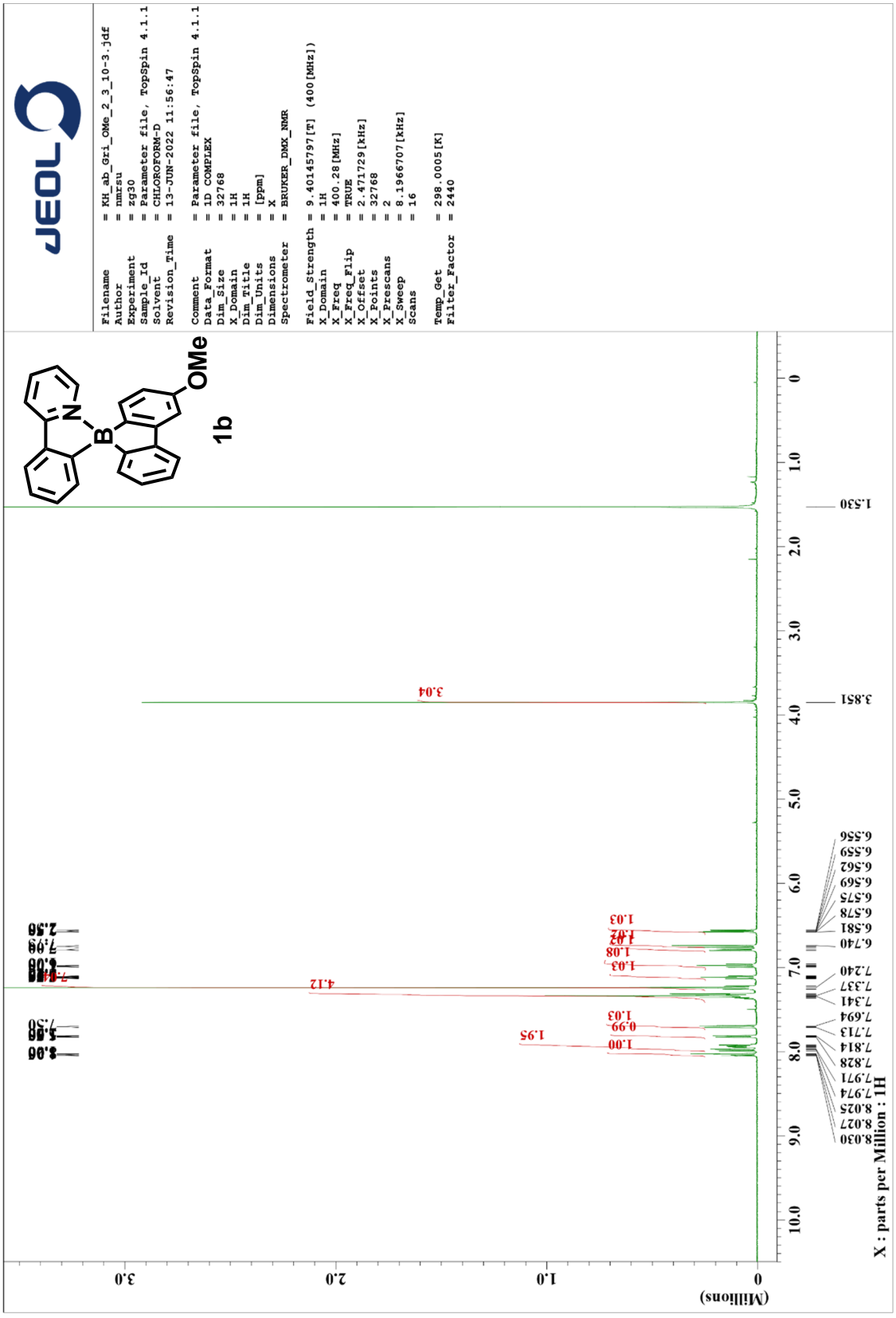

^{13}C NMR Spectrum of 1b (100 MHz, $CDCl_3$, rt)

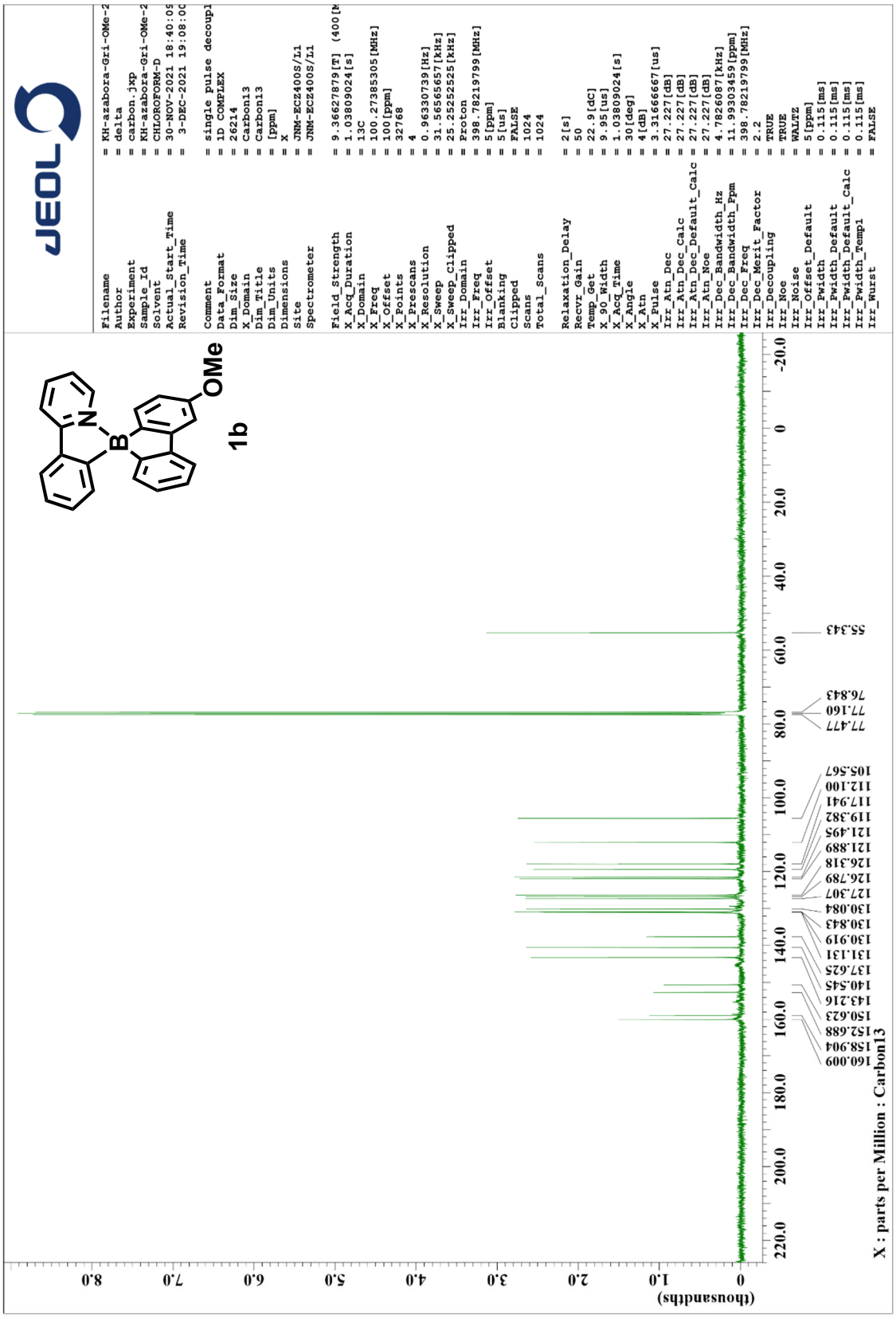

^{11}B NMR Spectrum of 1b (128 MHz, $CDCl_3$, rt)

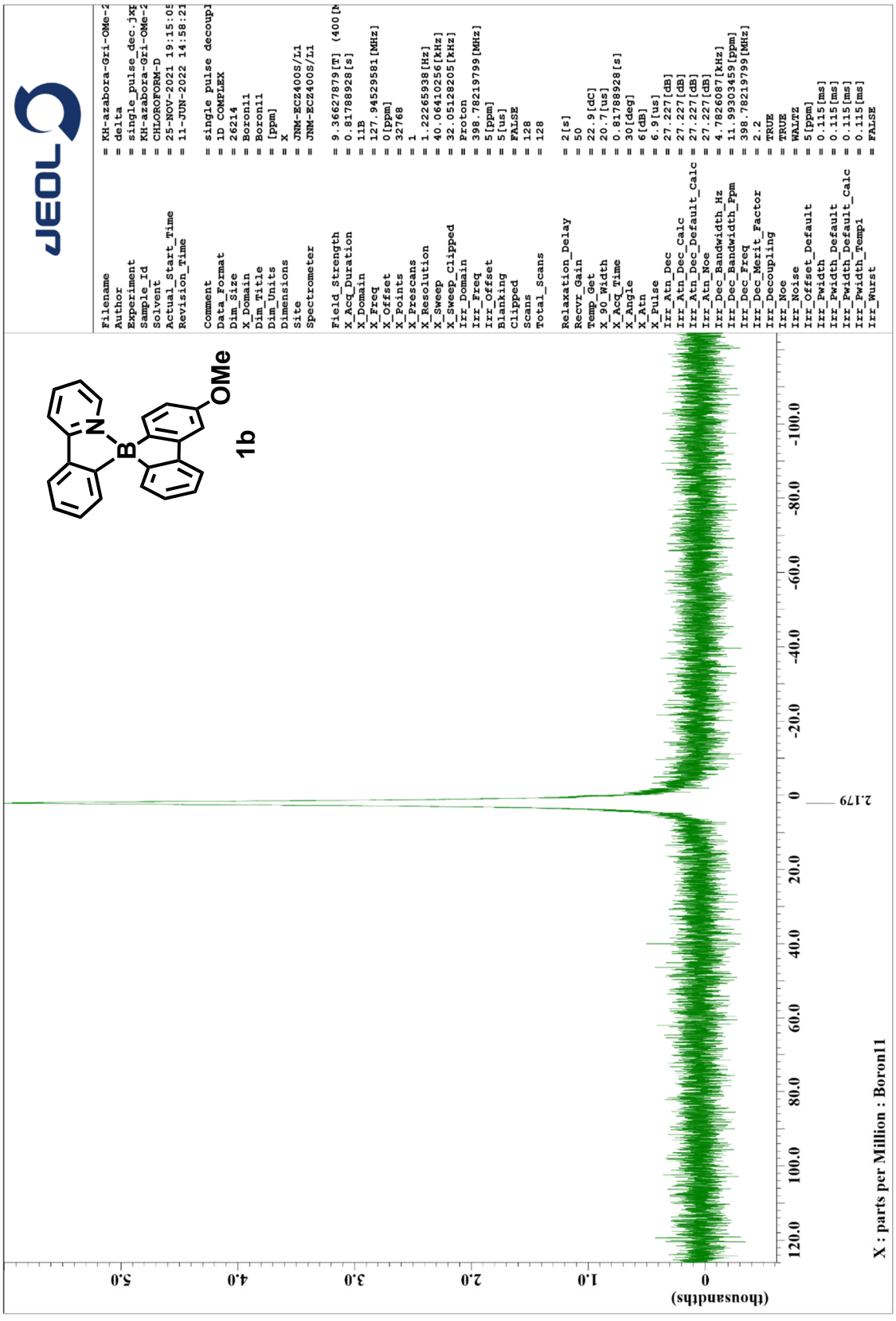

^{1}H NMR Spectrum of 1c (400 MHz, $CDCl_3$, rt)

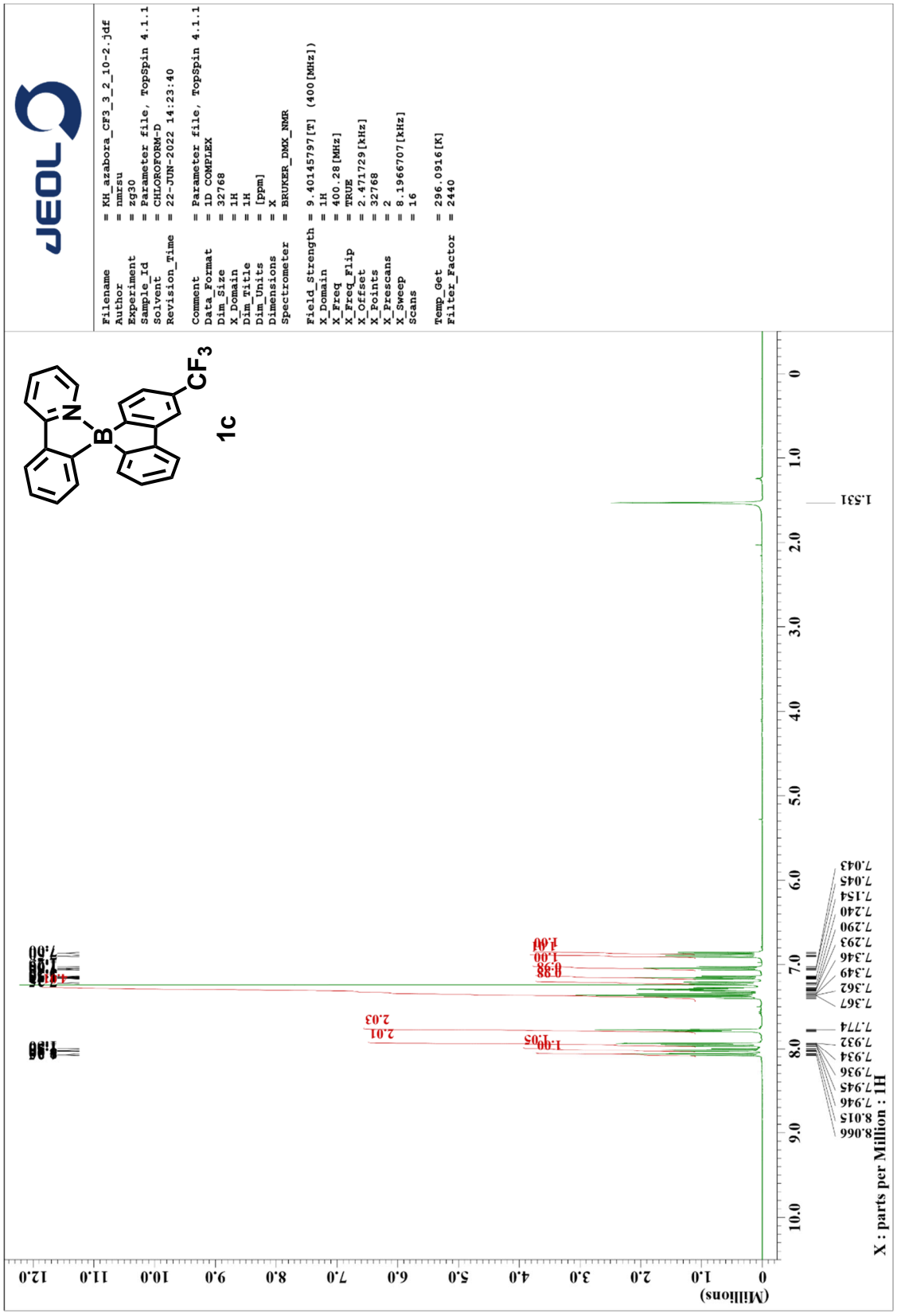

^{13}C NMR Spectrum of 1c (100 MHz, $CDCl_3$, rt)

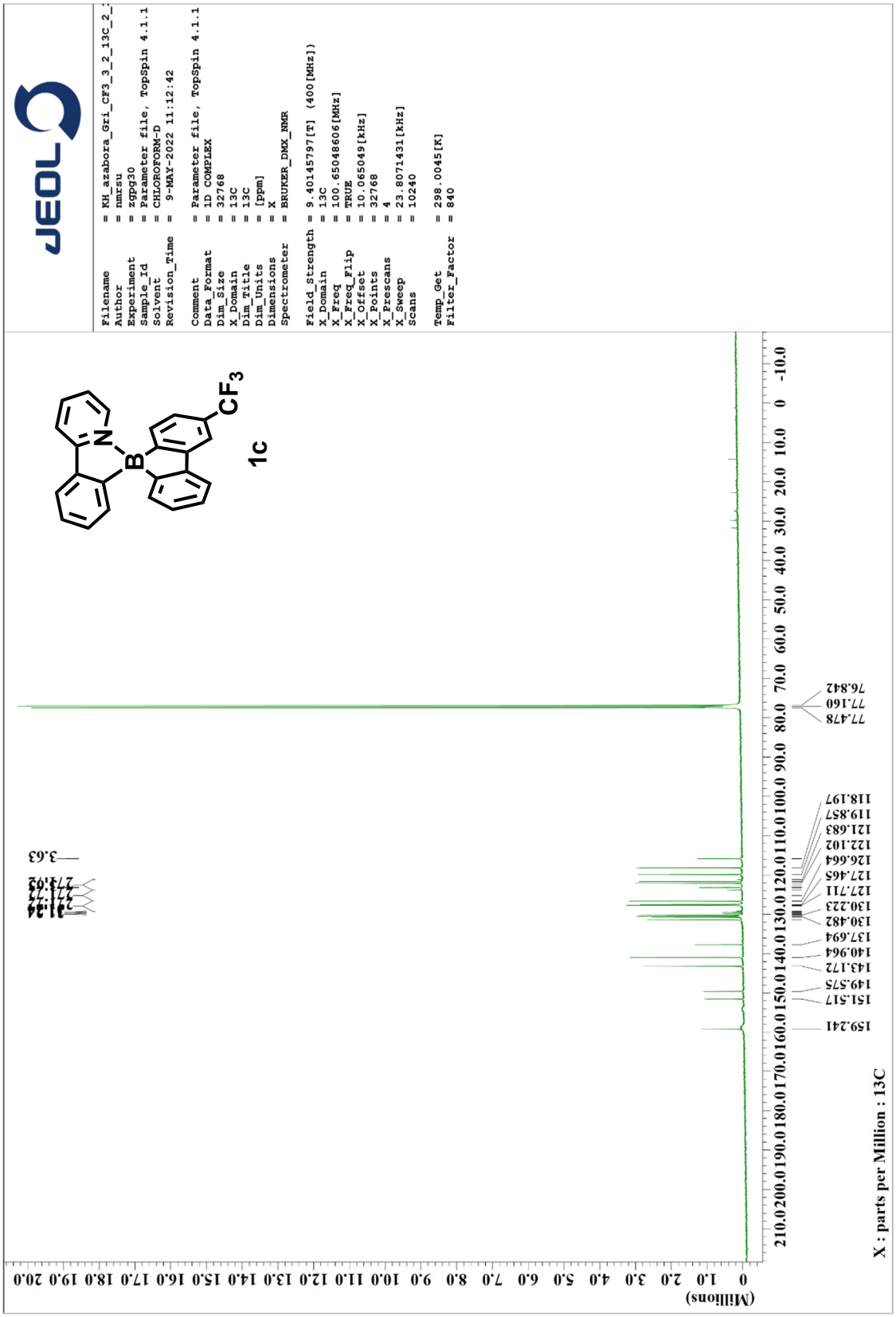

^{11}B NMR Spectrum of 1c (128 MHz, $CDCl_3$, rt)

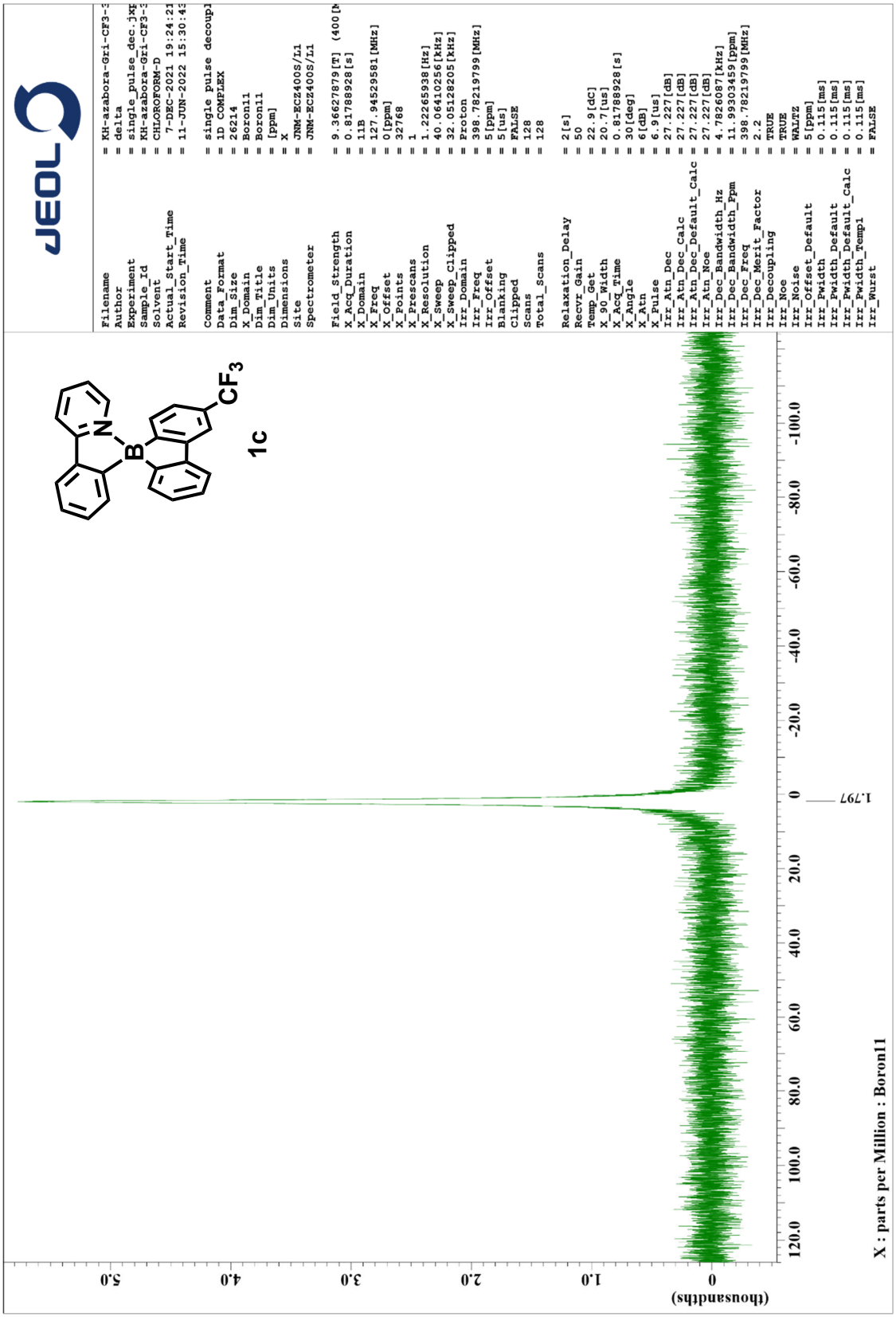

^{19}F NMR Spectrum of 1c (375 MHz, $CDCl_3$, rt)

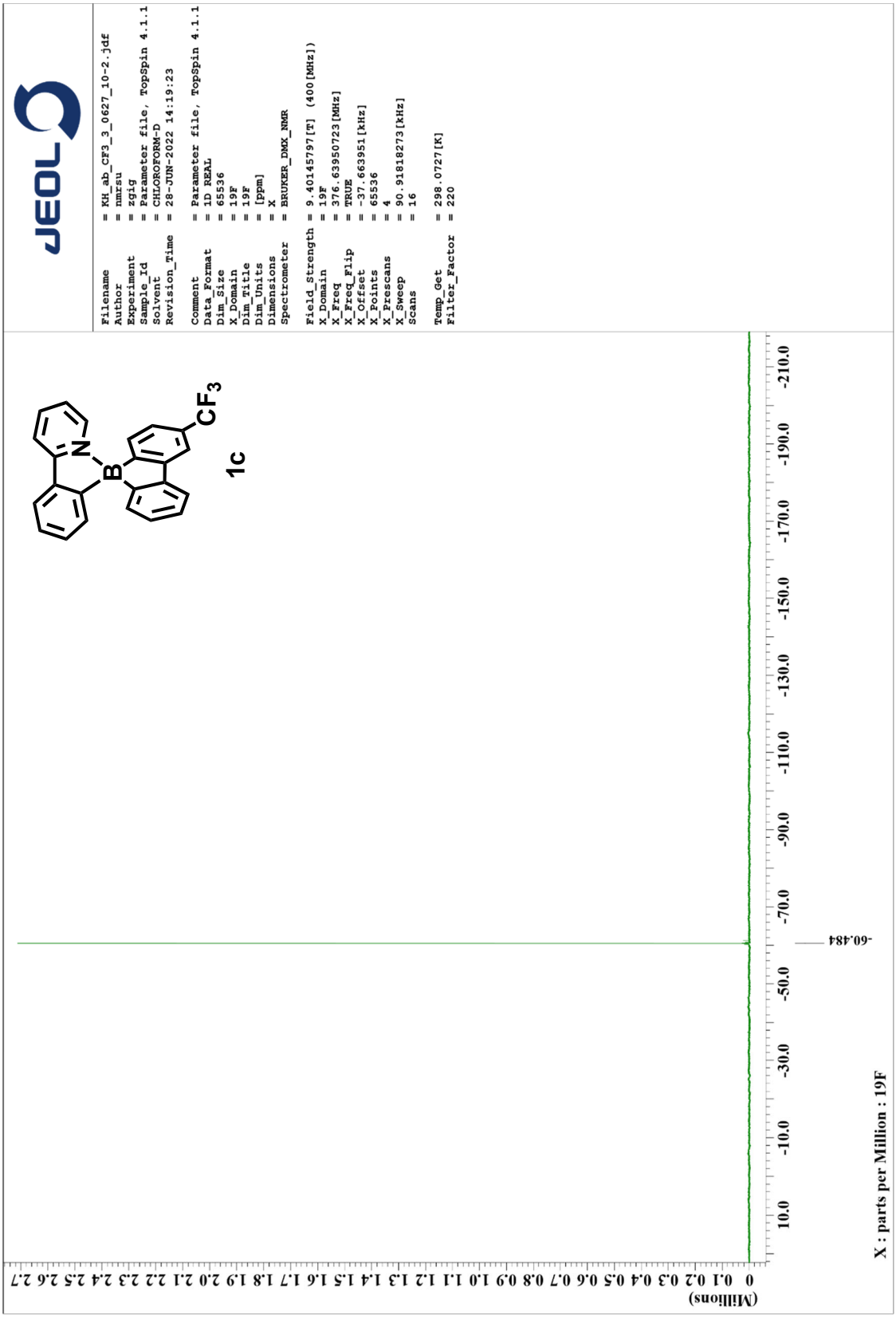

^{1}H NMR Spectrum of 1d (400 MHz, $CDCl_3$, rt)

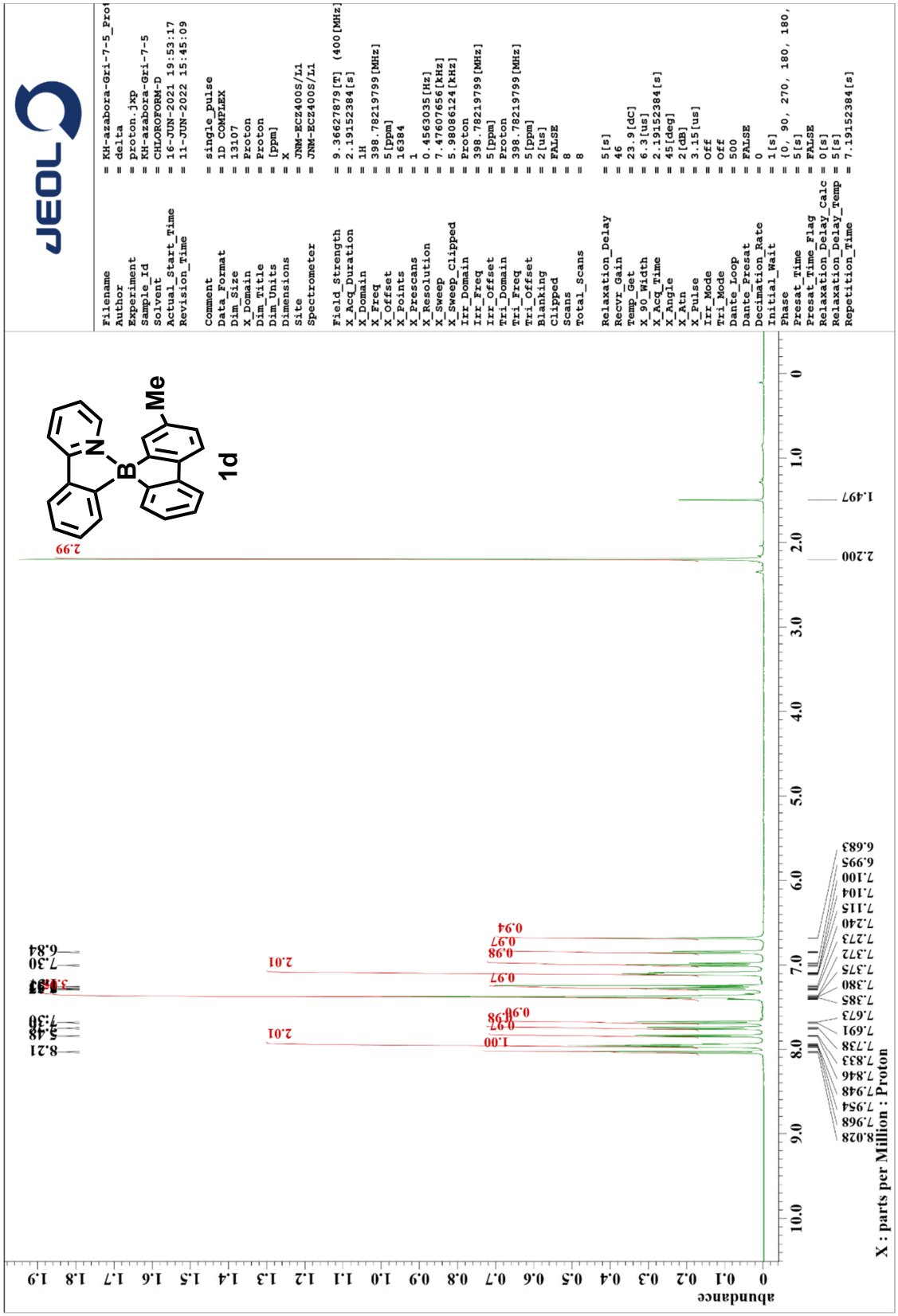

^{13}C NMR Spectrum of 1d (100 MHz, $CDCl_3$, rt)

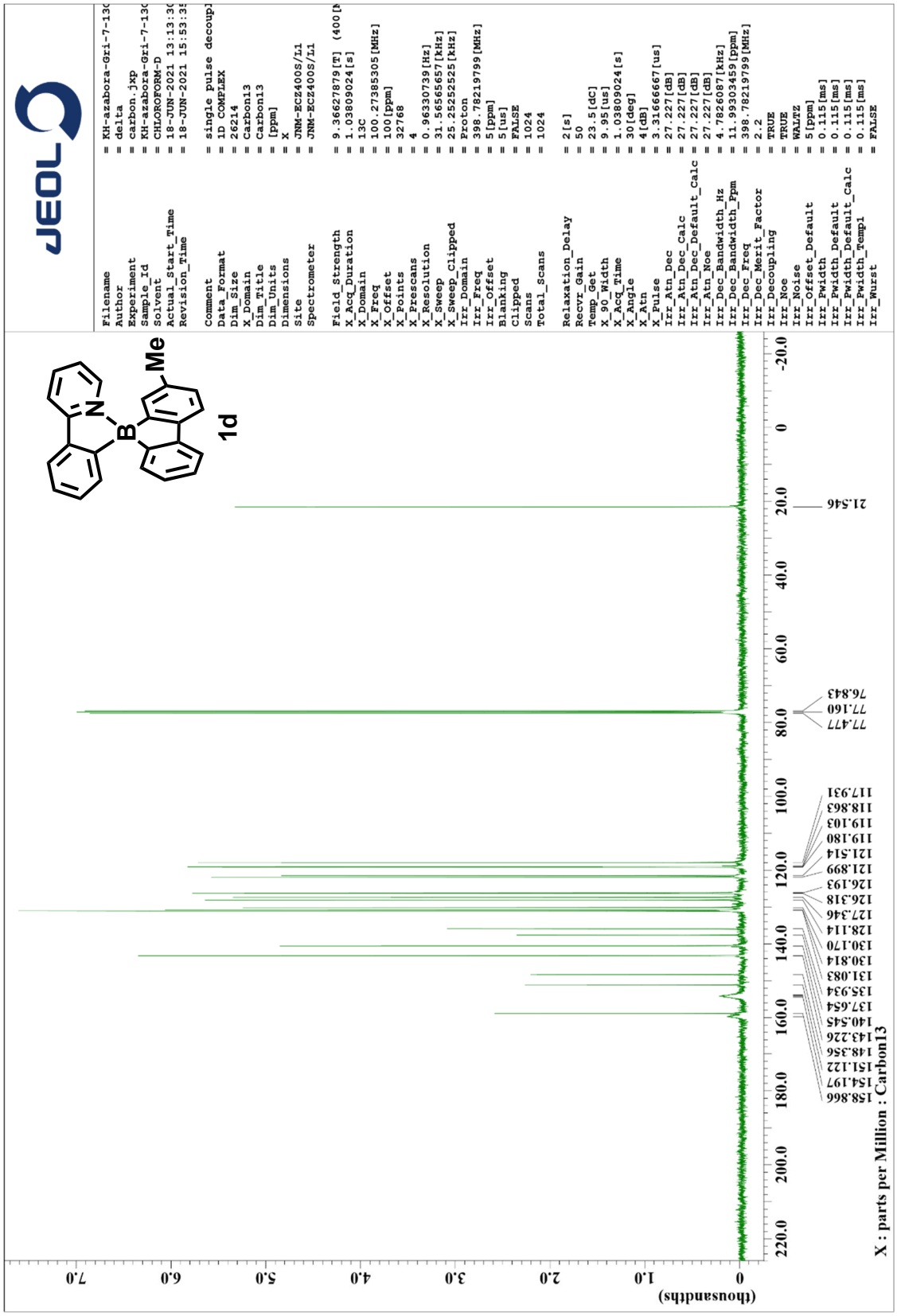

^{11}B NMR Spectrum of 1d (128 MHz, $CDCl_3$, rt)

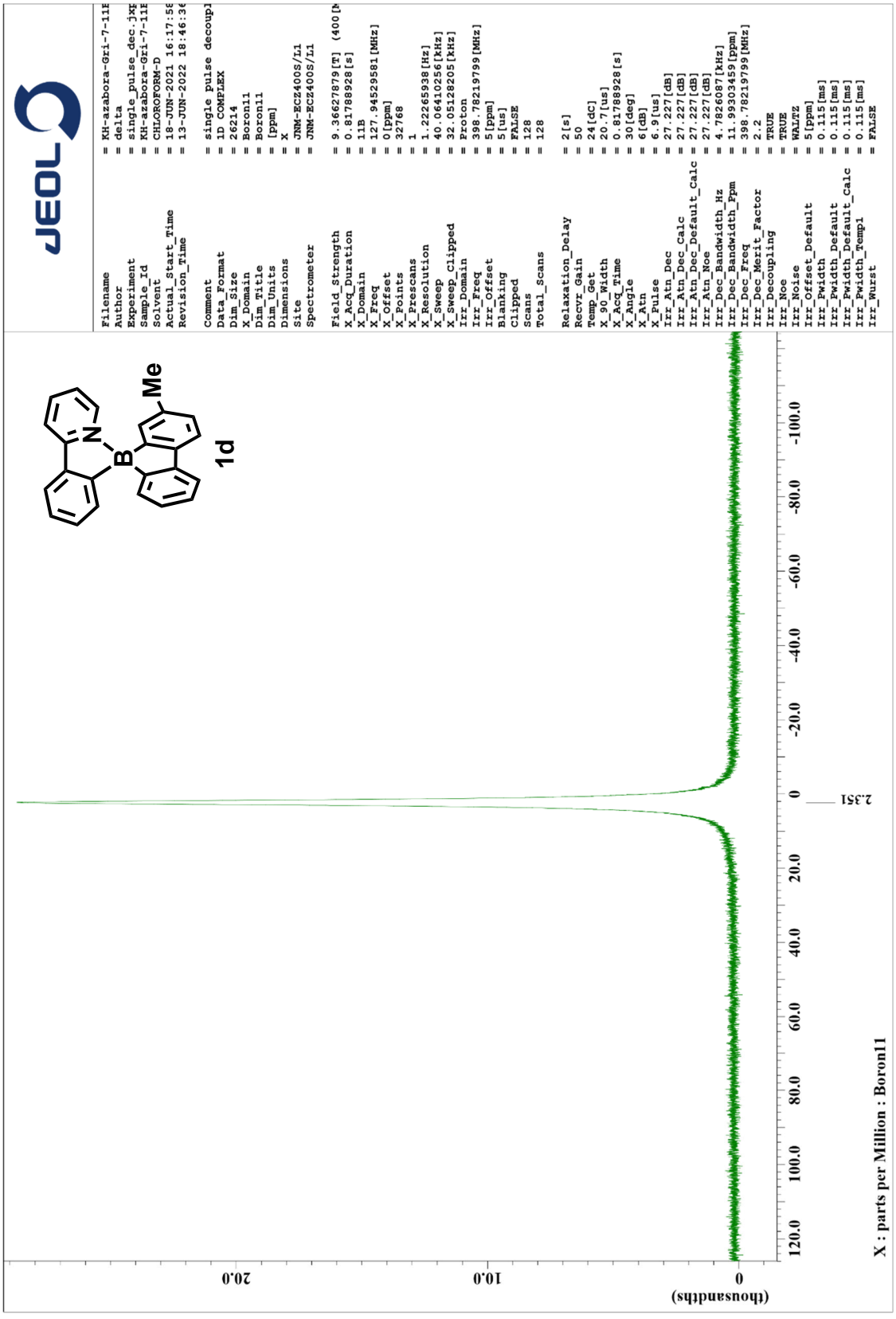

^{1}H NMR Spectrum of 1e (400 MHz, $CDCl_3$, rt)

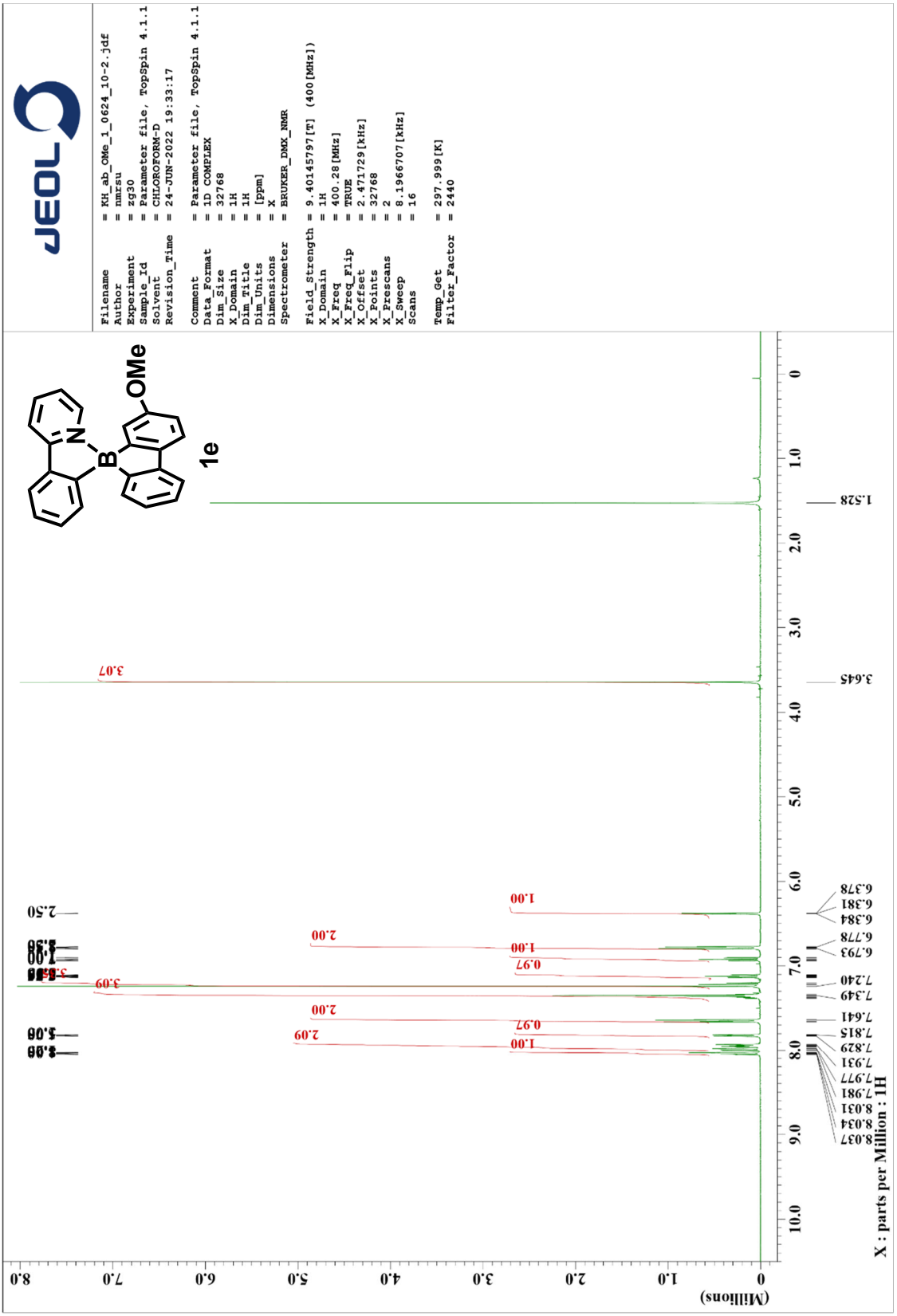

^{13}C NMR Spectrum of 1e (100 MHz, $CDCl_3$, rt)

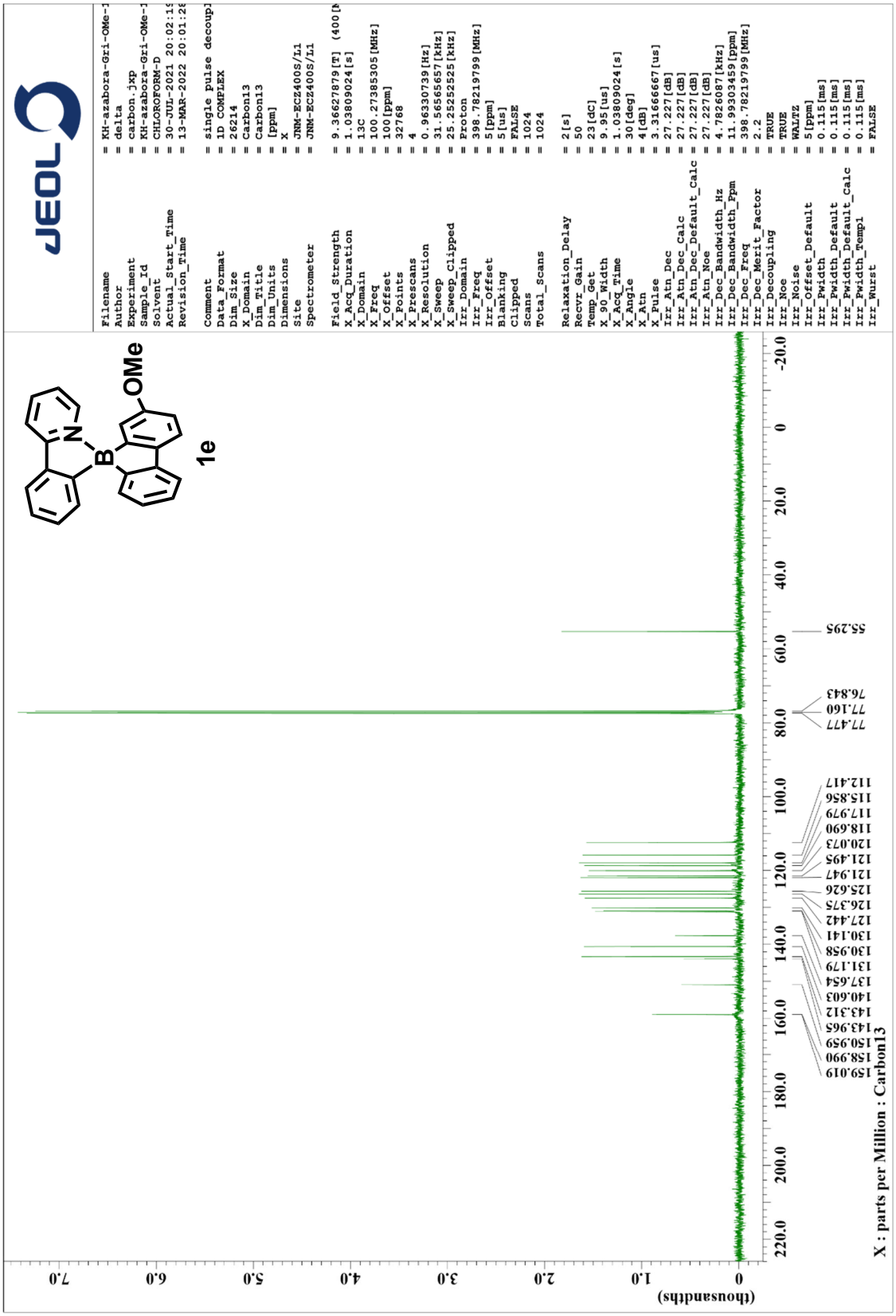

^{11}B NMR Spectrum of 1e (128 MHz, $CDCl_3$, rt)

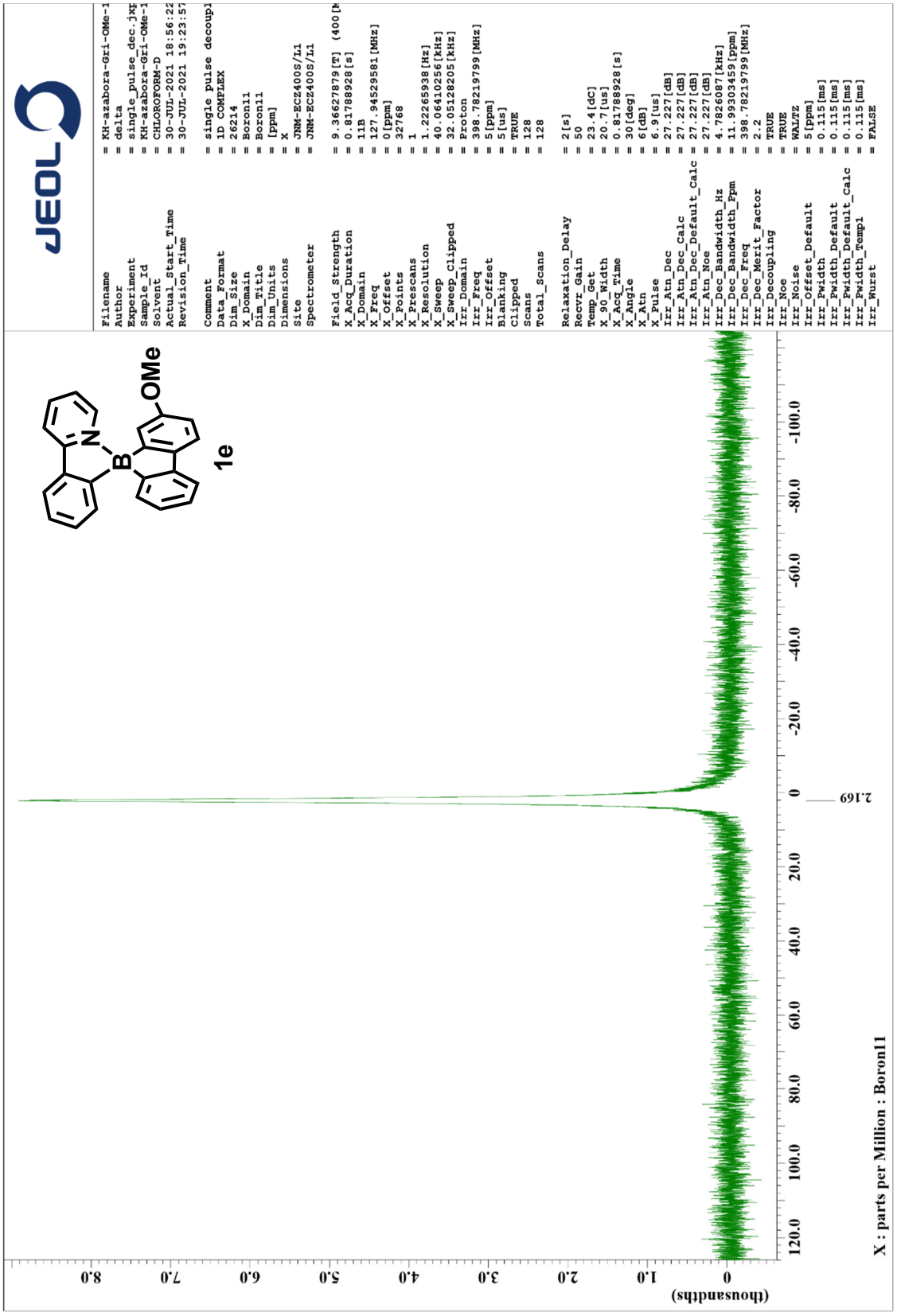

^{1}H NMR Spectrum of 1f (400 MHz, $CDCl_3$, rt)

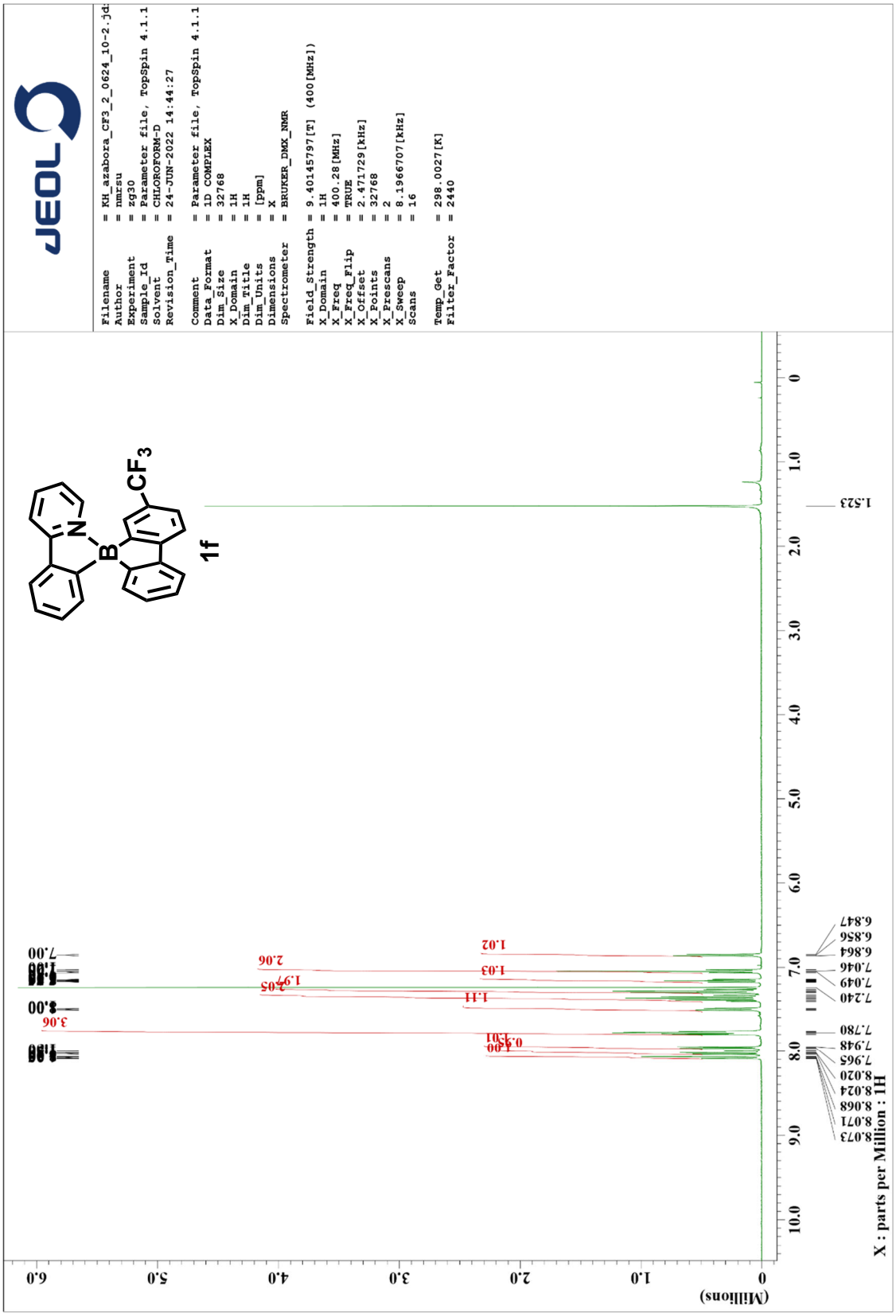

^{13}C NMR Spectrum of 1f (100 MHz, $CDCl_3$, rt)

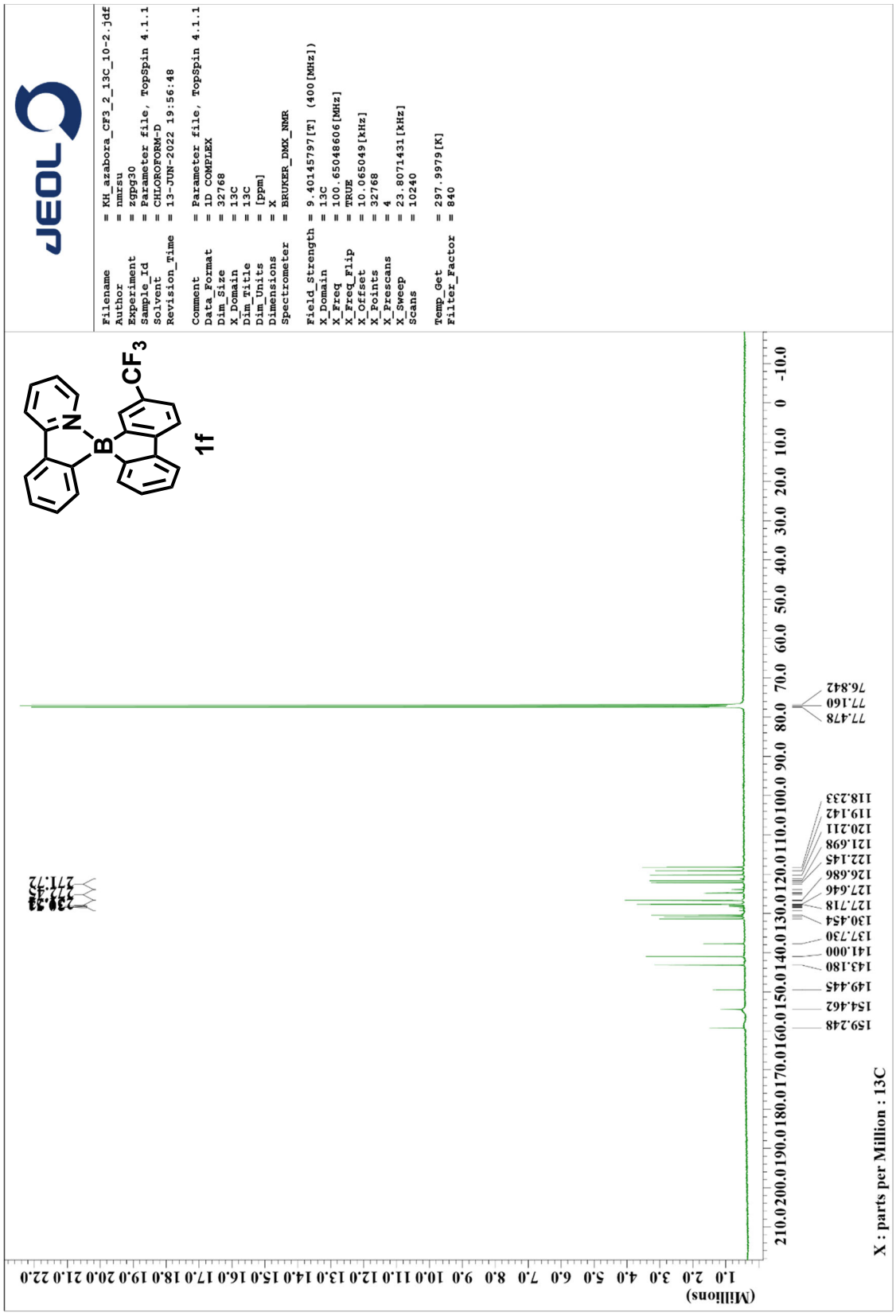

^{11}B NMR Spectrum of 1f (128 MHz, $CDCl_3$, rt)

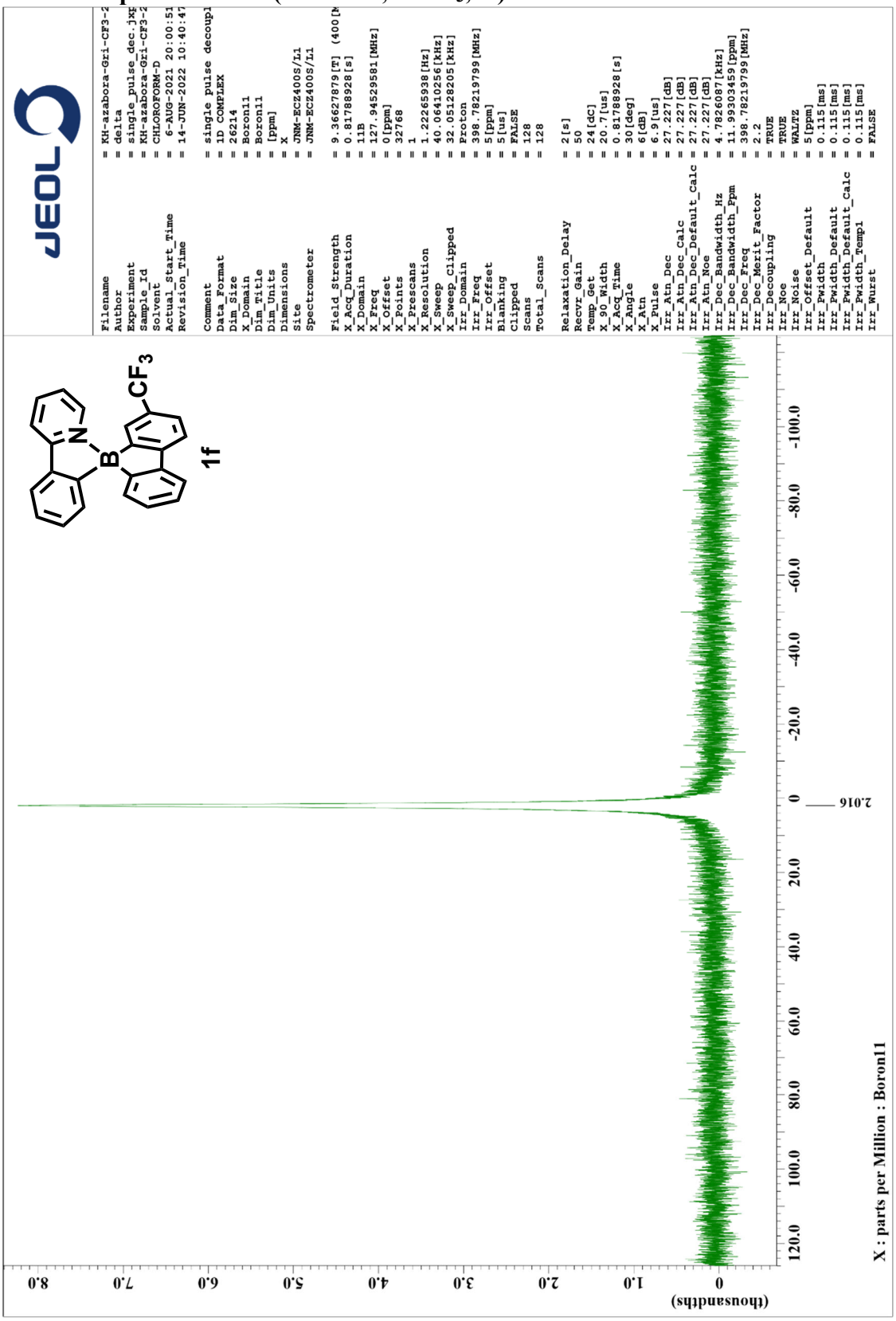

^{19}F NMR Spectrum of 1f (375 MHz, $CDCl_3$, rt)

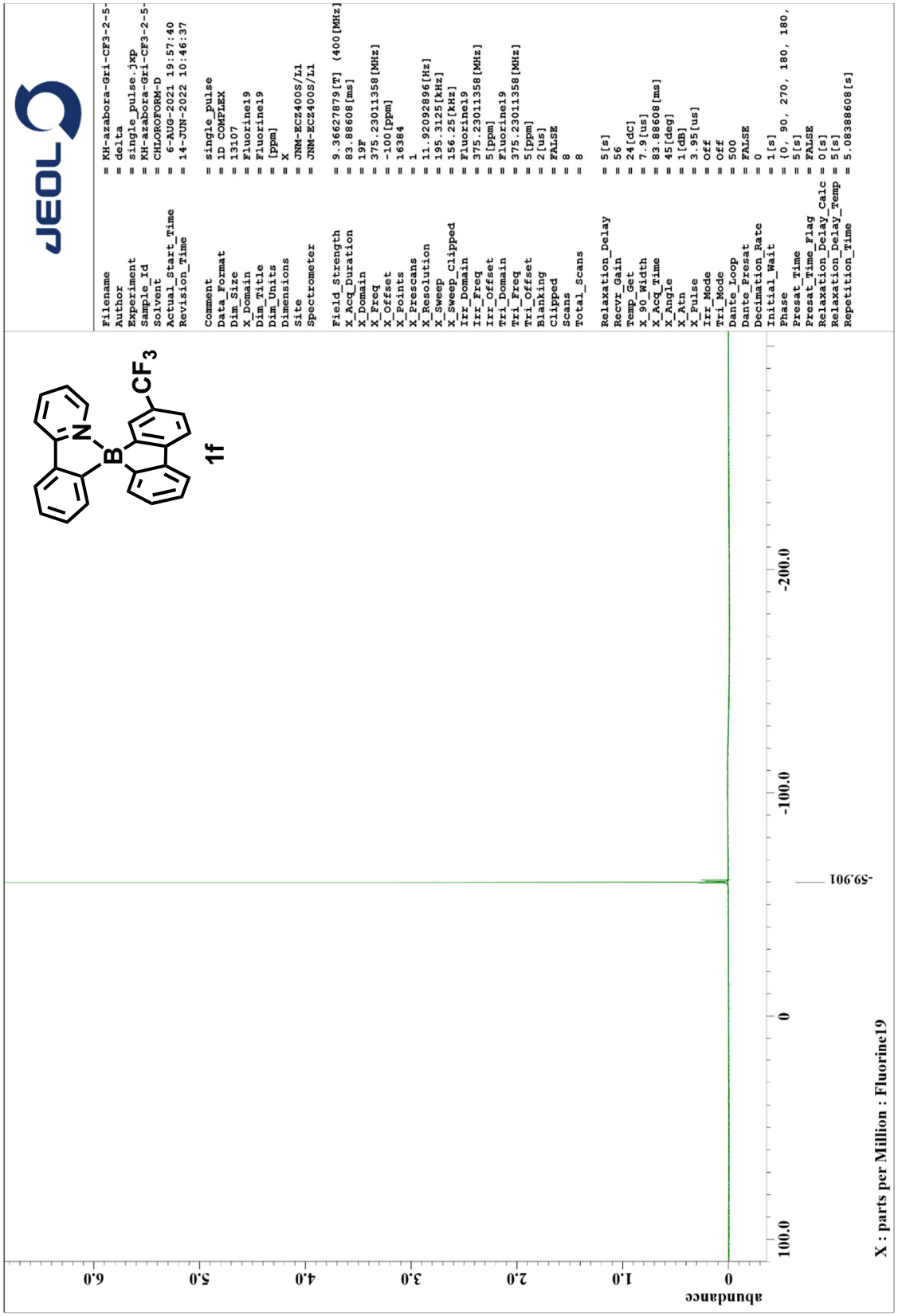

^{1}H NMR Spectrum of S7 (400 MHz, $CDCl_3$, rt)

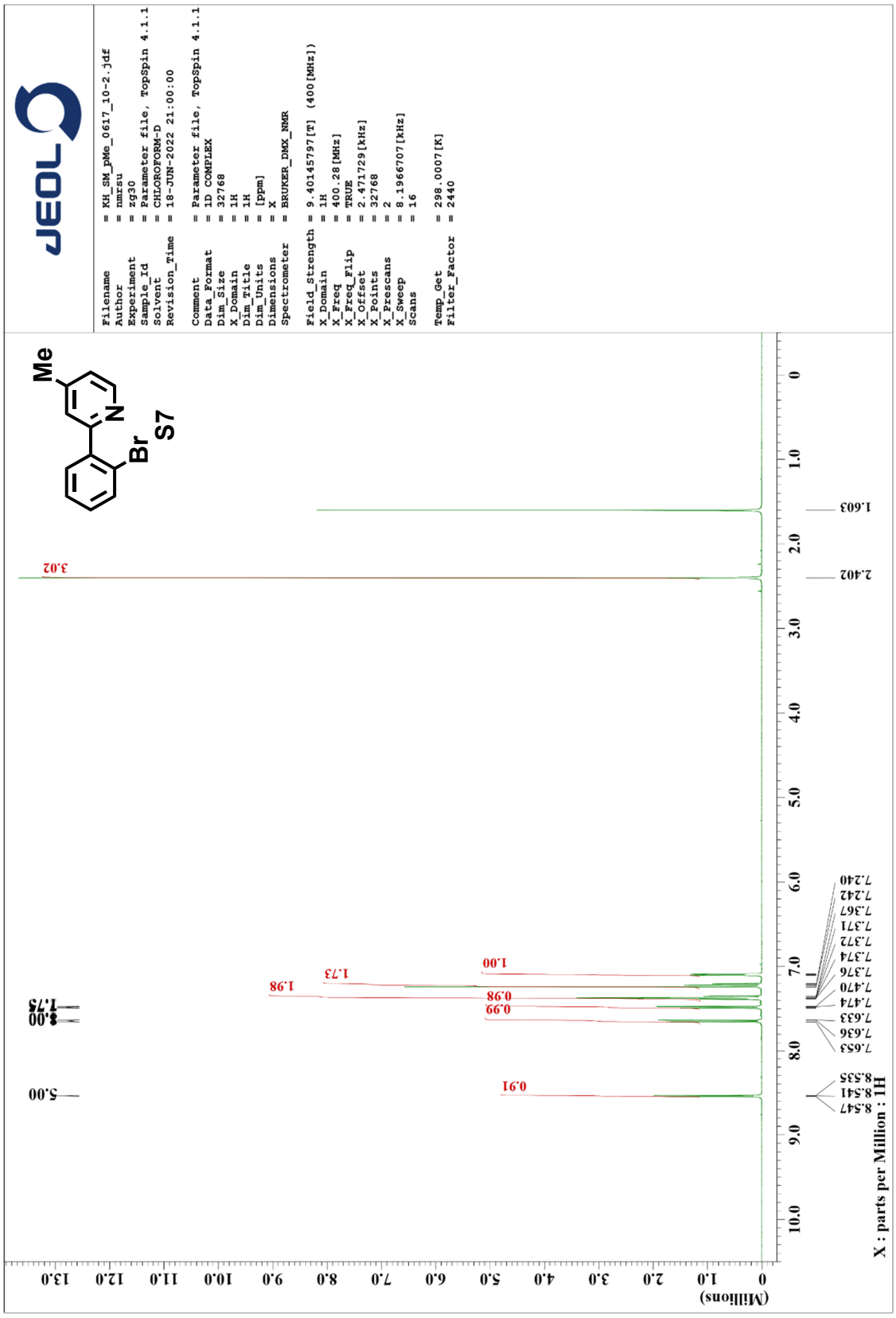

^{1}H NMR Spectrum of S8 (400 MHz, $CDCl_3$, rt)

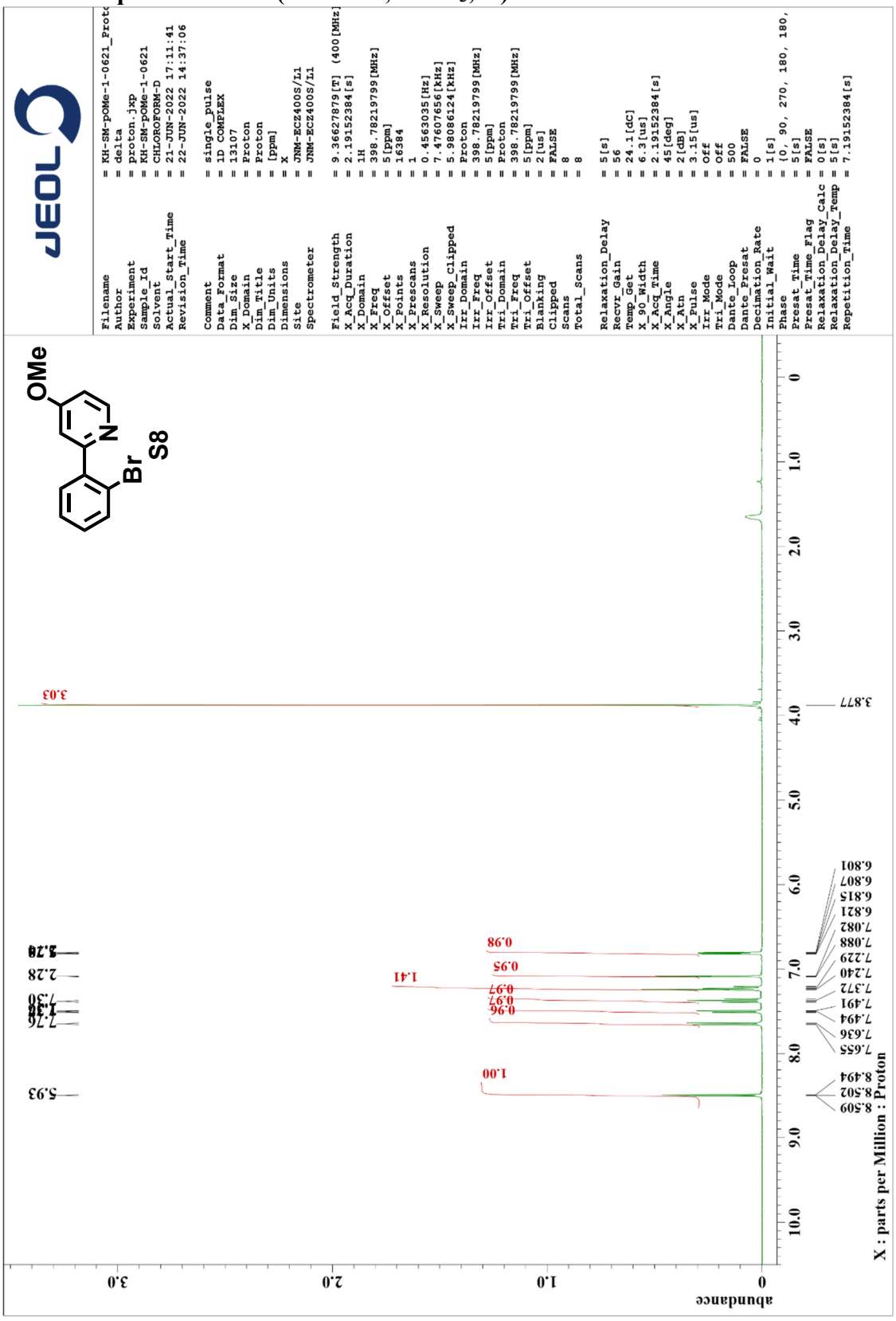

^{13}C NMR Spectrum of S8 (100 MHz, $CDCl_3$, rt)

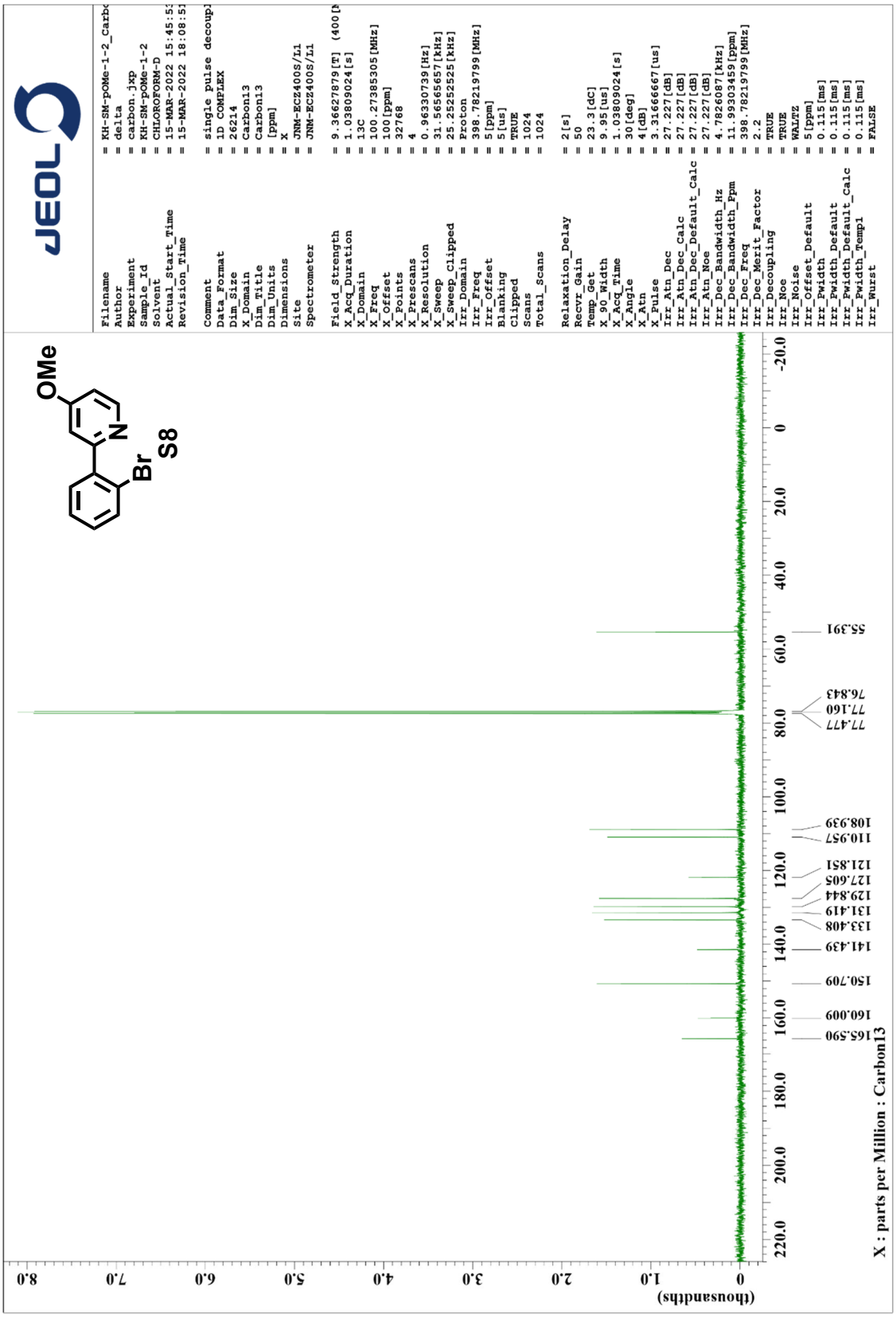

^{1}H NMR Spectrum of S9 (400 MHz, $CDCl_3$, rt)

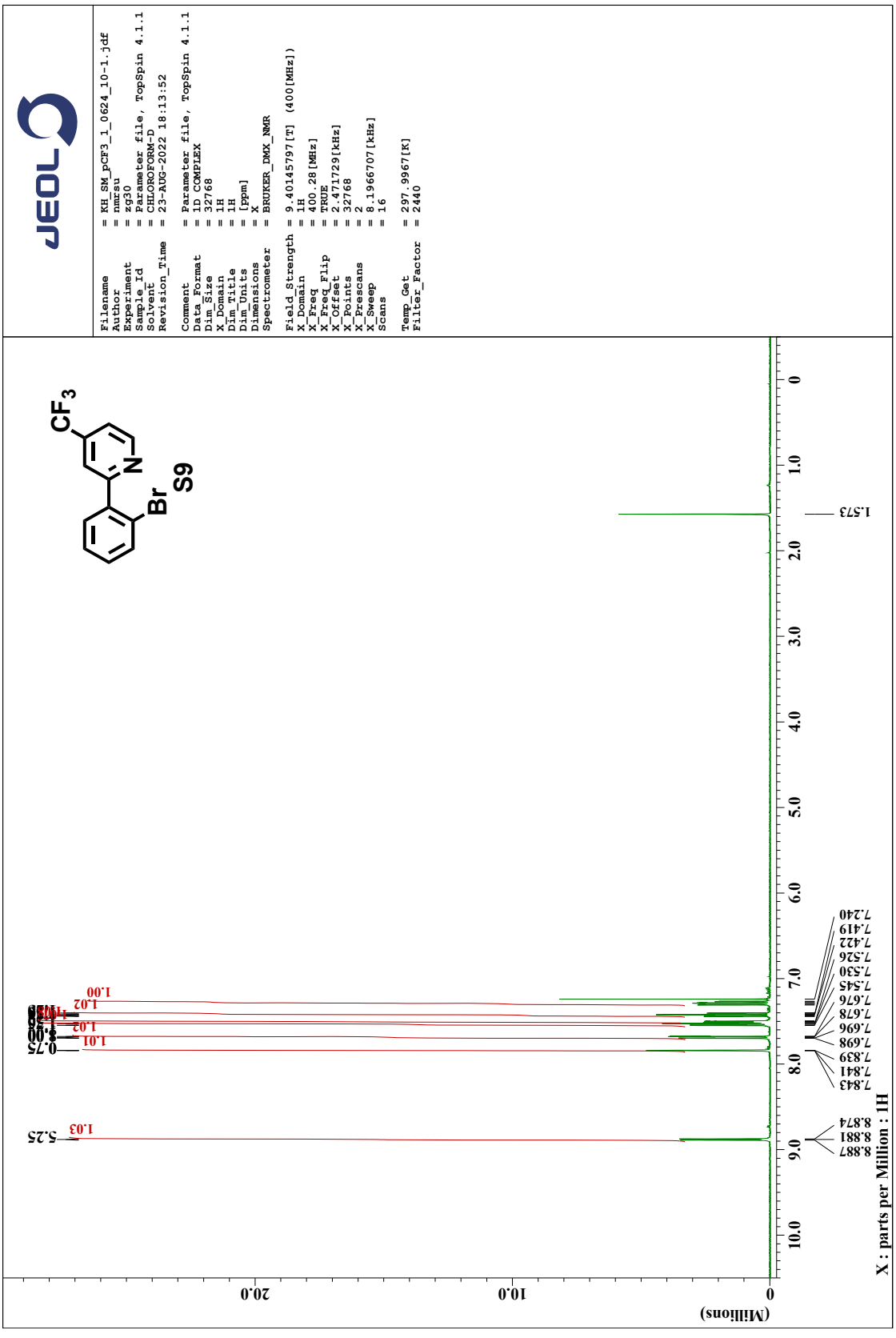

^{13}C NMR Spectrum of S9 (100 MHz, $CDCl_3$, rt)

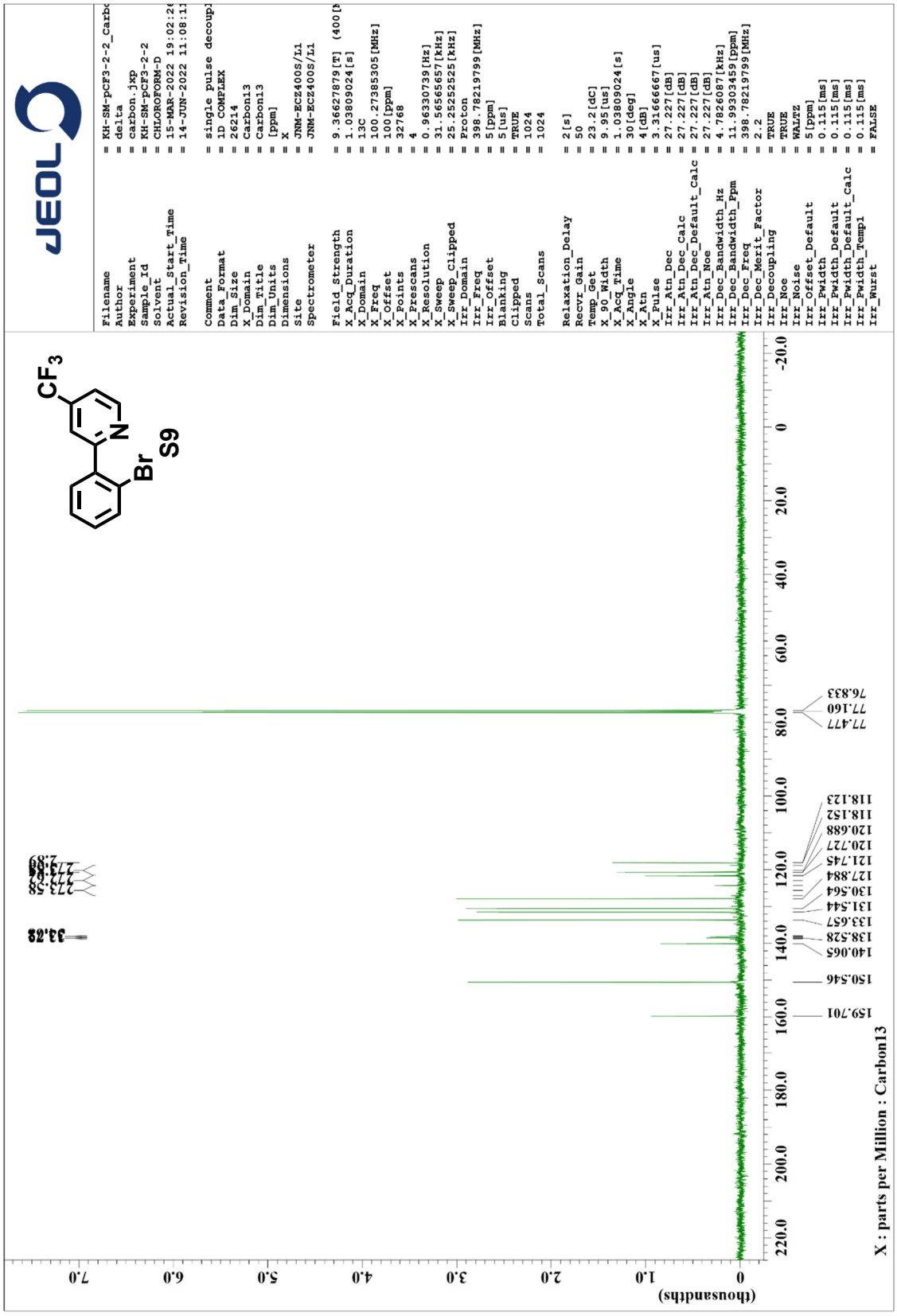

^{19}F NMR Spectrum of S9 (375 MHz, $CDCl_3$, rt)

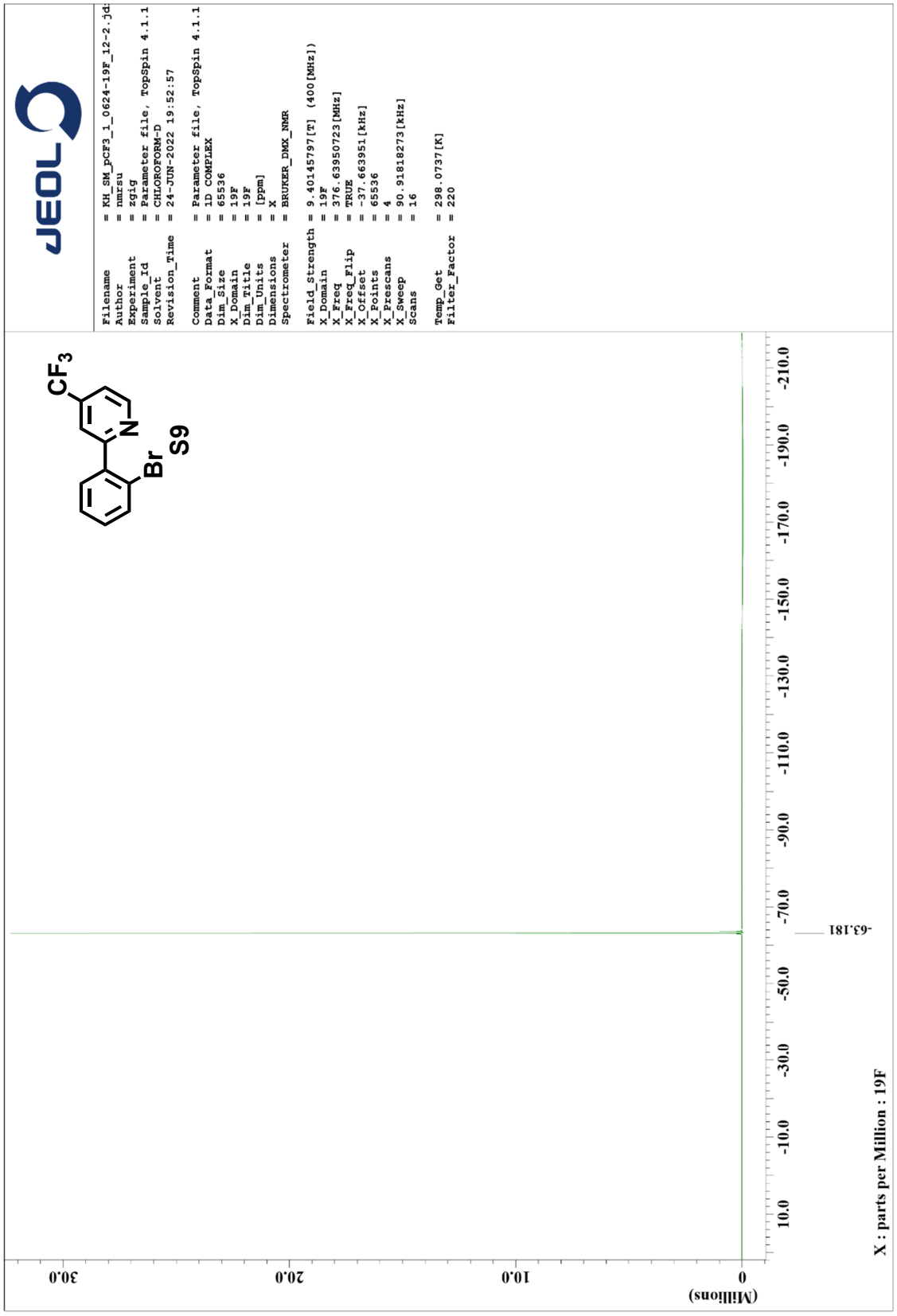

^{1}H NMR Spectrum of 1g (400 MHz, $CDCl_3$, rt)

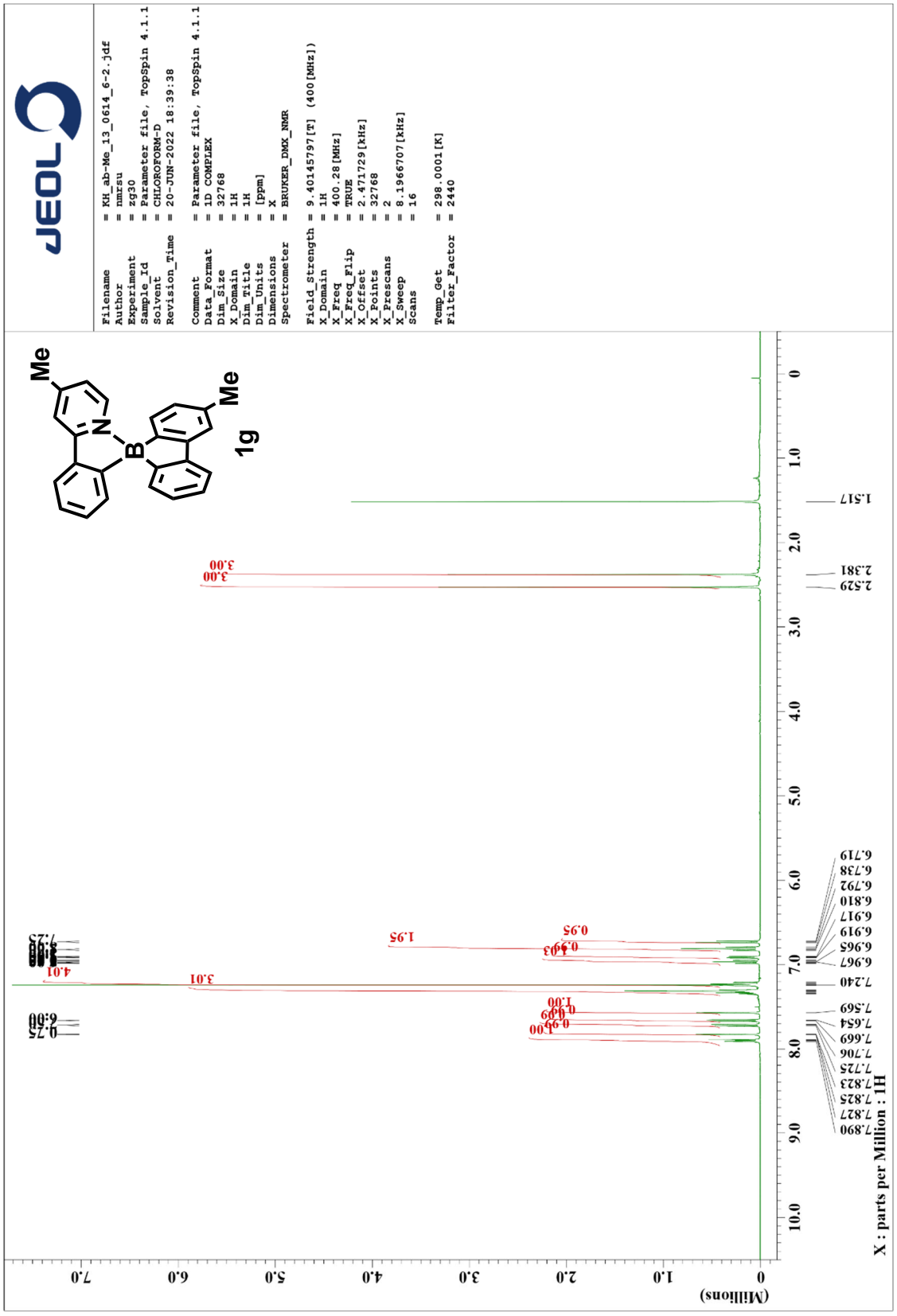

^{13}C NMR Spectrum of 1g (100 MHz, $CDCl_3$, rt)

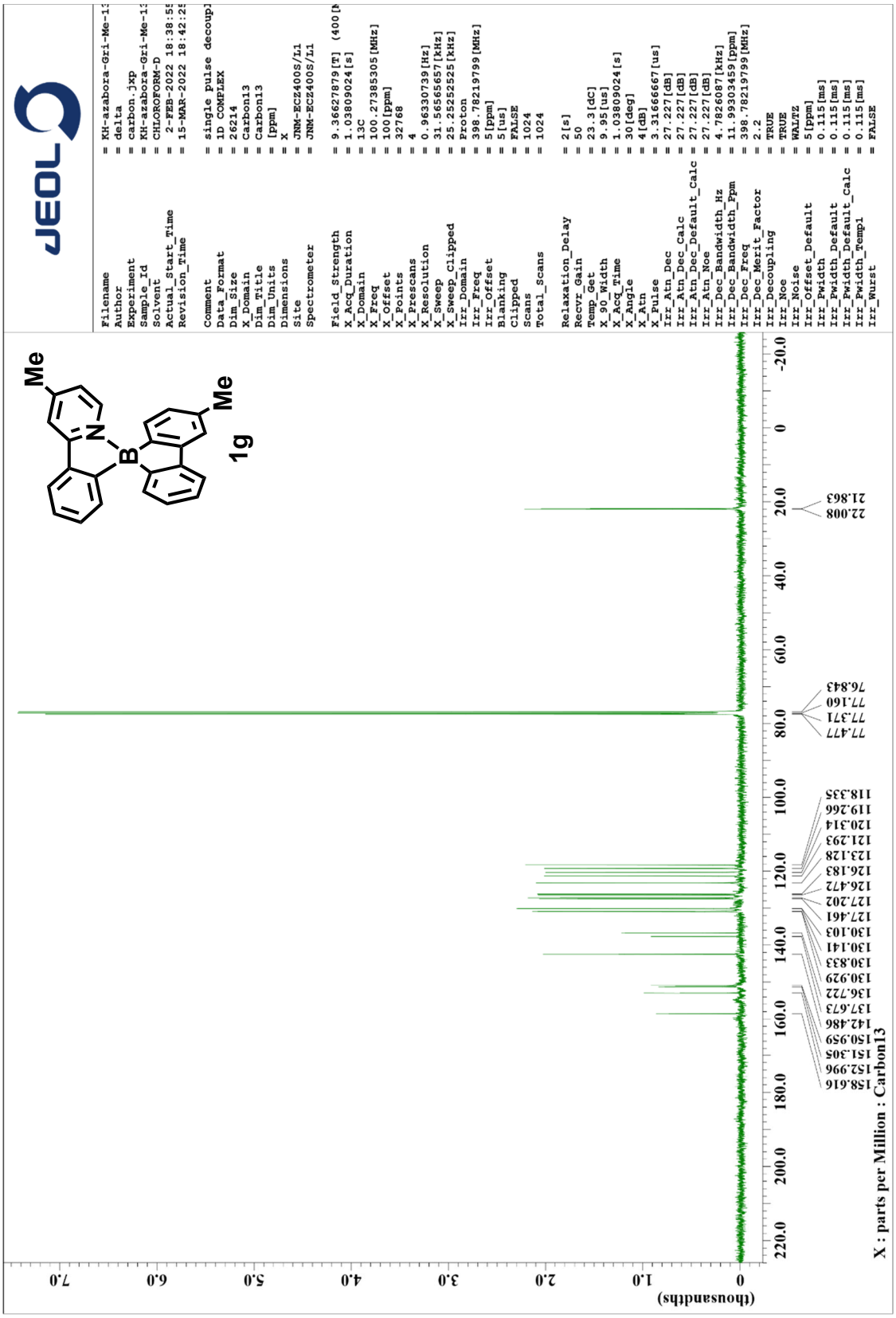

^{11}B NMR Spectrum of 1g (128 MHz, $CDCl_3$, rt)

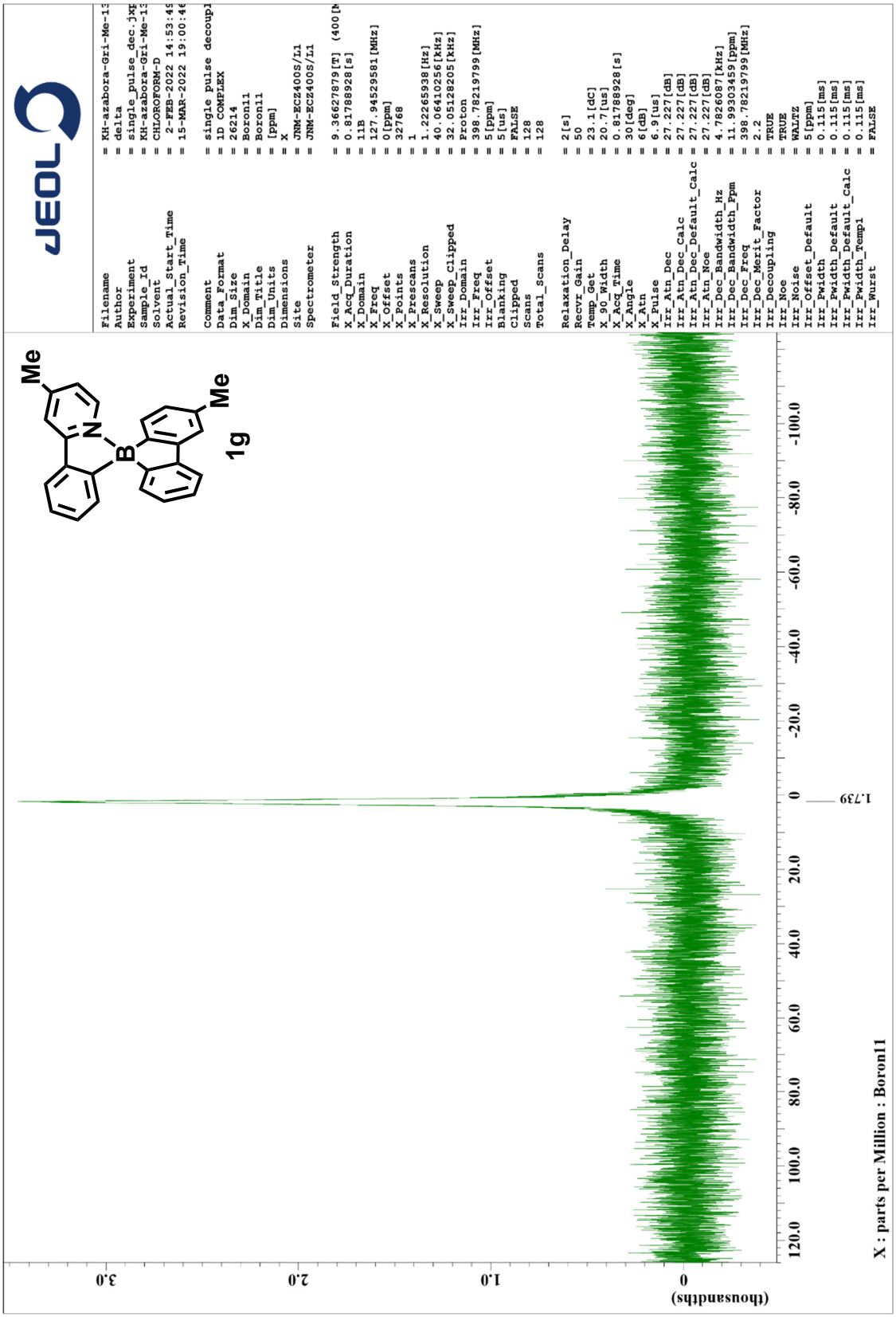

^{1}H NMR Spectrum of 1h (400 MHz, $CDCl_3$, rt)

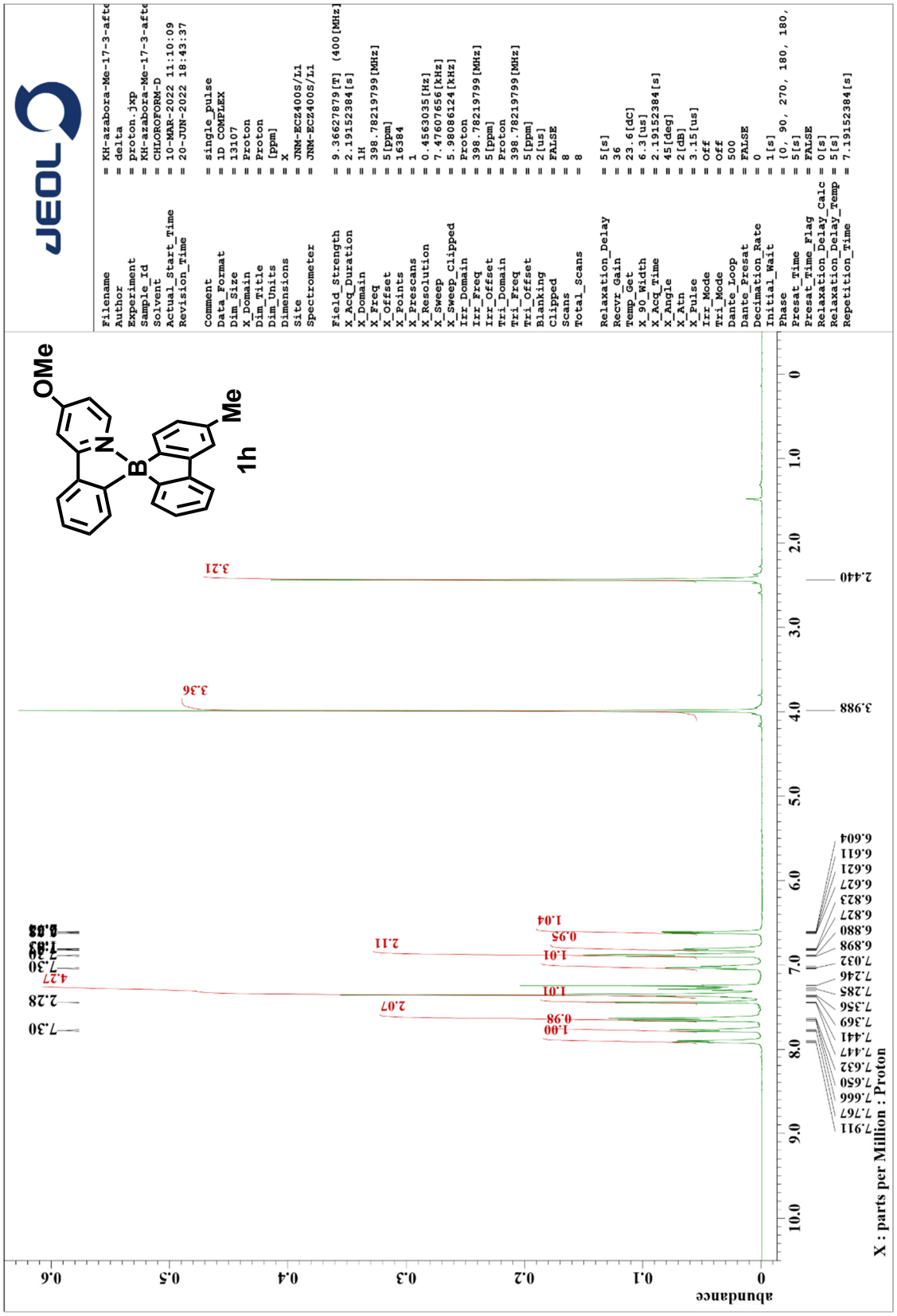

^{13}C NMR Spectrum of 1h (100 MHz, $CDCl_3$, rt)

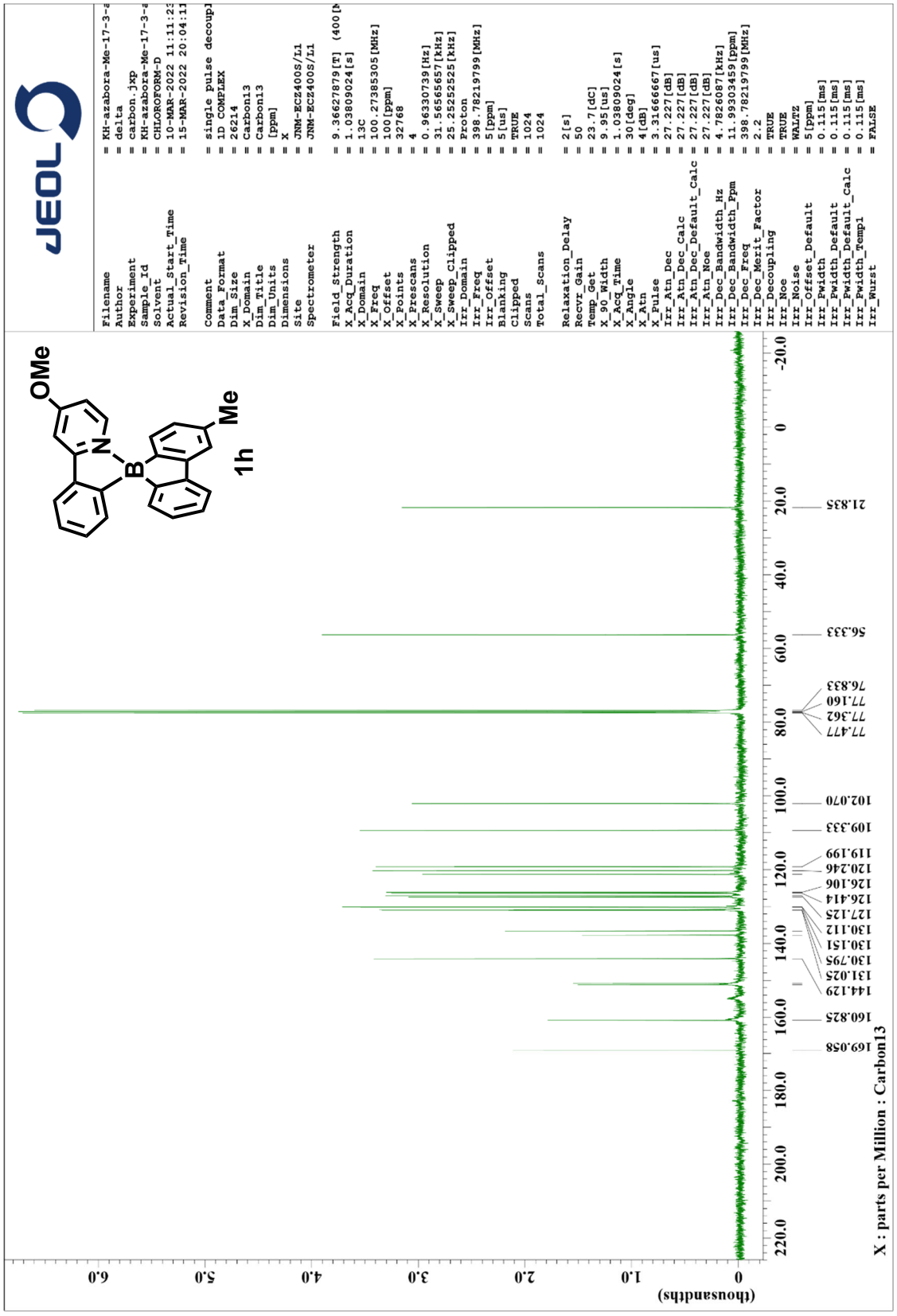

^{11}B NMR Spectrum of 1h (128 MHz, $CDCl_3$, rt)

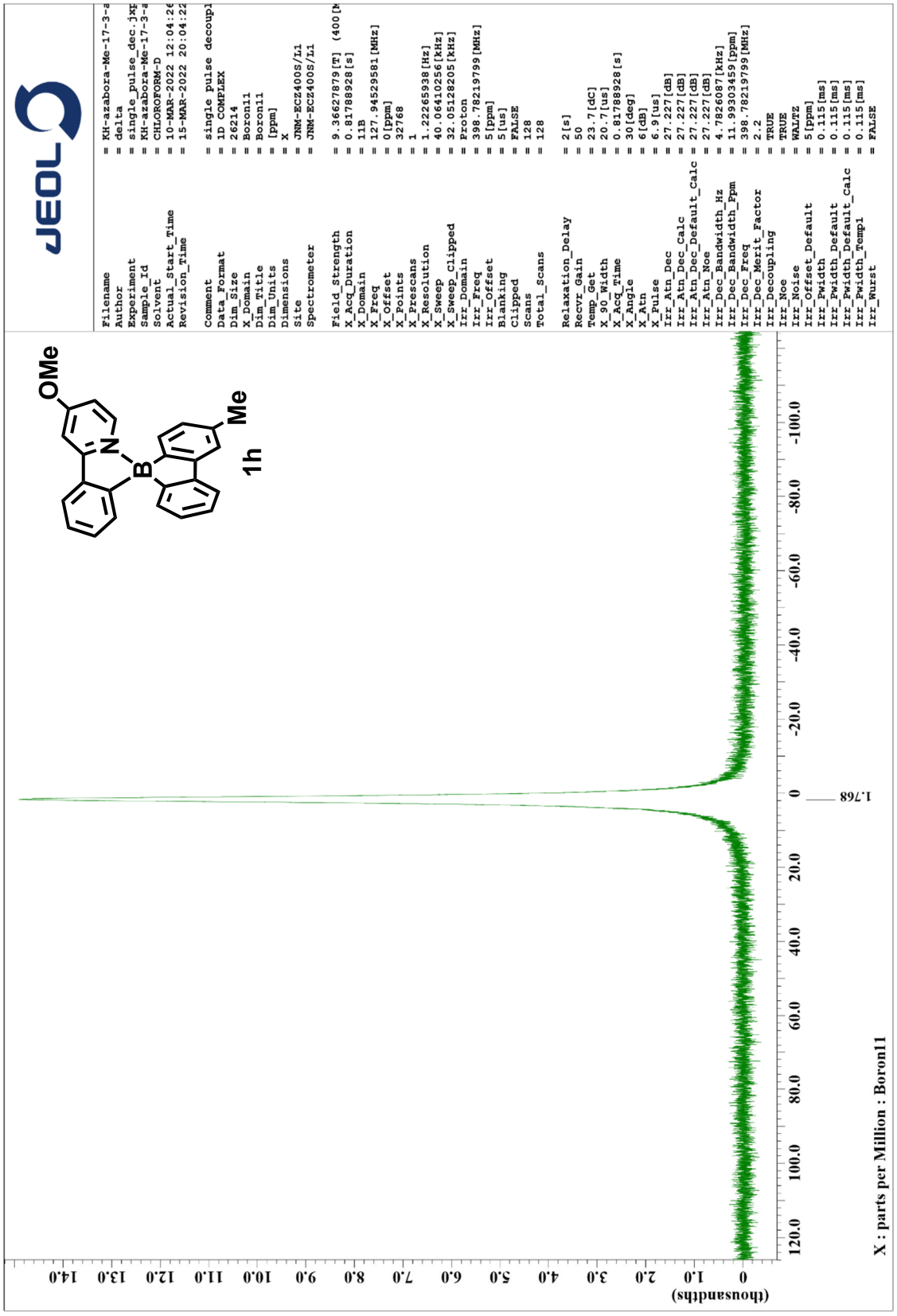

^{1}H NMR Spectrum of 1i (400 MHz, $CDCl_3$, rt)

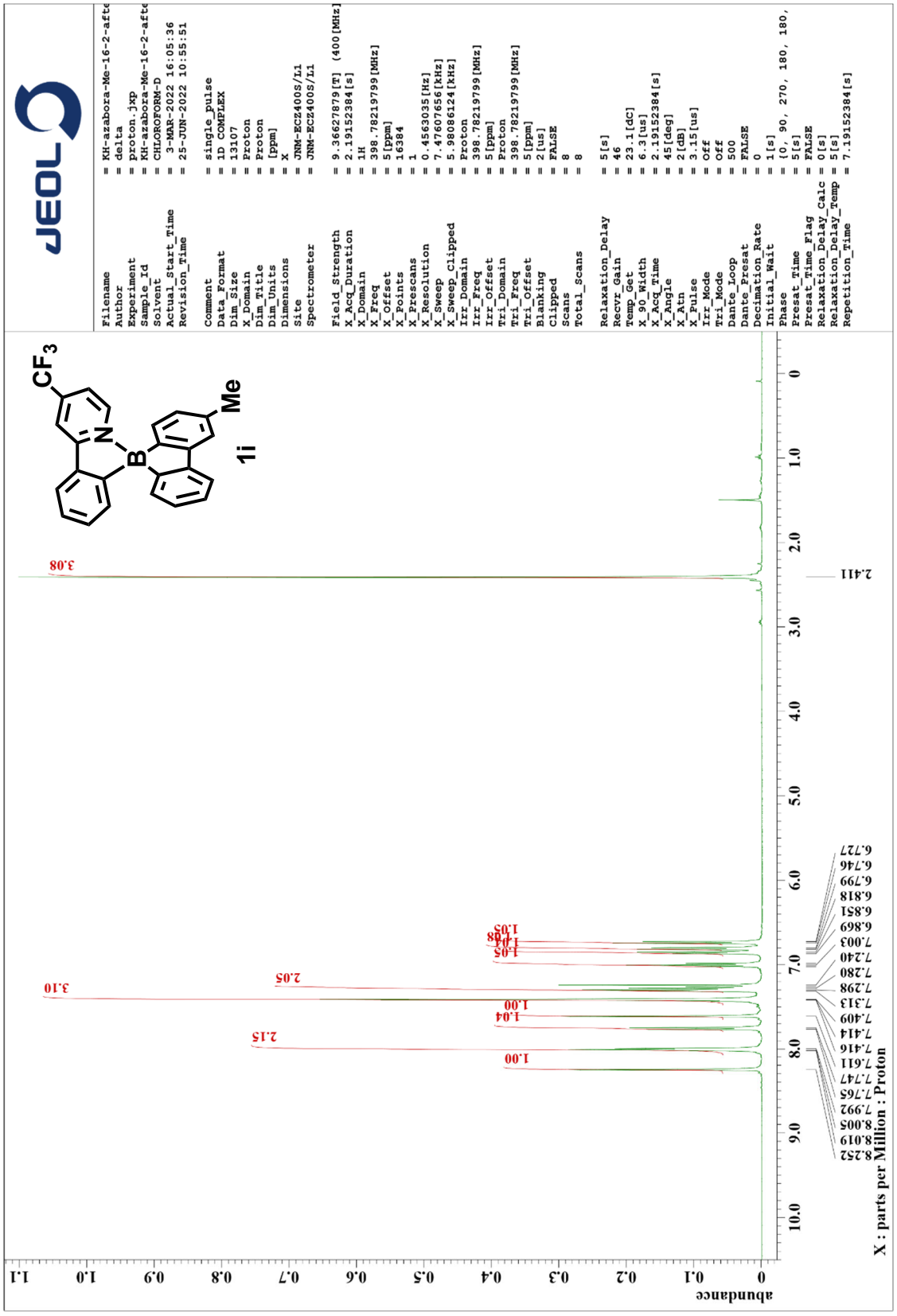

^{13}C NMR Spectrum of 1i (100 MHz, $CDCl_3$, rt)

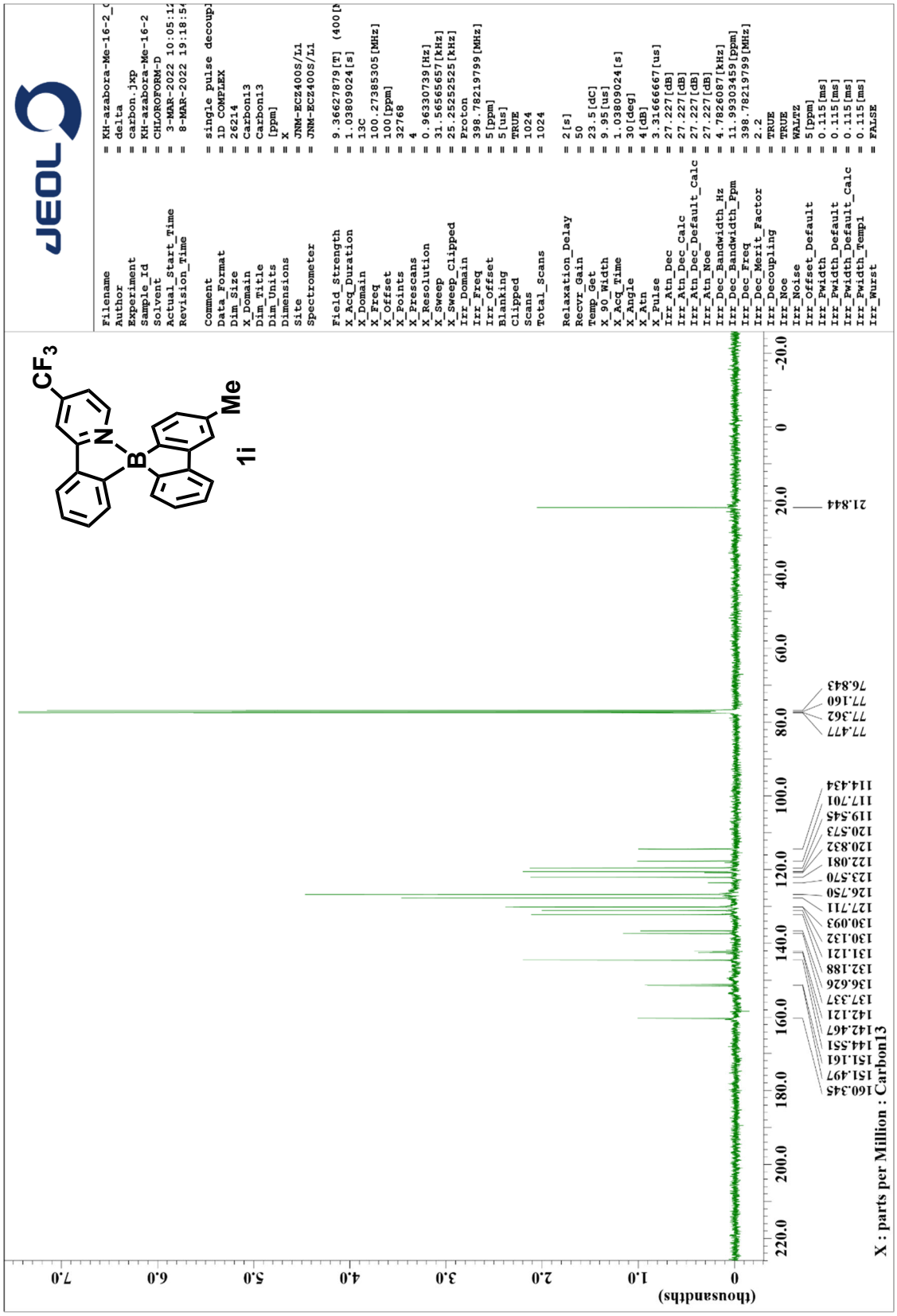

^{11}B NMR Spectrum of 1i (128 MHz, $CDCl_3$, rt)

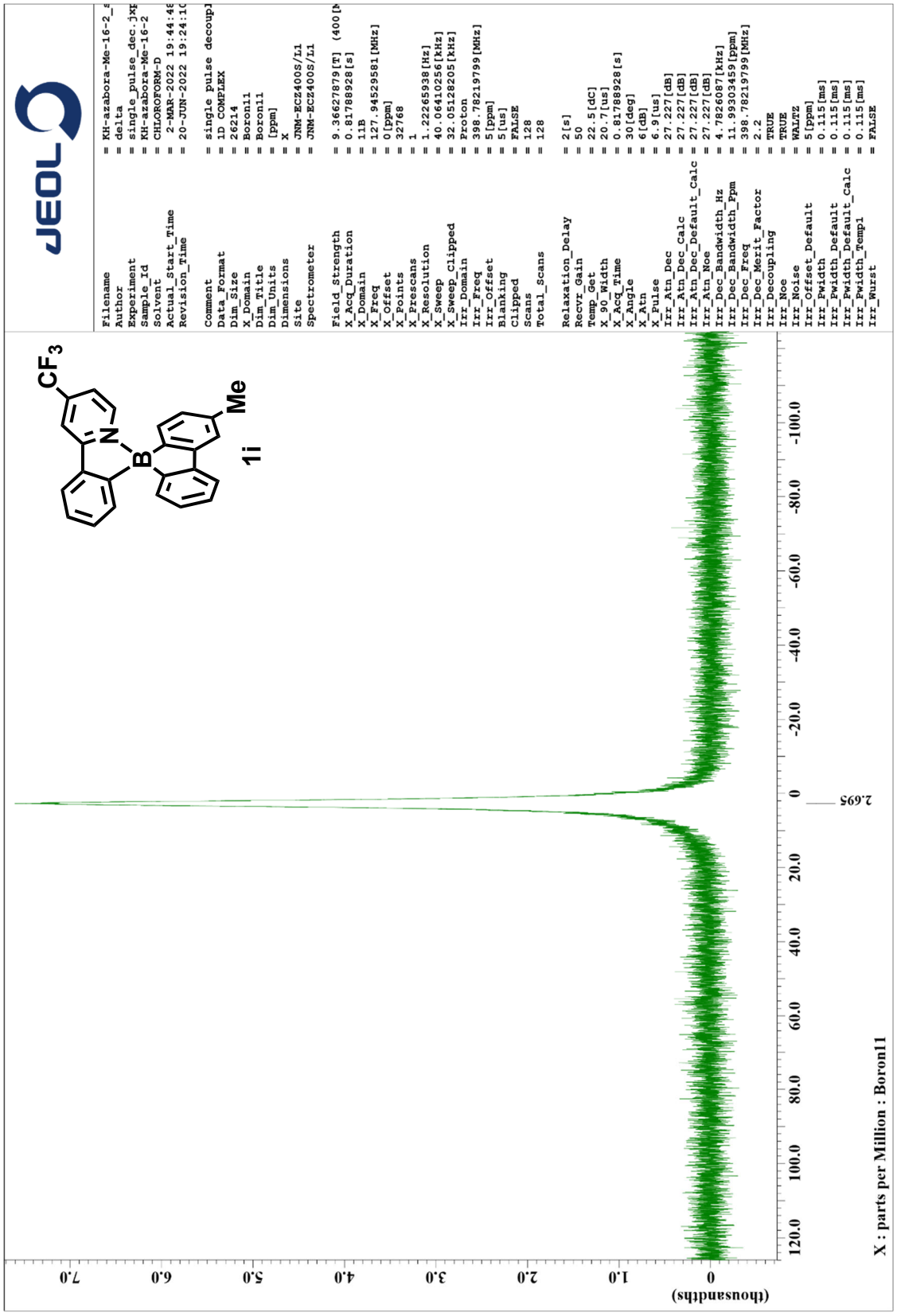

^{19}F NMR Spectrum of 1i (375 MHz, $CDCl_3$, rt)